UNDERSTANDING THE SOLUTION PHASE CHEMISTRY AND SOLID STATE THERMODYNAMIC BEHAVIOR OF PHARMACEUTICAL COCRYSTALS

by

Chinmay Maheshwari

A dissertation submitted in the partial fulfillment
of the requirements for the degree of
Doctor of Philosophy
(Pharmaceutical Sciences)
in the University of Michigan
2012

Doctoral Committee:

Associate Professor Naír Rodríguez-Hornedo, Chair

Professor Gordon L. Amidon

Professor Anton Van der Ven

Research Professor Gregory E. Amidon

Dedicated to

My parents, my wife Priya and daughter Rhea

ACKNOWLEDGMENTS

I cherish this opportunity to thank many individuals who supported me in my graduate research endeavor. Their support and encouragement made these years full of rich experiences and lasting memories. First, I would like to acknowledge my research mentor Dr. Naír Rodríguez-Hornedo. You have been a great inspiration throughout my graduate studies and will continue to do so in my future research path. I truly admire your commitment to research and your relentless exploration for excellence. It has been a privilege to be part of your research group and benefit from your guidance. Thank you very much for believing in me and for all the scientific and philosophical discussions we have had over the years. I would also like to express my sincere thanks to the doctoral committee members, Dr. Gregory Amidon, Dr. Gordon Amidon and Dr. Anton Van der Ven for your thoughtful and timely input in my research. Sincere thanks to Dr. Rodolfo Pinal of Purdue University for your insights with several aspects of my research.

This research was made possible by financial contributions from the Everett Hiestand fellowship, Warner Lambert/Parke Davis endowment fellowships from the University of Michigan, College of Pharmacy. Funding from the Purdue-Michigan Consortium on Supramolecular Assemblies and Solid State Properties is also acknowledged. Thank you very much for providing financial assistance for my education.

A very big thanks to the past and present members of the Rodríguez laboratory including Sarah Bethune, Adivaraha Jayasankar (Jay), David Good, Neal Huang,

Sreenivas Reddy, Phil Zocharski, Lilly Roy, Maya Lipert and visiting members, Toshiro Fukami and Vania Andre. It was a pleasure to spend time with you and learn a great deal from each one of your strengths. Many thanks to my friends in Ann Arbor, for giving me great times and helping me unwind with all the laughter and joy.

I would like to acknowledge my family members, my mother Sudha Maheshwari for her love, courage and never to give up attitude, and for her prayers to provide me strength; my sisters and my brother as well as their families for their support and encouragement. Although my father, Dr. R.D. Maheshwari is not living to witness my graduation, he has always been the strongest inspiration, especially during the difficult times. Thank you all for your blessings, patience and for helping me carry on with enthusiasm.

Most importantly, I would like to thank my wife Priya and my now seven year old daughter Rhea for altering their lives so I could pursue my goals. I am short of words to express my gratitude to both of you, I am truly blessed. It wouldn't have been possible without your support, patience, endurance and sacrifice. I have constantly learned from Rhea's exceptional maturity and depth in personality at such a young age. Thank you.

TABLE OF CONTENTS

LIST OF FIGURES

CHAPTER 1

CHAPTER 2

CHAPTER 3

CHAPTER 5

LIST OF TABLES

ABSTRACT

UNDERSTANDING THE SOLUTION PHASE CHEMISTRY AND SOLID STATE THERMODYNAMIC BEHAVIOR OF PHARMACEUTICAL COCRYSTALS

by

Chinmay Maheshwari

Chair: Naír Rodríguez-Hornedo

Cocrystals have drawn a lot of research interest in the last decade due to their potential to favorably alter the physicochemical and biopharmaceutical properties of active pharmaceutical ingredients. This dissertation focuses on the thermodynamic stability and solubility of pharmaceutical cocrystals. Specifically, the objectives are to; (i) investigate the influence of coformer properties such as solubility and ionization characteristics on cocrystal solubility and stability as a function of pH, (ii) to measure the thermodynamic solubility of metastable cocrystals, and study the solubility differences measured by kinetic and equilibrium methods, (iii) investigate the role of surfactants on the solubility and synthesis of cocrystals, (iv) investigate the solid state phase transformation of reactants to cocrystals and the factors that influence the reaction kinetics and, (v) provide models that enable the prediction of cocrystal formation by

calculating the free energy of formation for a solid to solid transformation of reactants to cocrystals.

Cocrystal solubilities were measured directly when cocrystals were thermodynamically stable, while solubilities were calculated from eutectic concentration measurements when cocrystals were of higher solubility than its components. Cocrystal solubility was highly dependent on coformer solubilities for gabapentin-lactam and lamotrigine cocrystals. It was found that melting point is not a good indicator of cocrystal solubility as solute-solvent interactions quantified by the activity coefficient play a huge role in the observed solubility. Similar to salts, cocrystals also exhibit pH_{max}, however the salts and cocrystals have different dependencies on the parameters that govern the value of pH_{max}. It is also shown that cocrystals could provide solubility advantage over salts as lamotrigine-nicotinamide cocrystal hydrate has about 6 fold higher solubility relative to lamotrigine-saccharin salt.

In the case of mixtures of solid reactants, it was observed that cocrystals can form spontaneously when the reactants are in physical contact and that temperature, relative humidity, and disorder in the reactants caused by mechanical stress such as milling can enhance the reaction rates. Prediction of spontaneous cocrystal formation was investigated by developing models to calculate the Gibbs free energy of formation. Thermal behavior of cocrystal reactants was investigated by calorimetry and the interaction between the reactants is explained by investigating the heats of mixing in the melt. These principles are applied on cocrystals that are divided into two categories;
(i) Where the cocrystal melting point is between that of its reactants and, (ii) where the cocrystal melting point is below that of its components. Generalized equations were

developed that enable the calculation of Gibbs free energy of formation from fusion temperatures, enthalpy and entropy of fusion.

CHAPTER 1

INTRODUCTION

This chapter introduces cocrystals in the context of their design and synthesis, physicochemical properties, the current understanding of solid state and solution chemistry, and the role additives can play in cocrystal research. Cocrystal solid-solution equilibria that describe solubility product behavior are presented. Mechanisms of cocrystal formation are discussed with emphasis on reaction crystallization method which incorporates the solubility product behavior. Reaction crystallization method and solubility product behavior is applied in the synthesis and solubility assessment of cocrystals presented in chapters 2 and 3. A few case studies are presented from published literature where cocrystals have shown favorable pharmaceutical properties such as solubility, dissolution and stability enhancements. The model compounds used are mentioned where applicable, however a detailed description of compounds can be found in relevant chapters. The chapter concludes with the key questions this research will address, statement of dissertation research and brief summaries of the contents in the research chapters.

What are Cocrystals?

Cocrystals are a single homogenous crystalline phase containing multiple distinct molecules often linked by hydrogen bonds. Cocrystals are not physical blends of pure components. Cocrystal physical and chemical properties are a function of unique solid-state arrangement of the molecules in the crystal lattice. Cocrystals are able to alter the physicochemical properties of active drug substances by combining drugs and coformers in the same crystal structure thereby altering solid-state properties and solution phase behavior without modifying the active's chemical structure. Properties that have a basis in the underlying crystal structure are therefore affected when a cocrystal is formed.[1-3] This ability of cocrystals to alter material properties of pharmaceutical relevance using crystal engineering principles and strategies has motivated the discovery of a large number of pharmaceutical cocrystals for drug development.[4-8] One of the most commonly faced challenge in drug development is the poor aqueous solubility of the active, which often results in dissolution rate limited bioavailability. Lipinski reported that between 1987 and 1994, nearly one-third of newly synthesized compounds in academic laboratories had solubilities less than 20 μg/mL.[9] Serajuddin reports that one-third of newly synthesized compounds have aqueous solubilities less than 10 μg/mL, and another one-third have aqueous solubilities between 10 and 100 μg/mL.[10] Cocrystals have been proven useful in addressing this issue by modulating the aqueous solubility of the drug as well as tailor the solubility based on coformer solubility and ionization properties.[11, 12] Depending on the desired pharmacokinetic effect, alternative solid forms such as salts, cocrystals and prodrugs can also be used to prolong the release of active compounds. Controlling release kinetics is of importance in the case of drugs exhibiting

short half lives, large C_{max} values or toxicity due to high solubility as well as for taste masking.[13-16] Cocrystals are unique relative to current options for altering physicochemical drug properties in pharmaceutical development because of the number of suitable drugs and possible coformers as well as the large number of intramolecular associations and supramolecular structures that can lead to cocrystal formation.

Cocrystals provide a unique advantage over other alternative solid forms in altering physico-chemical properties. For example, salts are commonly used to alter solubility, stability, mechanical properties of the API but only drugs with ionizable groups are candidates for salt formation and successful salt formation is in part a function of the drug pKa value(s). Amorphous solids can significantly change the solubility of a drug by eliminating crystal lattice energy as a barrier to solubilization,[17] however thermodynamic stability issues limit their applications. Cocrystals expand the options for drugs with challenging physicochemical properties by offering a large number of suitable coformers to change solution and solid-state chemistry. Furthermore cocrystals afford the preferred solid-state stability of a crystalline solid form for drug delivery. An overview of the classification and nomenclature of solid forms relevant to pharmaceutical development is presented in Figure 1.1 which, includes multi-component crystalline forms and cocrystals.

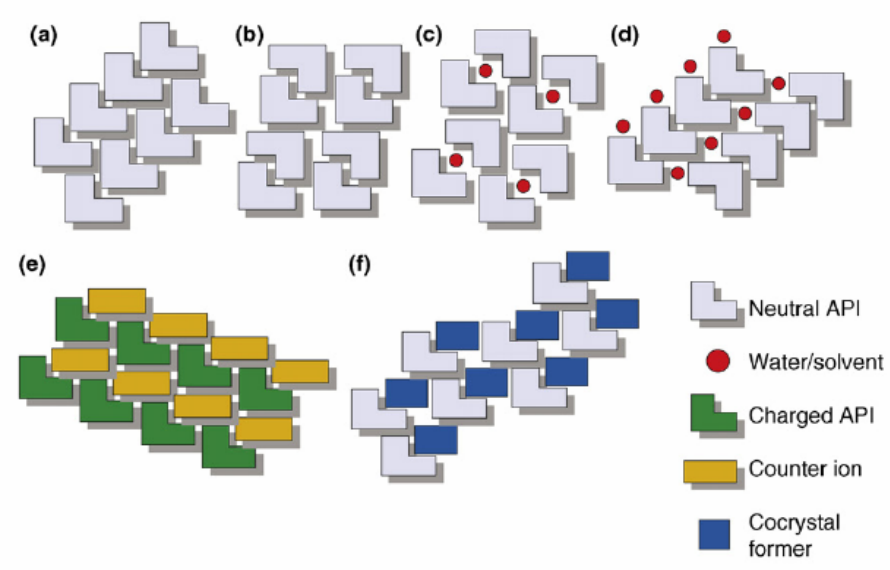

Figure 1.1: The range of single crystalline forms that are possible for an API: (a) pure API; (b) polymorph of pure API; (c) clathrate hydrate/solvate of API; (d) hydrate/solvate of API; (e) salt of API; (f) pharmaceutical cocrystal. Salts and cocrystals can also form hydrates, solvates, and polymorphs.[18]

Design Elements of Cocrystals

Hydrogen bonds play an important role in organic materials due to their ability to form weak intermolecular interactions. The products of these intermolecular interactions are hydrogen-bonded molecular aggregates, defined by connectivity patterns arising from hydrogen. Such aggregates could be formed in solution or in solid state.[19] As a result of molecular recognition phenomenon, hydrogen bonded supramolecular assemblies are formed. These supramolecular assemblies could either be single component crystals or multiple component cocrystals. The types of hydrogen-bond synthons and molecular aggregates likely to form between cocrystals components can be predicted by several general rules developed by Etter.[1, 20] There are three very useful rules, commonly referred to as hydrogen bond rules that reflect molecular recognition,[19] these are,

– All acidic hydrogen available in a molecule will be used in hydrogen bonding in the crystal structure of that compound.
– All good acceptors will be used in hydrogen bonding when there are available hydrogen bond donors.
– The best hydrogen bond donor and the best hydrogen bond acceptor will preferentially form hydrogen bonds to one another.

As a result of formation of hydrogen bonds between molecules, synthons are formed. Some examples of hydrogen bonded synthons are shown in the figure below.

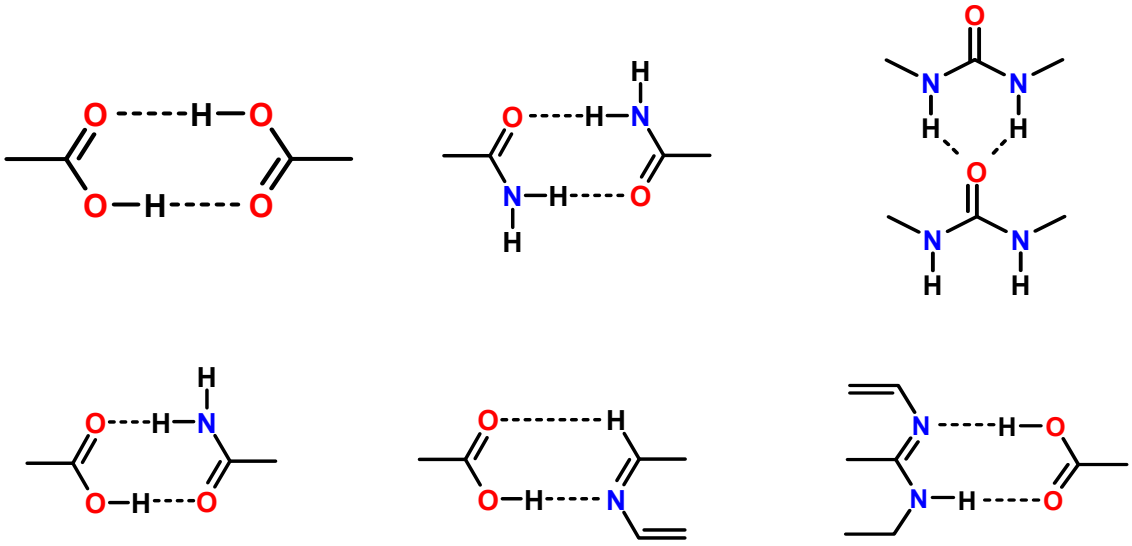

Figure 1.2: Common synthons in the supra molecular assemblies.

Synthons are classified as homosynthons and heterosynthons depending on the nature of the interacting functional groups in molecules. Homosynthons are formed by the interaction of similar functional groups while heterosynthons are formed by the interaction of different functional groups. These interacting functional groups form synthons through hydrogen bond formation. The term homosynthons or heterosynthons does not indicate if the synthons are formed between similar or dissimilar chemical

entities. A homosynthon can be formed in a multi component cocrystal whereas a heterosynthon can be formed in a single component crystal. Examples of homosynthons and heterosynthons are shown in Figure 1.3.

amide-amide homosynthon acid-amide heterosynthon

Figure 1.3: Example of homosynthon and heterosynthon.

Depending on the nature of the interacting molecules the terms homomers or heteromers is used to describe the molecular aggregate formed. If the interacting molecules are the same, then the resulting aggregate is a homomer, whereas a heteromer is said to be formed when the result is a multi component cocrystal. Cocrystals are a result of hydrogen bond formation between neutral molecules of two or more different components. The term cocrystal is generally used when it is formed from components which in their pure states are solids at room temperature.[21] While these rules are good general considerations they do not predict crystal structure, molecules capable of cocrystallizing with each other, conditions that promote cocrystallization, or the properties of cocrystals that might form.[22] Exceptions to these guidelines often occur due to competition of multiple hydrogen bonding, dipole, or ionic sites as well as steric or conformational limitations. Considerations of van der Waals interactions and stereochemistry of the components are also relevant for cocrystal design and coformer selection.[22] Symmetry elements and conformational energies of molecules play essential roles in determining crystal structures. The formation of stable crystal structures is

additionally based on minimizing electrostatic energies (e.g. bond or molecular dipoles) and minimizing free volume (i.e. maximizing density). A search of the Cambridge Structural Database (CSD) showed that molecules containing carboxamide moieties form multicomponent crystal forms with carboxylic acids via $R_2^2(8)$ synthon. Zaworotko and coworkers published a CSD survey of compounds containing primary amides and carboxylic acid groups that suggested that 47% of the structures formed acid ··· amide heterosynthons while 44% and 6% structures formed amide ··· amide and acid ··· acid homosythons respectively.[23] Recent analysis of coformers published in the CSD indicated that shape, polarity, and available synthons were key parameters for designing cocrystals, however the number of hydrogen bond donors and acceptor was not statistically significant.[24] Together all these structural considerations of the crystalline state influence the design and stability of cocrystals.

Cocrystal Synthesis

Currently the most established methods for cocrystal formation are solvo-thermal and mechanical techniques. In solvo-thermal cocrystal synthesis, stoichiometric ratios of reactants are dissolved in a solvent of choice and supersaturation is achieved either through a temperature difference or through evaporation of the solvent. In mechanical cocrystal synthesis, stoichiometric ratios of reactants are mechanically agitated (*e.g.* by grinding in a mill) to induce phase transformations from a physical mixture into cocrystal.[7, 25-27] Drops of solvent, which are considered plasticizers, have been shown to impact the crystallization outcome.[28-31] Mechanical methods are often favored due to their speed, procedural simplicity, and potential for green chemistry.

While grinding experiments are attractive because of small requisite quantities of components and rapid synthesis. Some limitations include the difficulty of readily discerning the formation mechanism or pathway, the chemical stability of components subjected to high kinetic energy process, purity of products (i.e. extent of transformation), empirical nature, and challenges regarding scalability. Solvo-thermal techniques often rely on empirical choices of solvent, temperature conditions, and molar ratio of reactants. There is a risk of crystallizing one or more undesirable phases if conditions are chosen such that cocrystal is not the thermodynamically stable phase. Mechanical techniques are also subject to empirically selected conditions (such as selection of solvent drop and grinding time), but the main challenges include process scalability, reactant stability during mechanically/thermally energetic processes, and extent of transformation.

Reaction crystallization is an emerging solution-mediated cocrystal synthesis method that complements the other more established methods.[32] The reaction crystallization method (RCM) relies on creating supersaturation through cocrystal solution phase chemistry. The solubility product behavior of cocrystals described by Nehm and Rodríguez-Hornedo et al. provided the basis for their development of RCM wherein cocrystal had lowest solubility, was thermodynamically stable, in solutions containing excess of one of the cocrystal components.[33] Cocrystal solubility is described by solubility product behavior, which indicates that cocrystal solubility decreases as coformer concentration increases.[33, 34] Cocrystal solubility is decreased below that of the drug by adding coformer at or near the coformer solubility. Therefore, conditions are chosen to maximize the likelihood of obtaining cocrystal by operating in a region of the phase diagram where cocrystal is least soluble and maximum supersaturation with respect

to the cocrystalline solid phase can be generated (Figure 1.4). Supersaturation affects the nucleation rate, high supersaturation achievable in the reaction crystallization leads to fast nucleation rates. The nucleation rate is given by the equation below,

$$J = N_0 \nu \exp\left(\frac{-16\pi\gamma^3\upsilon^2}{2(k_b T)^3 (\ln\sigma)^2} \right)$$

N_o is the number of molecules of the crystallizing phase per unit volume

v is the frequency of molecular transport at the nucleus-liquid interface

υ is the molecular volume of the crystallizing phase

k_b is the Boltzmann constant

γ is the interfacial energy between the crystal nuclei and supersaturated solution

T is the temperature

Mechanisms of Cocrystal Formation

Phase Diagram - Reaction Crystallization Method (RCM)

The driving force for crystallization is the difference between the chemical potential at a supersaturated state (liquid) and at equilibrium. At the solubility, the equilibrium phases have equal molar free energies or chemical potentials. In the case of cocrystals this is the sum of the molar free energies or chemical potentials of each cocrystal component. The molar free energy of a cocrystal A_mB_n in equilibrium with solution phase is given by,

$$G_{A_mB_n} = G_{solution} = mG_A^L + nG_B^L = m\mu_A + n\mu_B \quad (1.1)$$

The activity of each component a_i is defined as,

$$\mu_i = \mu_i^o + RT \ln a_i \quad (1.2)$$

where μ_i^o is the chemical potential of the reference state for i. Combining equations (1.1) and (1.2) gives,

$$\Delta G_{A_mB_n} = \Delta G_{solution} = RT(m \ln a_A + n \ln a_B)$$

$$\exp\left(\frac{\Delta G_{A_mB_n}}{RT}\right) = (a_A)^m (a_B)^n$$

$(a_A)^m(a_B)^n$ is the solubility product, K_{sp} of the cocrystal. Figure 1.4 shows the phase diagram that explains the cocrystal formation pathways and stability domains. A is the drug and B is the ligand (cocrystal former). Cocrystals follows the solubility product (K_{sp}), i.e., with increasing ligand concentration, higher supersaturation with respect to the cocrystal is generated and the cocrystal precipitates out of the solution.[35] The transition concentration at which the concentration of cocrystal is equal to the concentration of the drug is known as the ligand transition concentration shown in Figure 1.4 as $B_{tr.}$ At the ligand transition concentration the drug and the cocrystal solid phases are in equilibrium with each other. Details of all the four regions of the phase diagram are described below.

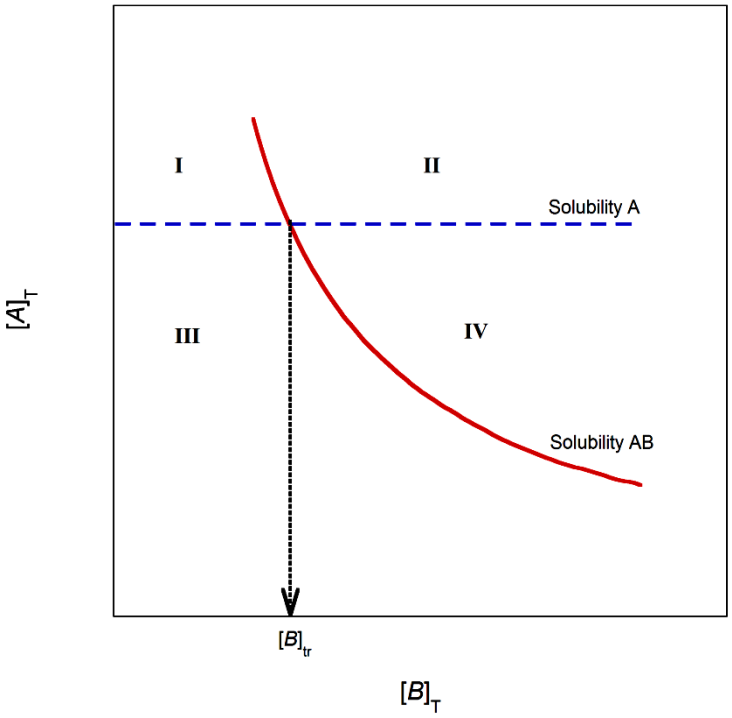

Figure 1.4: Solubility phase diagram for crystal A and cocrystal AB, showing the transition concentration, $[B]_{tr}$.

Region I: Supersaturated with respect to A and undersaturated with respect to AB, therefore in region I crystalline form AB will transform to crystalline form A.

Region II: Supersaturated with respect to A and AB and the thermodynamically more stable phase AB will precipitate as the stable solid phase.

Region III: Undersaturated with respect to both A and AB resulting in a solution.

Region IV: Supersaturated with respect to AB and undersaturated with respect to A and crystalline form A will transform to cocrystalline form AB.[35]

The transition concentration is also referred as a eutectic point, this is because at the transition concentration Gibbs phase rule constraint is invoked. According to the Gibbs phase rule at constant pressure, $P + F = C+1$, the term 1 represents the temperature variable.

Phases (P): For a cocrystal system, at the eutectic point (transition concentration), there are three phases, solid which is composed of two separate homogeneous solid phases (cocrystal and drug) and liquid (solution), together constituting three phases.

Components (C): Coformer, Drug and Solvent

Thus, $P = 3$ and $C = 3$ resulting in $F=1$. This implies that the eutectic concentration is temperature dependent and when the temperature is constant, there are zero degrees of freedom. This is compared with the more widely used eutectic point for a melt at constant pressure below where,

Phases (P): Solid and liquid, where solid is composed of A and B components. Thus there are 3 phases, namely Solid A, solid B and melt (liquid).

Components(C): A and B.

Thus, when $P = 3$ and $C = 2$ the resulting $F = 0$, this type of solid-liquid eutectic is rigidly defined by the temperature and can be achieved only at a particular temperature when the pressure is constant. Multiple eutectic points can exist depending on what solid phases coexist at equilibrium. In the case of a cocrystal AB with no other stoichiometries or polymorphs, two eutectics exist; the first is between solid drug, cocrystal, and solution, and the second is between solid coformer, cocrystal, and solution.

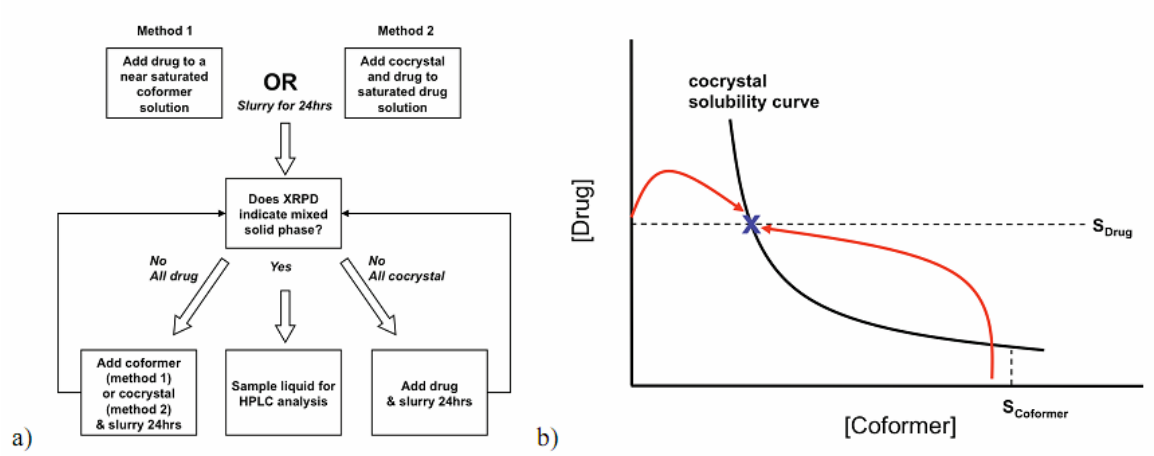

Figure 1.5: (a) Flowchart of method used to establish the invariant point and determine equilibrium drug and coformer eutectic concentrations, (b) Schematic phase solubility diagram that illustrates two pathways to the eutectic point (marked X).[11]

Figure 1.5 shows the schematic pathway to determine the solubility of cocrystal via the eutectic point. The intersection of cocrystal and drug solubilities is the eutectic between solid drug, cocrystal, and solution. From the concentrations of drug and coformer at the eutectic, the cocrystal solubility product K_{sp} can be calculated.

Eutectic and Vapor Phase Mediated Cocrystal Formation

Cocrystal formation via cogrinding of solid reactants has been explained by eutectic formation when the reactants are milled together.[36, 37] Milling the reactants raises the mill temperature significantly above room temperature, which can cause the reactants to melt and initiate the reaction. However, the temperature at which the reactants melt is lower than the melting temperature of the individual reactants. Eutectic melt-mediated cocrystal formation at room temperature has been reported for benzophenone and diphenylamine.[36] Similar behavior has been shown for cocrystals of CBZ with carboxylic

acids at temperatures above 85°C.[37] Solid-vapor interactions due to sublimation of reactants have also been reported to form cocrystals.[38-40]

Deliquescence Mediated Cocrystallization

It has been shown that cocrystal formation can occur during storage by vapor sorption of reactant components.[41] Phase transformations of APIs in the presence of moisture sorbed by hygroscopic materials are well known and are suggested to proceed through a solution mediated process.[42] It is reasonable to expect solution mediated phase transformation of drug to cocrystal in solid mixtures of cocrystal components with deliquescent materials.

Deliquescent and hygroscopic cocrystal components or excipients have been shown to facilitate solution-mediated formation of cocrystals. Deliquescent excipients including sucrose, fructose, and citric acid led to cocrystal formation for various components.[43] The mechanism indicated consisted of deliquescence of the excipient, followed by dissolution of the cocrystal components in the sorbed moisture, then subsequent crystallization of cocrystal from solution. In this solution mediated mechanism supersaturation with respect to cocrystal was generated from dissolution of components in the sorbed moisture. Cocrystal nucleation was observed near the surface of undissolved carbamazepine crystals presumably due to the high drug concentrations at this boundary producing the greatest supersaturation in the concentrated nicotinamide/sucrose solution. Cocrystal formation in solid blends of cocrystal components and deliquescent materials involves 4 essential processes: (i) moisture sorption by deliquescent material (ii) dissolution of cocrystal components in the moisture sorbed by deliquescent material (iii) supersaturation with respect to cocrystal and (iv)

crystallization of cocrystal. Thus the rate of cocrystal formation in solid blends containing deliquescent materials will depend on the rate of moisture sorption, dissolution of reactants and supersaturation. The driving force for moisture sorption depends on the difference between the relative humidity of the surroundings (RH_s) to which the sample is exposed and the deliquescent point of the material (RH_o).[44]

Thermal Methods

Less common synthetic methods include melt processes such as the Kofler mixed fusion method and differential scanning calorimetry (DSC) of components in physical blends. Kofler's methods have been used to efficiently determine the formation and phase behavior of many multicomponent crystals and their polymorphs. A recent example is the work of Berry et al. who screened for cocrystals of seven drugs with nicotinamide and determined the structures of three novel cocrystals including that of R/S-ibuprofen-nicotinamide.[45] DSC and hot stage microscopy are also shown as an efficient thermal method for screening cocrystals of carbamazepine, theophylline, caffeine, lamotrigine and sulfamethazine.[37, 46]

Solubility and Solution Chemistry of Cocrystals

Cocrystal Solution Chemistry

Cocrystal solubilities have been commonly expressed using a variety of equilibrium and kinetic measurements. Kinetic solubility measurements reported are typically powder dissolution or intrinsic rotating disk dissolution. Both equilibrium and kinetic experiments present valuable information on the solution properties and performance of cocrystals relative to the components. Crystallization of other drug forms

can occur in kinetic studies particularly when cocrystal is highly soluble relative to the components.

The true stoichiometric solubility of a cocrystal is often difficult to measure directly because of purity issues, unknown or complex solubility phase behavior, and potential transformations to other solid forms such as components or other cocrystal stoichiometries or solvates. The measurement of an equilibrium or steady state drug concentration from a cocrystal placed in solution does not always reflect the actual stoichiometric solubility depending on the final solid phase(s) that persist at equilibrium point. Isolation and analysis of solid phase(s) is critical in describing solubility because the final solid form is associated with the measured concentration(s). Only when the initial cocrystal form is observed as the single solid phase after equilibration with pure solvent are the equilibrium concentrations descriptive of the true stoichiometric solubility. When a solid phase other than the starting cocrystal is observed, the corresponding steady state drug concentration is not the true cocrystal solubility. In these instances both component concentrations should be recorded to best describe solubility behavior of the solid phase(s) in equilibrium with the solution. If one of the stable equilibrium solid phases is a cocrystal of known stoichiometry, the Ksp can be calculated and reported to describe the thermodynamic cocrystal solubility.

Cocrystal solution phase behavior was first investigated by Higuchi, Connors, and coworkers, though their focus was on solution complexation between cocrystal components.[47-49] Their experiments showed that cocrystals adhered to solubility product behavior, where increasing coformer concentration led to decreasing drug concentration at equilibrium. The theoretical framework developed for cocrystal solubility allows for

rational selection of solvent and solute concentrations to control and optimize cocrystallization processes. RCM is a scalable technique, amenable to both large and small scales. RCM has been successfully used in addition to other methods to screen for carbamazepine and piroxicam cocrystals,[4, 5] and can be applied with equal success in green solvents such as water. A recent screening of twenty-seven carbamazepine cocrystals by four different methods including RCM identified all of the forms generated by grinding of components were also found by at least one of the other solution methods.[5] Cocrystals are often selected for their high solubilities relative to the drug. Cocrystals that are highly soluble relative to drug can transform, sometimes very rapidly, to the less soluble crystalline drug. Equilibrium solubilities that use drug concentration as a measure of cocrystal solubility are confounded by such conversions, which can lead to underestimation of true cocrystal solubilities. Kinetic solubility measurements are limited by the kinetics of transformation and depend highly on experimental conditions, which are often empirically selected. This dissertation establishes the fundamental solution behavior of cocrystals wherein cocrystal solubility is shown to be highly dependent on the nature of its components. Lower solubility coformers are shown to decrease cocrystal solubility and corresponding drug concentrations, while non-ionizable compounds can exhibit pH dependent solubility when ionizable coformers are selected. Also this work demonstrates that thermodynamic methods to evaluate solubility can yield large discrepancies with values estimated from kinetic methods. These methods are derived from the mathematical models that describe cocrystal solubility in terms of cocrystal solubility product (K_{sp}), solution complexation constant (K_{11}) and the pH dependent

solubility behavior introduced by Nehm *et al*.[33] The chemical equilibria that describe cocrystal AB solubility, where A is drug and B is coformer are,

$$AB_{solid} \overset{K_{sp}}{\rightleftharpoons} A_{soln} + B_{soln} \tag{1.3}$$

$$A_{soln} + B_{soln} \overset{K_{11}}{\rightleftharpoons} AB_{soln} \tag{1.4}$$

where K_{sp} and K_{11} are the cocrystal solubility product and the complexation constant for a 1:1 solution complex between A and B. K_{sp} and K_{11} are given by

$$K_{sp} = [A][B] \tag{1.5}$$

$$K_{11} = \frac{[AB]}{[A][B]} \tag{1.6}$$

under the assumption of dilute conditions where activities are approximated by concentrations. By mass balance, where $[A]_T$ and $[B]_T$ are the total analytical concentrations of A and B,

$$[A]_T = [A] + [AB] \tag{1.7}$$

$$[A]_T = \frac{K_{sp}}{[B]_T} + K_{11}K_{sp} \tag{1.8}$$

Equation (1.8) is an expression of the cocrystal solubility (in terms of drug concentration) as a function of the coformer concentration at equilibrium. Figure 1.6 shows the solubility of a 1:1 cocrystal of carbamazepine and nicotinamide (CBZ-NCT) in three organic solvents. Figure 1.6 shows that cocrystal solubility decreases as a function of coformer concentration.

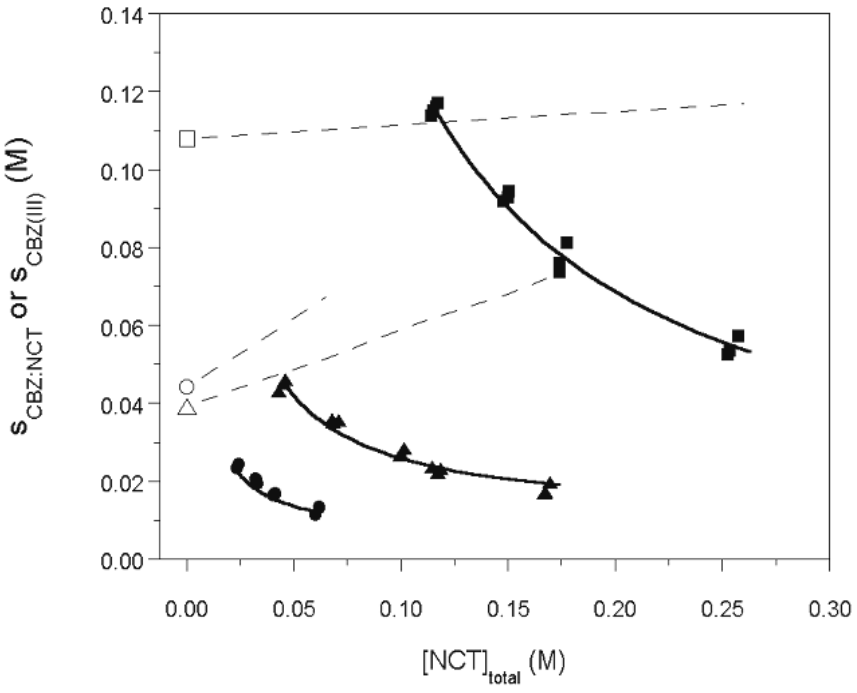

Figure 1.6: Solubility of 1:1 CBZ-NCT cocrystal at 25 °C as a function of total NCT concentration in ethanol, 2-propanol, and ethyl acetate.[33] The solid lines represent the predicted solubility according to Equation (1.8). Filled symbols are experimental cocrystal solubility values in (■) ethanol, (▲) 2-propanol, and (●) ethyl acetate.

For a 1:1 cocrystal, the cocrystal solubility in solutions containing stoichiometric solution concentrations of A and B, S_{AB}, is given by

$$S_{AB} = [A]_T = [B]_T \tag{1.9}$$

$$S_{AB} = \sqrt{K_{sp}} \tag{1.10}$$

if we assume $K_{11}K_{sp} << S_{AB}$.

Cocrystal Solubility Dependence on Coformer Solubility

Solid state properties are often considered as a basis to predict solubilities, while solution phase contributions are not weighed upon. When solubility is limited by the strength of the crystal lattice, solubility is dependent on melting of the solid solute given by the ideal solubility equation,

$$\ln \chi_{ideal} = -\frac{\Delta H_m}{R}\left(\frac{T_m - T}{T_m T}\right) \qquad (1.11)$$

where χ_{ideal} is the ideal solubility expressed as mole fraction, R is the gas constant, T is the reference temperature, T_m and H_m are melting temperature and enthalpy in Kelvin. Equation (1.11) assumes that the heat capacity change upon melting is negligible, and that solubility is a property of the solid solute only and is not solvent dependent. Such a behavior only applies to ideal solutions or to different solid state forms of the same chemical components such as polymorphs. Solids with different chemical composition can exhibit an inverse proportionality between solubility and melting point when solvation energy changes are parallel to lattice energy changes. However, melting point is a poor indicator of observed solubility due to the fact that solubility is often limited by solvation and not by lattice energy alone. The observed aqueous solubilities are highly dependent on the solvation barrier (hydrophobicity) due to solute solvent interactions. Coformer solubility has also been shown to influence cocrystal solubility. This is due to coformer altering the solvation barrier for the cocrystal Figure 1.7.[50]

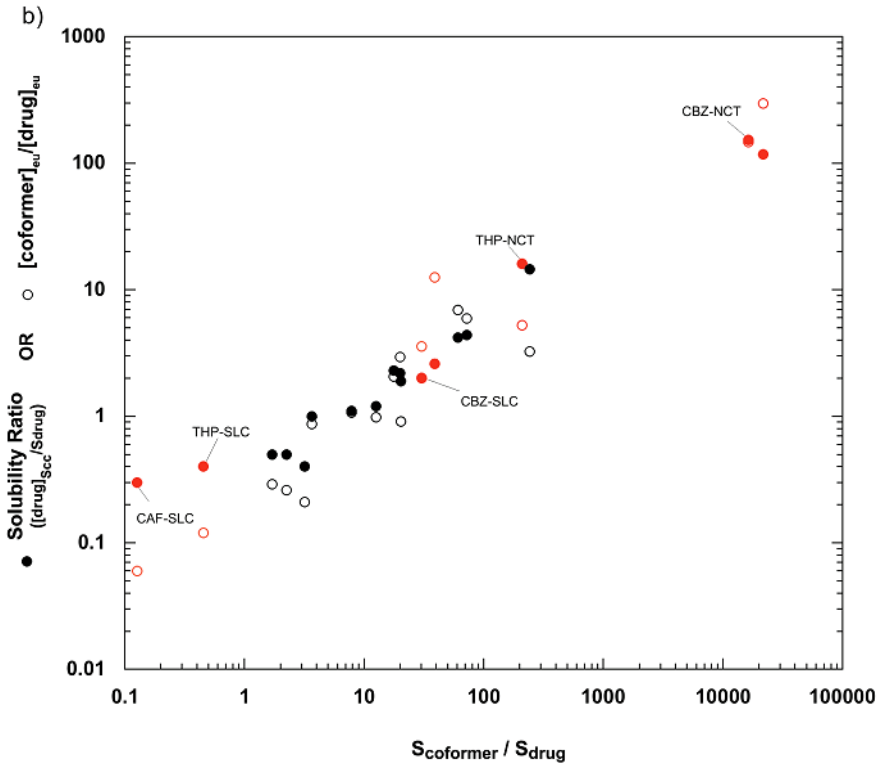

Figure 1.7: The ratio of coformer to drug solubility plotted against the cocrystal solubility ratio (filled circles) and the ratio of coformer to drug eutectic concentrations (open circles).[11] All aqueous samples are shown in red. Several cocrystals with the same coformers are labeled.

Figure 1.7 shows the cocrystal to drug solubility ratio against the coformer to drug solubility ratio for several cocrystals. The solubilities of twenty-five cocrystals were ranked according to their solubility advantage over drug.[11] The cocrystals were various combinations of three drugs (carbamazepine, theophylline, and caffeine) and seven coformers (malonic acid, nicotinamide, salicylic acid, saccharin, succinic acid, glutaric acid, and oxalic acid) in four solvents (water, isopropyl alcohol, methanol, and ethyl acetate). The measured cocrystal solubilities ranged from 0.1 to over 100-fold their respective drug solubilities and the coformer solubilities spanned several orders of magnitude, from 10^{-2} m to 10^{1} m. The dependence was demonstrated to be linear, where larger coformer to drug solubility ratios resulted in cocrystals that were more soluble

relative to the drug. This work demonstrated that cocrystal solubility enhancement could be rationally selected based on knowledge of the coformer solubility.

Role of Additives in Cocrystal Research

Role of differential solubilization by sodium lauryl sulfate (SLS) on cocrystal solubility is recently demonstrated by Huang and Rodríguez. Cocrystal and drug show different solubility dependencies as a function of SLS concentration, resulting in a critical stabilization concentration (CSC) with respect to SLS beyond which cocrystal is less soluble and thermodynamically stable solid phase (Figure 1.8).[51]

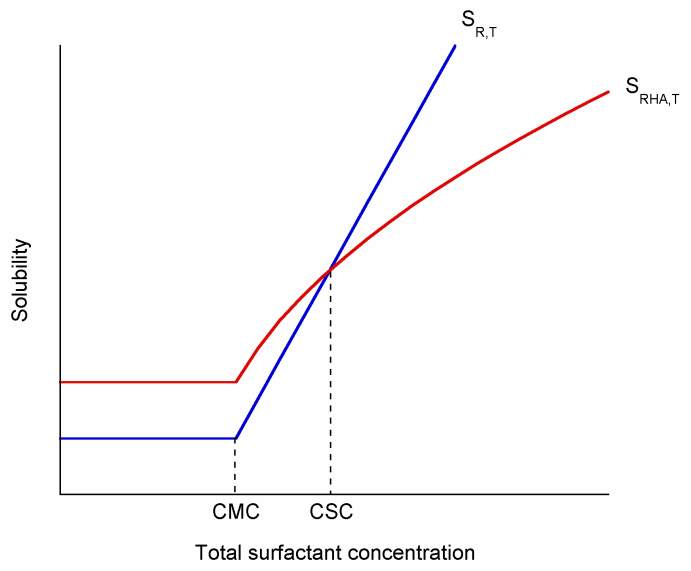

Figure 1.8: Schematic representation of the cocrystal (RHA) and drug (R) solubility with respect to the total surfactant concentration. The differential solubilization of cocrystal and drug results in the intersection of solubility curves yielding a CSC (critical stabilization concentration) at which both cocrystal and drug are in equilibrium with the solution.

Surfactants are important additives that have range of pharmaceutical applications such as solubilizers, emulsifiers, detergents, foaming agents, lubricants, etc.[52-54] Dissolution of celecoxib-nicotinamide cocrystal into aqueous media (pH 6.5) containing

1% SLS demonstrated that a 5-minute "pre-suspension" process could lead to variable dissolution rates based on extent of transformation from cocrystal to drug, which could compromise a potential dosage form. This implies that excipients such as SLS can affect which solid forms are favorable in solution as well as the kinetics of transformation to those solid forms. Remenar *et al.* investigated the influence of SLS and polymer polyvinylpyrollidone (PVP) mixtures on dissolution and phase stability of a 1:1 cocrystal of celecoxib and nicotinamide.[8] Celecoxib-nicotinamide cocrystal was suspended in aqueous media with varying pH, ionic strength and SLS concentration. Cocrystal was found to transform to drug in all cases, but in the presence of SLS transformation resulted to different polymorphs of celecoxib. Thus, mixtures of cocrystal, PVP K-30, and SLS were formulated to inhibit the transformation to less soluble drug. Dissolution of cocrystal, PVP, and SLS mixtures into aqueous media (pH 6.5) containing 1% SLS exhibited dissolution rates comparable to amorphous form/PVP mixtures in the same media. This investigation demonstrated that solution conditions (such as pH) and excipients (PVP, SLS) affected cocrystal solution phase behavior, although further investigation is needed to understand the mechanisms involved in these phase transitions. One limitation of this work is the lack of quantitative theoretical treatment and mechanistic understanding of excipient effects on cocrystal solution chemistry that can be applied across different cocrystal systems and solution conditions.

Properties of Pharmaceutical Cocrystals: A Few Case Studies

Solubility is a critical property of pharmaceutical materials, since an active must be in solution to be absorbed. Solubility is defined by thermodynamic equilibrium of the solid phase of a solute with its solution. The structure and properties of cocrystals are distinct from that of their individual components. Cocrystals have been shown to change the hygroscopicity, melt temperature, chemical and thermal stability, solubility and dissolution rate, bioavailability, hydrate/solvate formation as well as mechanical properties. Any chemical or physical properties that are a function of the supramolecular structure are potentially modified by cocrystal formation. The design and formation of a cocrystal to change a particular physicochemical drug property will likely change additional properties since the structure and supramolecular chemistry are not exclusive to any one physicochemical property. If designing a cocrystal for improved drug solubility one should anticipate changes to many other properties, such as possibly the crystal density or habit, that are dependent on supramolecular structure. A few case studies are presented below where increased bioavailability or maximum plasma concentration (Cmax) has been demonstrated for several drug substances.

Itraconazole Cocrystal

Itraconazole, an antifungal agent with low solubility (~1ng/ml) in its free base form, has been reported to form several cocrystals with 1, 4 dicarboxylic acids. All of the cocrystals demonstrated an enhanced dissolution profile as compared with itraconazole free base. In some cases the dissolution profiles of the cocrystals approached that of amorphous itraconazole.[55] The three cocrystals studied achieved sustained (>400 minutes) dissolution concentrations from 4 to 20-fold of the crystalline itraconazole level.[55]

Remenar also showed for the celecoxib-nicotinamide cocrystal that formulation with surfactant (SDS) and polymer (PVP) provided similar dissolution rates as amorphous blends of drug and PVP. Here the cocrystal formulation produced an amorphous/crystalline blend with small particulates (~380nm) of a metastable drug polymorph (celecoxib IV).[8] This study demonstrated formulation methods to exploit the high cocrystal solubility relative to celecoxib to design rapidly dissolving drug products.

API-Glutaric Acid Cocrystal

2-[4-(4-chloro-2-fluorophenoxy)phenyl]pyrimidine-4-carboxamide, which is a sodium channel blocker with low dissolution rate and bioavailability. This API belongs to BCS class II (low solubility-high permeability). Traditional methods of forming salts and amorphous material failed to produce a viable solid form for continued development. However, cocrystal with glutaric acid resulted in higher bioavailability when tested in dogs. These in vivo studies were in agreement with aqueous rotating disk intrinsic dissolution results that indicated significant improvement for the cocrystal (~18-fold increase) over the pure drug at 37˚C.[56]

Fluoxetine·HCl Cocrystals

Another example of altered dissolution was observed for three cocrystals of fluoxetine HCl, an active ingredient to treat depression. This is an interesting case as the researchers designed the cocrystals by combining a carboxylic acid with the hydrochloric acid (HCl) salt of fluoxetine, generating three novel cocrystals of salts with three different acid coformers. The individual cocrystals were found to have dissolution rates above, below and comparable to the salt form of the drug.[57] Using different ligands,

dissolution rates could be controlled. This is due to the ligand properties such as pK_a (pH-solubility profile) and aqueous solubility. Cocrystals of different ligands also have different lattice energies which may govern their solubility and dissolution behavior.[57]

AMG 517 – Sorbic Acid Cocrystal

In a recent study, a new chemical entity inadvertently formed a cocrystal with one of the formulation components. AMG 517 is a poorly soluble VR1 (vanilloid receptor 1) antagonist. In animal studies good exposure of the drug was seen from a 10% (w/v) Pluronic F108 in OraPlus suspension. This was due to the fact that the drug had formed a cocrystal with sorbic acid, a preservative in Ora Plus.[58] This also emphasizes the importance to understand the possibility of unintentional cocrystallization. Such uncontrolled events can occur during development and/or storage depending on the reaction kinetics. Thus a molecular level understanding of cocrystallization mechanisms and physico-chemical factors responsible will have positive implications on drug development.[58]

Additionally a cocrystal of Merck L-883555, a developmental phosphodiesterase-IV inhibitor, and L-tartaric acid (0.5:1) showed more than 10 and 20-fold increase of C_{max} and AUC, respectively, for 3mg/kg dose given orally in methocel to rhesus monkeys.[59] Carbamazepine-saccharin (1:1) cocrystal has exhibited higher average cocrystal C_{max} and AUC values relative to the marketed form III of carbamazepine in beagle dogs. Three different cocrystals of lamotrigine-nicotinamide were shown to have powder dissolution rates that were improved or equivalent to free lamotrigine at acidic and neutral pH conditions, respectively. However, the two nicotinamide cocrystal forms administered to rats demonstrated lower serum concentrations.[60] This discrepancy could

be caused by several factors such as the influence of the coformer on oral absorption or the oral suspension vehicle (PEG400 and methyl cellulose) that could change the thermodynamic stability or solubility of the cocrystal. Whatever the case, future animal experiments should carefully consider the thermodynamic solubility of cocrystals and the relevant solubility equilibrium associated with excipients and *in-vivo* or biorelevant conditions.

Stability

Caffeine converts to caffeine hydrate at high RH, which limits the processing and storage conditions of caffeine during development. However, the cocrystal of caffeine with oxalic acid was physically stable even at 98%RH up to 7 weeks. Moisture uptake studies done in our lab have also demonstrated the stability potential of the CBZ-NCT and CBZ-SAC cocrystals at high RH values [61] (Figure 1.9).

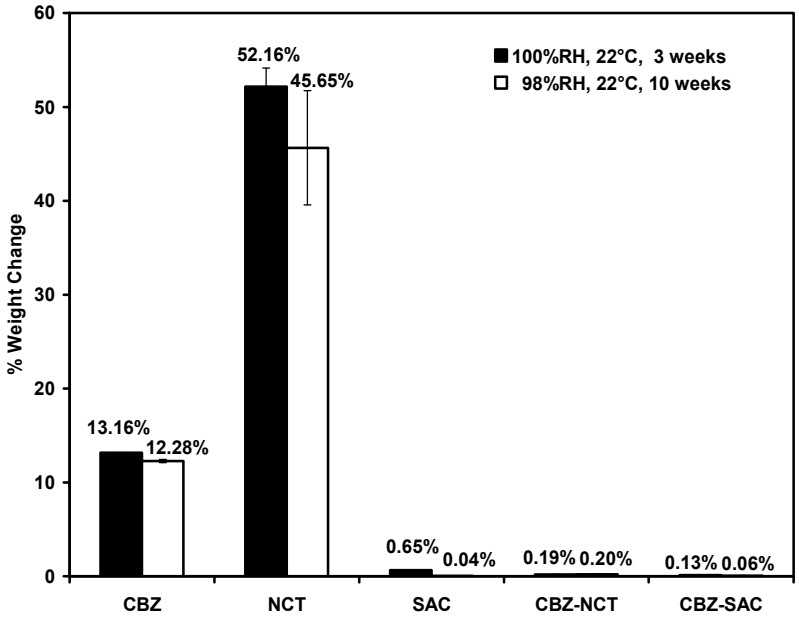

Figure 1.9: Moisture uptake of CBZ:NCT, CBZ:SAC, and single components. Measured by thermal gravimetric analysis.[61]

Research Objective and Hypotheses: Key Questions

- Can lower solubility cocrystals be synthesized by selecting coformers of lower solubility relative to a reference compound? How does the solid and solution phase mechanisms influence solubility behavior?
- Can cocrystals provide solubility advantage over salts, and what are the key differences in the solubility-pH behavior of cocrystals and salts?
- How can additives influence cocrystal synthesis?
- Can cocrystal form in the solid state upon storage without cogrinding the reactants? Is there a thermodynamic driving force for spontaneous cocrystallization in the solid state?
- What are the factors that influence the kinetics of cocrystal formation in the solid state during storage (temperature, relative humidity, disorder, material properties)?

Statement of Dissertation Research

The purpose of this dissertation is to investigate the solution phase chemistry and solids state properties of pharmaceutical cocrystals and analyze the thermodynamic basis for their solubility and stability. This research is focused on determining cocrystal properties in relation to the properties of their components, their environment such as solvent, pH, common ions, fusion properties, temperature and relative humidity. The goal is to gain insights with respect to cocrystal solid state and solution chemistry in order to improve the systematic approach for cocrystal design, synthesis, screening, selection and applications in drug delivery. Phase behavior and solution equilibria are considered to provide general and accurate descriptions of the stoichiometric solubility of cocrystals that are either thermodynamically stable or unstable in pure solvent. Cocrystal solubility

can be influenced by solid-state chemistry and solution chemistry including solute-solvent interactions as well as ionization properties of its components and pH. The influence of additives is also investigated, specifically the role of SLS is studied due to its ubiquitous presence in pharmaceutical formulations and testing media. The chapters presented describe important aspects of both solution and solid-state chemistry of cocrystals.

Chapter 2 introduces four new cocrystals of a highly soluble compound gabapentin-lactam (GBPL). Crystallographic data is presented to resolve the crystal structure of these new cocrystals along with an in-depth analysis of solid state properties and solution phase chemistry to understand the aqueous solubility behavior. The thermodynamic basis for solubility and stability of GBPL cocrystals is discussed with the emphasis on how coformer solubility could influence cocrystal solubility. All GBPL cocrystals are less soluble than both the cocrystal components and their thermodynamic stability is highly dependent on pH. GBPL is non ionizable however, due to the ionic nature of coformers, cocrystal solubility is pH dependent. All GBPL cocrystals exhibit pH_{max} where the cocrystal is in equilibrium with its component. Analogous to salts, detailed analysis of pH_{max} is presented with the generalized rules that will allow the estimation of pH_{max} for cocrystals as well as the parameters that will influence the magnitude of pH_{max}. The experimentally observed solubility of cocrystals is discussed and the differences in the experimental solubility from the calculated ideal solubility are explained on the basis of activity of the solute in solvent. Our analyses show that there is a huge discrepancy between the observed and calculated solubilities of cocrystals resulting from the hydrophobicity of the solid leading to high values of activity

coefficient. Melting point alone is therefore not the only criteria that govern the cocrystal solubility as two independent factors regulate cocrystal solubility.

Chapter 3 presents the solubility pH dependence of several crystalline forms of a poorly soluble drug lamotrigine (LAM). Thermodynamic solubility of LAM salts and cocrystals is estimated. For higher solubility cocrystals of LAM, solubility is estimated by measuring the eutectic concentrations of cocrystal components from which entire solubility pH profile is generated. All cocrystals and salts exhibit a pH_{max} which dictates the thermodynamic stability of the solid phase in the solvent. Key differences between the pH_{max} of cocrystals and salts are presented and generalized for applications to other such systems. We show how thermodynamic methods to determine solubility are more accurate than the reported kinetic methods, which can result in inaccurate values due to phase transformations. The effect of common ion is analyzed to determine the relative stability of LAM crystalline forms in the presence of Cl^- and its influence on phase transformations. This is critical since Cl^- is prevalent in physiological systems and physiologically relevant testing media. Also in this chapter we examine the role of SLS on the synthesis, solubility and thermodynamic stability of lamotrigine nicotinamide cocrystal hydrate (LAM-NCT·H_2O). The role of micellar solubilization on cocrystal solubility and stability is investigated. Mathematical equations are developed based on cocrystal dissociation, component ionization, and micellar solubilization equilibria that describe cocrystal solubility as a function of thermodynamic parameters (K_{sp}, K_a, and micellar solubilization constant K_s).

Chapter 4 investigates the mechanisms of cocrystal formation in the solid state. This chapter describes how cocrystals can form with no external energy applied such as

by applying mechanical stress as in milling, heating of the reactants, moisture induced etc, but simply from physical mixture of cocrystal components. The goal is to examine the factors that influence the kinetics of transformation of cocrysals from solid reactants. These factors include the effect of storage temperature and relative humidity, effect of milled vs. unmilled reactants and effect of annealing. It is observed that high temperature and relative humidity as well as milling of reactants prior to mixing enhance the rate of cocrystal formation.

Chapter 5 examines the solid state thermodynamic properties that impact the solid to solid conversion of reactants to cocrystals. Models have been shown previously for racemic compounds, however unlike racemic compounds, the components of cocrystals differ in their molecular structure, temperature and heat of fusion. Thermodynamic cycles were generated to develop mathematical equations for calculating free energy of cocrystal formation from its reactants. This type of investigation is developed for the first time for cocrystals. Reactant properties such as temperature and heat of fusion, heat capacity, entropy and enthalpy of mixing were used to derive these models to predict the cocrystal formation from reactants. Rigorous mathematical treatment is developed which is presented in a simplified manner for application along with general guidelines. Thermal behavior of carbamazepine-nicotinamide (CBZ-NCT) cocrystal has been studied by calorimetry. Thermal events are characterized, which are useful in understanding several features of cocrystals such as, interaction with reactants, eutectic melt behavior, purity as well as nature of the impurity. This data is used to generate a binary phase diagram which is very useful in understanding the general behavior of cocrystals as a function of temperature and composition.

Finally, the conclusions and future work of this dissertation research are provided in Chapter 6. Future challenges include, how surfactants can influence cocrystal formation and the mechanism of reaction involved at the molecular level resulting in cocrystal formation in the presence of surfactants. How the non-ideality influences the free energy of cocrystal formation in physical mixtures of its reactants? The role of reactants can influence mixing enthalpies thereby influencing the magnitude as well as the sign of free energy of formation of cocrystals in the solid state from its reactants. This will lead to generalized applications of these concepts and greater predictive power from simple thermodynamic calculations. Each chapter begins with its abstract and ends with a conclusion.

Several of these chapters have been published. Tailoring aqueous solubility of GBPL *via* cocrystallization and the effect of coformer ionization, pH_{max} and solute-solvent interactions described in Chapters 2 is published in *CrystEngComm* Vol. 14, pp. 4801-4811, 2012.

Factors that influence spontaneous formation of pharmaceutical cocrystals by simply mixing solid reactants described in chapter 4 is published in *CrystEngComm*, Vol .11, pp. 493-500, 2009.

Chapter 3 discussing the cocrystal solubility advantages over salts and the importance of thermodynamic solubility measurements to assess true solubility as well as the role of surfactants in cocrystal synthesis is in draft for submission at the time of writing this thesis.

References

1. Etter, M. C. Hydrogen Bonds as Design Elements in Organic Chemistry. Journal of Physical Chemistry 95, 4601-4610 (1991).

2. Fleischman, S. G. et al. Crystal engineering of the composition of pharmaceutical phases: Multiple-component crystalline solids involving carbamazepine. Crystal Growth & Design 3, 909-919 (2003).

3. Childs, S. L. & Hardcastle, K. I. Cocrystals of piroxicam with carboxylic acids. Crystal Growth & Design 7, 1291-1304 (2007).

4. Childs, S. L. & Hardcastle, K. I. Cocrystals of piroxicam with carboxylic acids. Crystal Growth & Design 7, 1291-1304 (2007).

5. Childs, S. L. et al. Screening strategies based on solubility and solution composition generate pharmaceutically acceptable cocrystals of carbamazepine. Crystal Engineering Communications 10, 856-864 (2008).

6. Caira, M. R. Sulfa Drugs as Model Cocrystal Formers. Molecular Pharmaceutics 4, 310-316 (2007).

7. Karki, S., Friscic, T., Jones, W. & Motherwell, W. D. S. Screening for pharmaceutical cocrystal hydrates via neat and liquid-assisted grinding. Molecular Pharmaceutics 4, 347-354 (2007).

8. Remenar, J. F. et al. Celecoxib:Nicotinamide Dissociation: Using excipients to capture the cocrystal's potential. Molecular Pharmaceutics 4, 386-400 (2007).

9. Lipinski, C. Poor aqueous solubility: an industry wide problem in drug discovery. American Pharmaceutical Reviews 5, 82-85 (2002).

10. Serajuddin, A. T. M. Salt formation to improve drug solubility. Advanced Drug Delivery Reviews 59, 603-616 (2007).

11. Good, D. J. & Rodriguez-Hornedo, N. True solubility advantage of cocrystals: measurement, relationships, and pharmaceutical implications. Crystal Growth & Design (2009).

12. Bethune, S. J., Huang, N., Jayasankar, A. & Rodríguez-Hornedo, N. Understanding and Predicting the Effect of Cocrystal Components and pH on Cocrystal Solubility. Crystal Growth & Design 9, 3976-3988 (2009).

13. Stahl, P. H. & Wermuth, C. G. Handbook of Pharmaceutical Salts: Properties, Selection and Use (Wiley-VCH, Zürich, 2002).

14. Nelson, E., Wagner, J. G., Knoechel, E. L. & Hamlin, W. E. Influence of Absorption Rate of Tolbutamide on Rate of Decline of Blood Sugar Levels in Normal Humans. Journal of Pharmaceutical Sciences 51, 509-& (1962).

15. Paluch, K. J. et al. Solid-State Characterization of Novel Active Pharmaceutical Ingredients: Cocrytsal of Salbutamol Hemiadipate Salt with Adipic Acid (2:1:1) and Salbutamol Hemisuccinate Salt. J. Pharm. Sci 100, 3268-3283 (2011).

16. Fritz, B., Lach, J. L. & Bighley, L. D. Solubility Analysis of Multicomponent Systems Capable of Interacting in Solution. Journal of Pharmaceutical Sciences 60, 1617-1619 (1971).

17. Miyako, Y., Tai, H., Ikeda, K., Kume, R. & Pinal, R. Solubility screening on a series of structurally related compounds: Cosolvent-induced changes on the activity coefficient of hydrophobic solutes. Drug Development and Industrial Pharmacy 34, 499-505 (2008).

18. Chency, M. L. et al. Effects of Crystal Form on Solubility and Pharmacokinetics: A Crystal Engineering Case Study of Lamotrigine. Crystal Growth & Design 10, 394-405.

19. Etter, M. C. hydrogen Bonds as Design Elements in Organic Chemistry. J. Phys. Chem. 95, 4601-4610 (1991).

20. Etter, M. C. & Reutzel, S. M. Hydrogen Bond Directed Cocrystallization and Molecular Recognition Properties of Acyclic Imides. Journal of the American Chemical Society 113, 2586-2598 (1991).

21. Rodríguez-Hornedo, N. Cocrystals: Design, Properties and Formation Mechanisms; In: Encyclopedia of Pharmaceutical Technology; 3rd Ed. DOI: 10.1081/E-EPT-120041485, 615-635 (2007).

22. Aakeroy, C. B. et al. Ten years of co-crystal synthesis; the good, the bad, and the ugly. Crystal Engineering Communications 10, 1816-1821 (2008).

23. McMahon, J. A. et al. Crystal engineering of the composition of pharmaceutical phases. 3. Primary amide supramolecular heterosynthons and their role in the design of pharmaceutical co-crystals. Zeitschrift Fur Kristallographie 220, 340-350 (2005).

24. Fábián, L. Cambridge Structural Database Analysis of Molecular Complementarity in Cocrystals. Crystal Growth & Design 9, 1436-1443 (2009).

25. Weyna, D. R., Shattock, T., Vishweshwar, P. & Zaworotko, M. J. Synthesis and Structural Characterization of Cocrystals and Pharmaceutical Cocrystals:

Mechanochemistry vs Slow Evaporation A from Solution. Crystal Growth & Design 9, 1106-1123 (2009).

26. Braga, D. et al. Making crystals from crystals: A solid-state route to the engineering of crystalline materials, polymorphs, solvates and co-crystals; considerations on the future of crystal engineering. Engineering of Crystalline Materials Properties, 131-156 (2008).

27. Friscic, T. & Jones, W. Recent Advances in Understanding the Mechanism of Cocrystal Formation via Grinding. Crystal Growth & Design 9, 1621-1637 (2009).

28. Friscic, T., Childs, S. L., Rizvi, S. A. A. & Jones, W. The role of solvent in mechanochemical and sonochemical cocrystal formation: a solubility-based approach for predicting cocrystallisation outcome. Crystengcomm 11, 418-426 (2009).

29. Braga, D. et al. Solvent effect in a "solvent free" reaction. Crystengcomm 9, 879-881 (2007).

30. Trask, A. V. & Jones, W. Crystal engineering of organic cocrystals by the solid-state grinding approach. Organic Solid State Reactions 254, 41-70 (2005).

31. Trask, A., V., Motherwell, W. D. S. & Jones, W. Solvent-drop grinding: green polymorph control of cocrystallisation. Chemical Communications, 890-891 (2004).

32. Rodríguez-Hornedo, N., Nehm, S. J., Seefeldt, K. F., Pagan-Torres, Y. & Falkiewicz, C. J. Reaction Crystallization of Pharmaceutical Molecular Complexes. Molecular Pharmaceutics 3, 362-367 (2006).

33. Nehm, S., Rodriguez-Spong, B. & Rodriguez-Hornedo, N. Phase Solubility Diagrams of Cocrystals Are Explained by Solubility Product and Solution Complexation. Crystal Growth & Design 6, 592-600 (2006).

34. Rodríguez-Hornedo, N., Nehm, S. J. & Jayasankar, A. Cocrystals: Design, Properties and Formation Mechanisms. Encyclopedia of Pharmaceutical Technology: Third Edition, 615 - 635 (2006).

35. Nehm, S., Seefeldt, K. F. & Rodríguez-Hornedo, N. Phase Diagrams to Predict Solubility and Crystallization of Cocrystals. The AAPS Journal 7, Abstract W4235 (2005).

36. Chadwick, K., Davey, R. & Cross, W. How does grinding produce co-crystals? Insights from the case of bezophenone and diphenylamine. CrystEngComm 9, 732-734 (2007).

37. Lu, E., Rodriguez-Hornedo, N. & Suryanarayanan, R. A rapid thermal method for cocrystal screening. Crystal Engineering Communications 10, 665-668 (2008).

38. Oguchi, T. et al. Specific complexation of ursodeoxycholic acid with guest compounds induced by co-grinding. Physical Chemistry Chemical Physics 2, 2815-2820 (2000).

39. Mattheus, C. C. et al. A 2:1 cocrystal of 6, 13-dihydropentacene and pentacene. Acta Crystallographica Section E 58, 1229-1231 (2002).

40. Nakai, Y., Yammamoto, K., Oguchi, T., Yonemochi, E. & Hanawa, T. New Methods for Preparing Cyclodextrin Inclusion Compounds. III. Preparation of Heptakis-(2,6-di-O-methyl)-β-cyclodextrin-Benzoic Acid Inclusion Compound by Sealed Heating Chem. Pharm. Bull. 38, 1345-1348 (1990).

41. Jayasankar, A., Good, D. & Rodríguez-Hornedo, N. Mechanisms by which moisture generates cocrystals. Molecular Pharmaceutics 4, 360-372 (2007).

42. Salameh, A. K. & Taylor, L. S. Physcial stability of crystal hydrates and their anhydrates in the presence of excipients. J. Pharm. Sci 95, 445-461 (2006).

43. Jayasankar, A., Good, D. J. & Rodriguez-Hornedo, N. Mechanisms by which moisture generates cocrystals. Molecular Pharmaceutics 4, 360-372 (2007).

44. Carstensen, J. T. An approach to the evaluation of hygroscopicity for pharmaceutical solids. International Journal of Pharmaceutics 5, 1-18 (1980).

45. Berry, D. J. et al. Applying Hot-Stage Microscopy to Co-Crystal Screening: A Study of Nicotinamide with Seven Active Pharmaceutical Ingredients. Crystal Growth and Design 8, 1697-1712 (2008).

46. Leksic, E., Pavlovic, G. & Mestrovic, E. Cocrysals of Lamotrigine Based on Coformers Involving Carbonyl Group Discovered by Hot-Stage Microscopy and DSC Screening. Crystal Growth & Design (2012).

47. Higuchi, T. & Connors, K. A. in Advances in Analytical Chemistry and Instrumentation (ed. Nurnberg, H. W.) 117-212 (Wiley-Interscience, New York, 1965).

48. Grant, D. J. W. & Higuchi, T. Solubility Behavior of Organic Compounds (John Wiley & Sons, Inc, New York, 1990).

49. Lachman, L., Ravin, L. J. & Higuchi, T. Inhibition of Hydrolysis of Esters in Solution by Formation of Complexes .2. Stabilization of Procaine with Caffeine. Journal of the American Pharmaceutical Association 45, 290-295 (1956).

50. Good, D. J. & Rodriguez-Hornedo, N. Solubility Advantage of Pharmaceutical Cocrystals. Crystal Growth & Design 9, 2252-2264 (2009).

51. Huang, N. & Rodriguez-Hornedo, N. Effect of Micelliar Solubilization on Cocrystal Solubility and Stability. Crystal Growth & Design 10, 2050-2053 (2010).

52. Moroi, Y. Micelles: Theoretical and Applied Aspects (Plenum Press, 1992).

53. Christian, S. D. & Scamehorn, J. F. Solubilization in Surfactant Aggregates (eds. Schick, M. J. & Fowkes, F. M.) (Marcel Dekker, Inc., 1995).

54. Rowe, R. C., Sheskey, P. J. & Quinn, M. E. Handbook of pharmaceutical excipients (APhA, (PhP) Pharmaceutical Press, 2009).

55. Remenar, J. F. et al. Crystal Engineering of Novel Cocrystals of a Triazole Drug with 1,4-Dicarboxylic Acids. Journal of the American Chemical Society 125, 8456-8457 (2003).

56. McNamara, D. P. et al. Use of a glutaric acid cocrystal to improve oral bioavailability of a low solubility API. Pharmaceutical Research 23, 1888-1897 (2006).

57. Childs, S. L. et al. Crystal Engineering Approach to Forming Cocrystals of Amine Hydrochlorides with Organic Acids. Molecular Complexes of Fluoxetine Hydrochloride with Benzoic, Succinic, and Fumaric Acids. Journal of the American Chemical Society 126, 13335-13342 (2004).

58. Bak, A. et al. The Co-Crystal Approach to Improve the Exposure of a Water-Insoluble Compound: AMG 517 Sorbic Acid Co-Crystal Characterization and Pharmacokinetics. Journal of Pharmaceutical Sciences (2007).

59. Variankaval, N. et al. Preparation and solid-state characterization of nonstoichiometric cocrystals off a phosphodiesterase-IV inhibitor annul L-tartaric acid. Crystal Growth & Design 6, 690-700 (2006).

60. Cheney, M. L. et al. Effects of Crystal Form on Solubility and Pharmacokinetics: A Crystal Engineering Case Study of Lamotrigine. Crystal Growth & Design 10, 394-405 (2009).

61. Rodriguez-Spong, B., Ph.D. Thesis, University of Michigan, 2005.

CHAPTER 2

TAILORING AQUEOUS SOLUBILITY OF A HIGHLY SOLUBLE COMPOUND *via* COCRYSTALLIZATION: *EFFECT OF COFORMER IONIZATION, pH_{MAX} AND SOLUTE-SOLVENT INTERACTIONS*

Abstract

Cocrystals of a nonionizable, water soluble compound (gabapentin-lactam (GBPL)) with less soluble coformers, are shown to be 2 to 17 times less soluble than GBPL. Cocrystals of GBPL with gentisic acid, 4-hydroxybenzoic acid, 4-aminobenzoic acid and fumaric acid are characterized by carboxylic acid---amide hydrogen bonds between coformer and GBPL, consistent with a previously reported structure of a benzoic acid cocrystal. The lattice and solvation contributions to cocrystal aqueous solubility were evaluated and solvation was found to be the main contribution to solubilization. Cocrystals exhibited pH-dependent solubility and pH_{max}, both of which are described by coformer pK_a and cocrystal K_{sp} values. These findings have important implications for the characterization and selection of cocrystals for desired drug delivery behavior.

Introduction

In the development of a dosage form, aqueous solubility is one of the principal attributes that must be considered in order to develop a safe, efficacious and consistent product. Some of the commonly used approaches for solubility modification are the use of amorphous materials, solid dispersions, prodrugs, molecular salts and cocrystals.[1-5] Cocrystals provide an alternative to salt formation for non-ionizable compounds and can impart pH dependent solubility behavior with the use of an ionizable coformer. Cocrystal aqueous solubility and its dependence on pH can be engineered by the choice of coformers and their ionization properties.[3, 6] From a solubility perspective, cocrystal research has mainly focused on enhancing drug solubility for achieving increased dissolution rate, thereby improving bioavailability. Depending on the desired pharmacokinetic effect, alternative solid forms such as salts, cocrystals and prodrugs can also be used to prolong the release of active compounds. Controlling release kinetics is of importance in the case of drugs exhibiting short half lives, large C_{max} values or toxicity due to high solubility. [2, 7-9]

Methods to alter the solubility are based on the free energy of solubilization, which involves crystal lattice interactions as well as interactions between solute and the solvent (solvation).[1, 10-12] Strategies that can modulate solute-solvent interactions to alter solubility include ionization, complexation, micellar solubilization, prodrugs and cosolvents. These two factors contribute to the associated overall free energy of solution of a compound, which is given by,

$$\Delta G_{solution} = \Delta G_{lattice} + \Delta G_{solvation}$$

where ΔG represents the Gibbs energies associated with the solubilization process, lattice and solvation. Several approaches can be utilized to alter the lattice energy of the solute, for example, formation of amorphous phases, polymorphs, solvates, salts and cocrystals. Solvation plays a critical role on solubility, especially for hydrophobic drugs.[10, 13] Cocrystals have the ability to modulate both solid and solution phase chemistry and consequently influence the associated lattice and solvation energies.

Enhancing the aqueous solubility of water insoluble drugs is well documented, [4, 14-19] the ability to decrease aqueous solubility is less recognized.[3, 8, 20] The purpose of the work presented here was to determine (i) the influence of low solubility coformers on cocrystals of a high solubility compound, (ii) the influence of crystal lattice energy on cocrystal aqueous solubility, (iii) the relationship between coformer ionization properties and cocrystal solubility-pH dependence, and (iv) the dependence of cocrystal thermodynamic stability on pH.

Cocrystal thermodynamic solubility has been correlated to the coformer solubility when solvation is the main barrier to solubilization. Cocrystals composed of coformers with a solubility of at least 10-fold higher than the drug have been observed to enhance cocrystal solubility.[4, 20] Cocrystallizing a highly soluble drug with a coformer exhibiting lower solubility will likely produce a cocrystal with a lower solubility than its drug component. For example, cocrystallizing the highly soluble gabapentin (GPB) with the less soluble 3-hydroxybenzoic acid (3HBA) results in a cocrystal which is 0.2 times the solubility of GBP (5 times less soluble).[3] 3HBA has an aqueous solubility of 0.06 (M) at pH 2.8 (pK_a – 4.06 and 9.92), which is 0.07 times the solubility of GBP (0.88 M) at pH 7.3 (pK_a – 3.68 and 10.70) at room temperature.[3]

The cyclization of the charged aminocarboxylic acid moiety of GBP results in a five membered uncharged cyclic lactam in gabapentin-lactam (GBPL) with secondary amine and carbonyl groups (Scheme 2.1). Gabapentin-Lactam (GBPL) is a non-ionizable compound with high aqueous solubility and potential pharmacologic activity.[21, 22]

Scheme 2.1: Chemical structures of GBP and GBPL

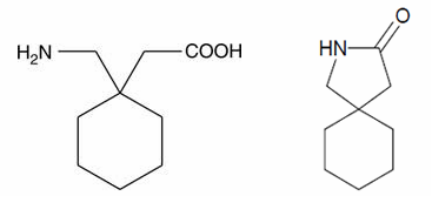

Due to its high aqueous solubility and non-ionizable nature in physiological pH range, GBPL was chosen as the model compound for investigation. Carboxylic acids were selected as coformers based on their low aqueous solubility relative to GBPL, ionizable characteristics, and their ability to form strong acid ··· amide heterosynthons. The reported aqueous solubilities of the selected coformers range from 0.14 to 0.75 relative to GBPL solubility and have pK_a values that range from 2.4 to 4.8.[23-30]

A search of the Cambridge Structural Database (CSD) showed that molecules containing carboxamide moieties form multicomponent crystal forms with carboxylic acids via $R_2^2(8)$ synthon. Zaworotko and coworkers published a CSD survey of compounds containing primary amides and carboxylic acid groups that suggested that 47% of the structures formed acid ··· amide heterosynthons while 44% and 6% structures formed amide ··· amide and acid ··· acid homosythons respectively.[31] The strength of acid ··· amide heterosynthon was exploited in the discovery of GBPL cocrystals with gentisic acid (GA), 4-hydroxybenzoic acid (4HBA), 4-aminobenzoic acid (4ABA) and fumaric acid (FA). The solubility behavior of a previously discovered cocrystal of GBPL with

benzoic acid (BA)[32] is also investigated in this manuscript. The molecular structures of compounds used are shown below.

Scheme 2.2: Compounds Used in Cocrystallization

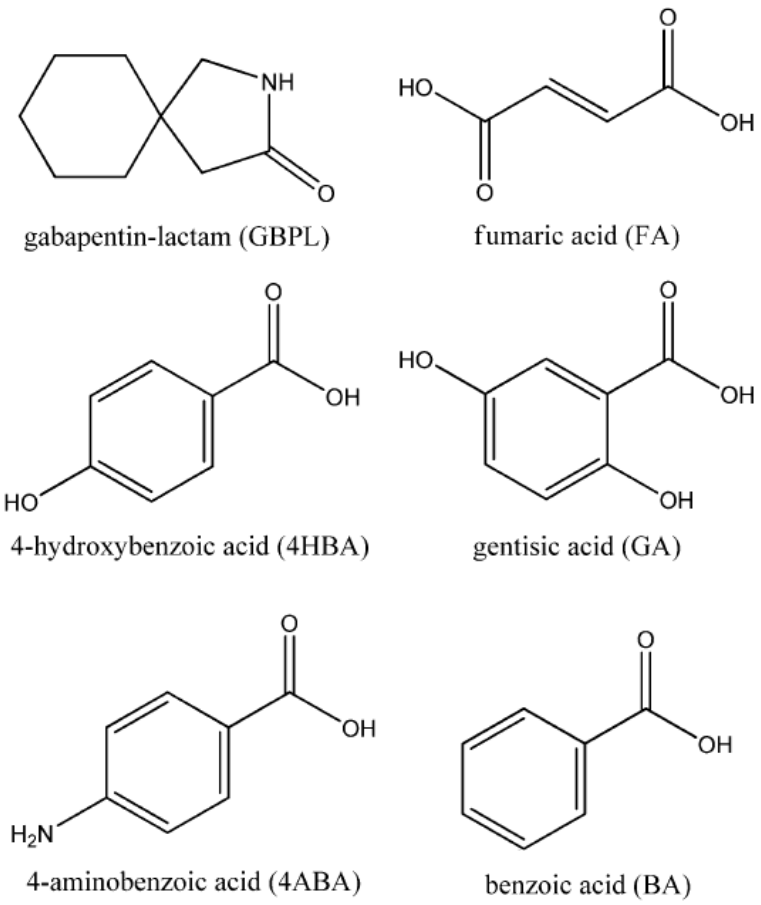

Materials and Methods

Materials

GBPL (97+% purity) was purchased from Waterstone-Technology, LLC., Carmel IN. Gentisic acid (GA), benzoic acid (BA), 4-hydroxybenzoic acid (4-HBA), 4-aminobenzoic acid (4ABA) and fumaric acid (FA) were obtained from Sigma-Aldrich and were of 99+ % purity. All materials were used as received. X-Ray powder diffraction (XRPD) and differential scanning calorimetry (DSC) were used to characterize the materials prior to use.

Cocrystal Synthesis

Cocrystals were synthesized from near saturated aqueous solutions of the higher solubility component, which is GBPL in these studies, according to the reaction crystallization method (RCM).[20, 33] An equimolar mass of coformer was added to the solution of GBPL in water at room temperature and stirred for 12 hours. The solid form recovered was analyzed by XRPD and DSC, and purity was confirmed by HPLC and DSC prior to single crystal determination.

X-ray Powder Diffraction (XRPD)

XRPD patterns of solid phases were recorded with a Rigaku MiniFlex X-ray diffractometer (Danvers, MA) using Cu Kα radiation (λ = 1.5418 Å), a tube voltage of 30 kV, and a tube current of 15 mA. The intensities were measured at 2θ values from 2° to 40° with a continuous scan rate of 2.5°/min. The X-ray powder diffraction patterns of new cocrystals of GBPL are provided in the supporting information.

Single-crystal X-ray Diffraction (SCXRD)

SCXRD data of new phases of GBPL-4HBA, GBPL-4ABA and GBPL-FA were determined at 293 and 150K on a Bruker AXS-KAPPA APEX II diffractometer with graphite-monochromated radiation (Mo Kα, λ=0.71069 Å). Data for GBPL-GA was collected on a Bruker SMART APEX CCD-based X-ray diffractometer (Mo Kα, λ=0.71069 Å) at 85K. All the data were corrected for Lorentzian, polarization and absorption effects using SAINT and SADABS programs. SIR97 [34] was used for structure solution and SHELXL-97 [35] was used for full matrix least-squares refinement on F^2. All non-hydrogen atoms were refined anisotropically, except in $GBPL_2$-FA where a disordered model on the carboxamide moiety of GBPL enforced an isotropic refinement of the C and N atoms. A disorder model was also applied to the cyclohexane ring in GBPL-4HBA. Both carboxylic groups of 4HBA and FA show some disorder with the H atom sharing two positions with split occupancy of 65:35%. H_{NH} atoms were located from a difference Fourier map and their positional coordinates and isotropic parameters were refined, except in the disordered $GBPL_2$-FA carboxamide moiety. H_{CH} atoms were added in calculated positions and refined isotropically riding on their C atoms. MERCURY 2.3 was used for molecular representations and packing diagrams. Single crystal data were used to simulate theoretical XRPD patterns that were compared with experimental data to ascertain the purity of the samples.

Thermal Analysis

Crystalline samples of 2-4 mg were analyzed by DSC using a TA instrument (Newark, DE) 2910 MDSC system equipped with a refrigerated cooling unit. DSC experiments were performed by heating the samples at a rate of 10 K/min under a dry nitrogen

atmosphere. High purity indium standard was used for temperature and enthalpy calibration of the instrument. Standard aluminum sample pans were used for all measurements. Cocrystal samples for DSC analysis comprised several large crystals grown by slow partial evaporation of solutions containing the reactants. These crystals were isolated from solution, washed, and characterized by X-Ray diffraction before DSC analysis. The mean result of a minimum of three samples is reported for each substance. Purity analysis of the cocrystal powder was analyzed and confirmed by the presence of a single endothermic event.

Solubility Measurement

All solubility measurements were carried out in aqueous medium at 25 ± 0.1ºC. pH was adjusted by adding 0.1N HCl or 0.1N NaOH. Solution concentrations of both cocrystal components were measured by HPLC. Solutions were considered to have reached equilibrium when less than 5% change in concentration was detected in either component of the cocrystal when measured subsequently over a period of 48-72 hours. Solubility product (K_{sp}) was calculated from measured concentration of cocrystal components at different pH values. Solid phases were characterized by XRPD and DSC at the end of the solubility experiments.

Nuclear Magnetic Resonance (NMR)

Chemical stability of GBPL in coformer aqueous solutions was confirmed by solution NMR. Solution NMR was also used to confirm the absence of interaction between GBPL and coformers in the solution phase. Proton decoupled ^{13}C NMR spectra were recorded

on a Bruker DRX500 spectrometer (11.75T) at a probe temperature of 298K, tuned to 125.7 MHz, using 5mm high resolution NMR tubes.

High-Performance Liquid Chromatography (HPLC)

Purity and stoichiometry of the GBPL cocrystals was analyzed by HPLC before carrying out pH dependent solubility studies. Solution concentrations of drug and coformer were analyzed by Waters HPLC (Milford, MA) equipped with a UV/vis spectrometer detector. A C18 Atlantis column (5 μm, 4.6 × 250 mm; Waters, Milford, MA) at ambient temperature was used to separate the drug and the coformer. An isocratic method with a mobile phase composed of 45% water, 55% methanol and 0.1% trifluoroacetic acid was used with a flow rate of 1 mL/min. Sample injection volume was 20 μL. Absorbance of the drug and coformer analytes was monitored between 210-300nm. Empower software from Waters Inc., was used to analyze the data. All concentrations, unless otherwise indicated are reported in molality (moles solute/kilogram solvent).

Results and Discussion

Four cocrystals of GBPL with GA, 4HBA, 4ABA and FA were discovered by reaction crystallization method (RCM). The hydrogen bonding patterns of these cocrystals as well as the previously discovered GBPL cocrystal with BA are presented in Figure 2.1. Crystallographic and structural data of GBPL cocrystals are listed in Table 2.1.

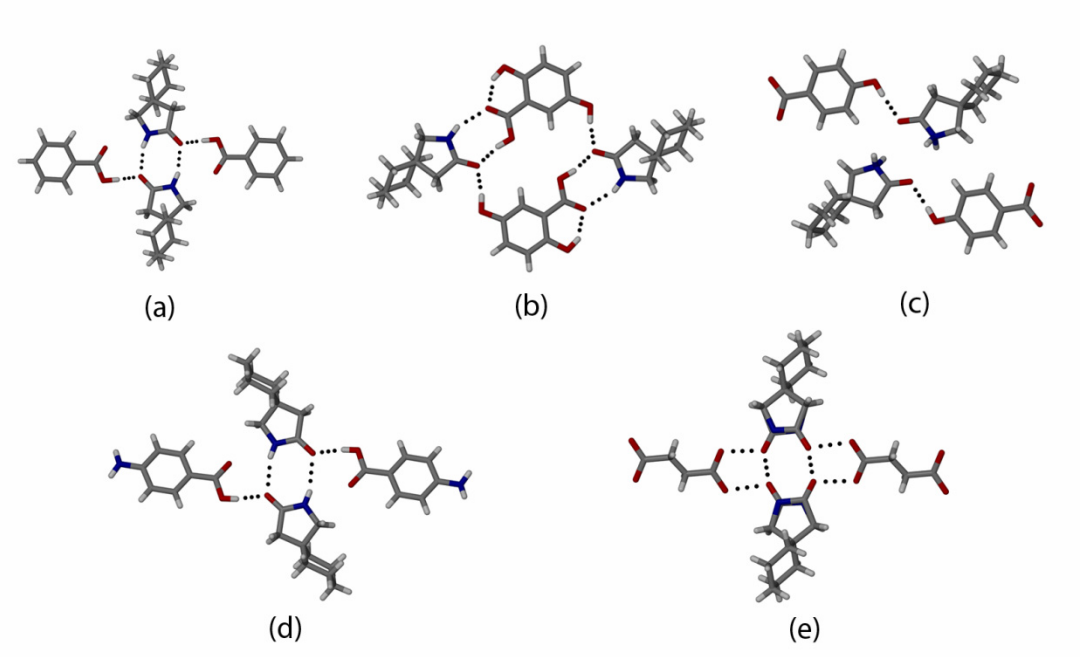

Figure 2.1: Hydrogen-bond patterns of GBPL cocrystals; (a) GBPL-BA (b) GBPL-GA (c) GBPL-4HBA (d) GBPL-4ABA and (e) $GBPL_2$-FA.

Table 2.1: Crystallographic data and structure refinement parameters of GBPL cocrystals

	GBPL-GA	GBPL-4HBA	GBPL-4ABA	$GBPL_2$- FA
Chemical formula	C16 H21 N O5	C16 H21 N O4	C16 H22 N2 O3	C11 H18 N O3
M_r	307.34	291.34	290.36	212.26
Temperature/K	85	150	150	150
Wavelength / (Å)	0.71073	0.71069	0.71069	0.71069
Morpholgy, colour	Needle, colorless	Thin plate, colorless	Parallelepiped, colorless	Needle, colorless
Crystal size/mm	0.40 x 0.19 x 0.04	0.08 x 0.04 x 0.02	0.22 x 0.05 x 0.04	0.20 x 0.03 x 0.02
Crystal system	Monoclinic	Triclinic	Monoclinic	Monoclinic
Space group	P21/n	P1	P21/n	P21/c
a/Å	5.9663(6)	6.3900(4)	5.9280(6)	10.7040(3)
b/Å	27.045(3)	10.0780(7)	18.465(2)	6.0110(4)
c/Å	9.470(1)	12.2260(8)	14.208(1)	17.802(6)
α/°	90	81.714(3)	90	90
β/°	107.008(2)	82.039(3)	99.259(5)	101.372(3)
γ/°	90	76.597(3)	90	90
V/Å^3	1461.3(3)	753.37(9)	1535.0(3)	1122.9(4)
Z	4	2	4	4
ρ/mg.m^{-3}	1.397	1.284	1.256	1.256
μ/mm^{-1}	0.104	0.092	0.087	0.091
Reflections collected/unique	32048/3647	8801 / 3034	10262/2922	7576 / 2097
R_{int}	0.0501	0.0277	0.0392	0.0466
Goodness of Fit	1.099	1.055	1.131	1.11
Final R indices [I>2σ(I)]	R_1 = 0.0445 wR_2 = 0.1067	R_1 = 0.0482 wR_2 = 0.1300	R_1 = 0.0446 wR_2 = 0.1539	R_1 = 0.0600 wR_2 = 0.2063

GBPL-GA cocrystal

GBPL-GA crystallizes in the $P2_1/n$ monoclinic space group, with one molecule of each component per asymmetric unit. Although the usual S(6) intramolecular O-H···O hydrogen bond between the hydroxyl and carbonyl moieties is maintained within gentisic acid molecules, the homomeric $R_2^2(8)$ synthon previously mentioned for gabapentin-lactam is disrupted and replaced by a heteromeric $R_2^2(8)$ synthon responsible for the formation of dimers enclosing GBPL and the coformer. This new synthon is based on N-$H_{GBPL}\cdots O_{GA}$ and O-$H_{GA}\cdots O_{GBPL}$ interactions. Two pairs of dimers are connected via O-$H_{GA}\cdots O_{GBPL}$ interactions between the hydroxyl donor moiety of the coformer and the carboxamide moiety of GBPL, giving rise to tetramers. These tetramers are different

from the ones based in the homosynthon as there are no external functional groups in the tetramer. The crystal packing of this compound shows alternated chains of API and coformer.

GBPL-4HBA cocrystal

GBPL-4HBA crystallizes in the $P\bar{1}$ triclinic space group, with one molecule of each compound per asymmetric unit. The C-O distances in the carboxylic moiety of the coformer are similar and the electron density map indicates disorder with the H atom sharing two positions with refined split occupancy of 65:35%. The carboxamide moiety interacts with hydroxyl of 4HBA via O-$H_{4HBA}\cdots O_{GBPL}$ to form a tetrameric motif. This pattern is repeated along the *b* axis via the homomeric $R_2^2(8)$ homosynthon, O-$H_{4HBA}\cdots O_{4HBA}$, between two coformer molecules, giving rise to chains of alternated GBPL and coformer dimers making a 35º angle. No supramolecular interactions are seen between consecutive chains.

GBPL-4ABA cocrystal

4ABA is an amphoteric coformer. GBPL-4ABA crystallizes in the $P2_1/n$ monoclinic space group, with one molecule of each component per asymmetric unit. GBPL crystal packing is based on N-H···O interactions inducing the formation of dimers through the homomeric $R_2^2(8)$ synthons between the carboxamide moieties. This motif is also the basis for GBPL-4ABA supramolecular arrangement. In this new cocrystalline form the carboxamide moiety interacts with the carboxylic moiety of the acid coformer via O-$H_{4ABA}\cdots O_{GBPL}$ bonds to form the tetrameric motif, exploiting the double acceptor ability of the carbonyl oxygen, reinforced by N-$H_{GBPL}\cdots O_{4ABA}$ interaction. The N-

$H_{4ABA}\cdots O_{4ABA}$ and N-$H_{4ABA}\cdots O_{GBPL}$ interactions are responsible for the linkage of these tetramers to other similar patterns along *a* and *b* axes. The extended supramolecular packing of this cocrystal is characterized by alternated zig-zag chains of coformer and GBPL interacting through N-$H_{GBPL}\cdots O_{4ABA}$, O-$H_{4ABA}\cdots O_{GBPL}$ and N-$H_{4ABA}\cdots O_{GBPL.}$

$GBPL_2$-FA cocrystal

FA is a diprotic acidic coformer. $GBPL_2$-FA crystallizes in the monoclinic $P2_1/c$ space group. It's asymmetric unit consists of one GBPL molecule and the fumaric acid resides on an inversion centre. The typical $R_2^2(8)$ homosynthon forming dimers of GBPL is observed. In this case, the amide moiety of GBPL works as a double donor, further interacting with the coformer via N-$H_{GBPL}\cdots O_{FA}$ forming tetramers, reinforced by O-$H_{FA}\cdots O_{GBPL}$. Tetramers are linked due to the special position of FA. GBPL dimers are intercalated by coformer, forming a chain.

The previously reported GBPL-BA cocrystal,[32] presents both resemblances and dissimilarities with the ones discussed herein. In the GBPL-BA cocrystal the GBPL $R_2^2(8)$ homosynthon is also present, forming dimers of GBPL. The tetramers are then formed by O-$H_{BA}\cdots O_{GBPL}$ interactions and similarly to what is seen in the GBPL-GA cocrystal, the tetrameric motifs are not hydrogen-bonded between them. Tetramers are extended to form alternated zig-zag chains of GBPL and BA. The cocrystal of GBP with 3HBA also exhibits a tetramer such that both carboxylic and phenolic OH donors form O-H$\cdots O^-$ interactions with GBP. However, unlike the GBPL-GA tetrameric motifs which are not hydrogen bonded, the GBP-3HBA tetrameric motifs are connected by charge assisted N^+- H$\cdots O^-$ hydrogen bonds forming a layered structure.[3]

Influence of Lattice and Solvation Energies on GBPL Cocrystal Solubility

The solubilization of a cocrystal involves two separate processes, (i) release of solute molecules from the crystal lattice and (ii) solvation of the released solute molecules. Each of these factors contributes to the free energy of solubilization and therefore to the observed solubility value. The lattice energy contribution is calculated from the ideal solubility given by

$$\log \chi_{\text{ideal}} = -\frac{\Delta H_f}{2.303R}\left(\frac{T_f - T}{T_f T}\right) \qquad (2.1)$$

where χ_{ideal} is the ideal mole fraction solubility of a solute at a temperature (T), T_f is the fusion temperature, and ΔH_f is enthalpy of fusion. This equation assumes that the heat capacity change upon melting is negligible.

Table 2.2 summarizes the ideal solubility values and measured aqueous solubilities of cocrystals and single components. Ideal solubility values were calculated according to equation (2.1) from measured fusion parameters. Table 2.2 shows that the melting points (MP) of GBPL cocrystals are in between that of its components, with the exception of GBPL-BA cocrystal, which has a MP lower than its components. The ideal solubilities range from 0.36 to 1.74 times that of GBPL ideal solubility, while the experimental solubilities range from 0.06 to 0.52 times GBPL solubility. This indicates that while cocrystals can increase solubility via changes in lattice energies, ultimately the lower coformer solubility relative to the drug results in observed lower cocrystal solubility.

Table 2.2: Ideal and experimental solubilities of cocrystals and components

Crystalline Phase	T_f (C°)	ΔH_f^* (kJ/mol)	Ideal Solubility [a] (χ_{ideal})	Experimental Solubility [b] (χ_{aq})	S_0 (m) and (pK_a)	$\frac{S_{0,coformer}}{S_{GBPL}}$	$\frac{S_{CC}}{S_{GBPL}}$
GBPL	92.0	19.0	2.44×10^{-1}	3.23×10^{-3}	1.80×10^{-1} (-0.84, 12.7)	-	-
BA	122.8	18.6	1.56×10^{-1}	4.68×10^{-4}	2.60×10^{-2} (4.2)	0.14	-
4ABA	188.9	27.2	2.02×10^{-2}	5.85×10^{-4}	3.25×10^{-2} (2.4, 4.8)	0.18	-
4HBA	219.3	30.3	7.95×10^{-3}	6.81×10^{-4}	3.78×10^{-2} (4.5)	0.21	-
FA[c]	300.0	31.8 [c]	2.37×10^{-3} [c]	8.07×10^{-4}	4.48×10^{-2} (3.0, 4.4)	0.25	-
GA[c]	200.0	26.7 [c]	1.85×10^{-2} [c]	2.43×10^{-3}	1.35×10^{-1} (2.9)	0.75	-
GBPL-BA	83.9	15.7	3.53×10^{-1}	3.34×10^{-4}	1.85×10^{-2} [d]	-	0.10
GBPL-4ABA	121.0	18.4	1.64×10^{-1}	5.22×10^{-4}	2.90×10^{-2} [d]	-	0.16
GBPL-4HBA	138.5	20.9	9.78×10^{-2}	2.65×10^{-4}	1.47×10^{-2} [d]	-	0.08
$GBPL_2$-FA	105.3	9.9	4.26×10^{-1}	8.45×10^{-4}	9.38×10^{-2} [d]	-	0.52
GBPL-GA	125.9	23.7	8.90×10^{-2}	2.07×10^{-4}	1.15×10^{-2} [d]	-	0.06

** Measured heats of fusion for cocrystals were normalized by moles of components per mole of cocrystal as shown by Black et. al., for salts.[36] (a) Ideal solubilities were calculated using equation (1) and are expressed as mole fraction cocrystal, this is equivalent to mole fraction GBPL for 1:1 cocrystals. (b) Experimental aqueous solubility measurements were carried out at 25°C and are expressed as mole fraction of cocrystal, this is equivalent to the mole fraction of GBPL for 1:1 cocrystals. (c) GA and FA sublime upon melting. Heat of fusion calculated from Walden's rule is used to calculate the ideal solubilities. Standard deviation in thermal data and solubility measurements is less than 2.5%. (d) Cocrystal solubilities were calculated from K_{sp} values listed in Table 2.3 and are expressed as moles GBPL/kg water.*

Figure 2.2 shows the experimental aqueous solubility values for all cocrystals are lower than the calculated ideal solubility values. Solvation in this series of cocrystals appears to be a significant barrier to the experimental aqueous solubility, which is lower than the ideal solubility by as much as 3 orders of magnitude. This difference between observed and ideal solubility values is quantitatively expressed by

$$\log \chi_{aq} = \log \chi_{ideal} - \log \gamma_{aq} \qquad (2.2)$$

where χ_{aq} is the observed solubility and γ_{aq} is the activity coefficient, which represents the contribution of solute-solvent interactions.[11, 13] Equations (2.1) and (2.2), were used to calculate the ideal solubilities and activity coefficients for GBPL cocrystals (Figure 2.2). A similar analysis has been presented to study the role of solvent and molecular structure on a series of organic compounds.[11, 13]

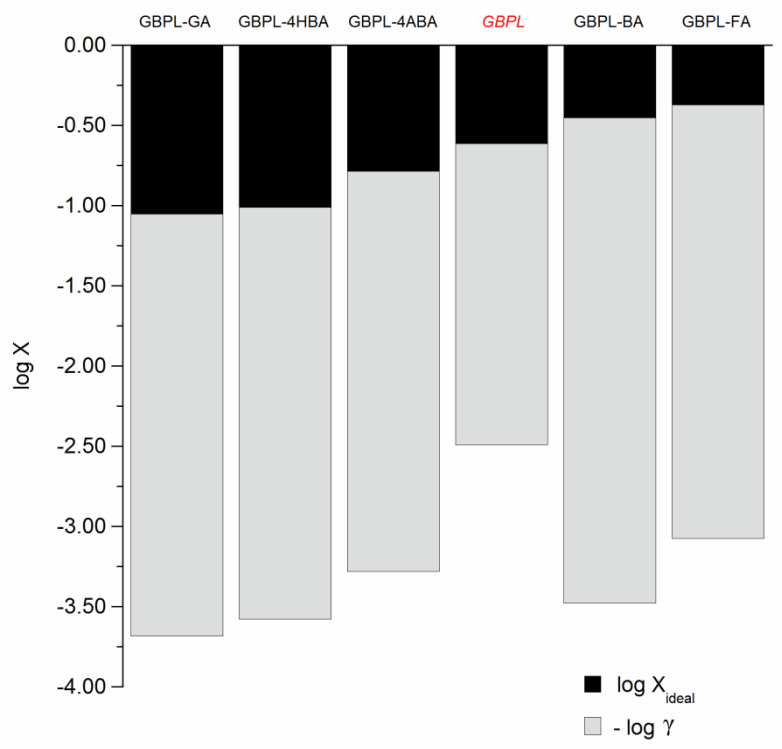

Figure 2.2: The lattice energy (log χ_{ideal}) and solvation energy (log γ_{aq}) contributions to the experimental aqueous solubility of GBPL and GBPL cocrystals is arranged in order of increasing ideal solubility (S_{ideal}). The black area of the bars represents S_{ideal} calculated from equation (2.1). The grey area represents the activity coefficient calculated from equation (2.2).

With respect to the series of GBPL cocrystals examined, lower solubility coformers led to cocrystals of lower solubility relative to GBPL, however the magnitude of solute-solvent interactions (γ_{aq}) is not proportional to the magnitude of their calculated ideal solubilities (χ_{ideal}). As a result melting point is not an accurate measure in predicting aqueous solubility of GBPL cocrystals. Similar solubility trends have been observed for other cocrystals,[4, 37] suggesting that it is often difficult to predict the solubility of a cocrystal in water based on its thermal properties alone, since solvation can be the factor determining cocrystal solubility.

Influence of Coformer Ionization on Cocrystal Solubility

GBPL forms cocrystals of 1:1 stoichiometry with monoprotic acidic coformers (GA, BA and 4HBA), 2:1 cocrystal with diprotic acidic coformer (FA) and a 1:1 cocrystal with amphoteric coformer (4ABA). The solubility dependence on coformer ionization for a 1:1 cocrystal of a non-ionic compound and a monoprotic acidic coformer can be calculated from:

$$S_{cc} = \sqrt{K_{sp}\left(1+\frac{K_{a,HA}}{[H^+]}\right)} \qquad (2.3)$$

where K_{sp} is the solubility product of the cocrystal, $K_{a,HA}$ is the ionization constant of the acidic coformer, and $[H^+]$ is the hydrogen ion concentration. The cocrystal K_{sp} can be calculated from the measured total drug $[GBPL]_T$ and the total coformer $[HA]_T$ solution concentrations at equilibrium with cocrystal using the following expression:

$$K_{sp} = \frac{[GBPL]_T[HA]_T}{\left(1+\frac{K_{a,HA}}{[H^+]}\right)} \qquad (2.4)$$

The solubility-pH dependence of GBPL-GA, GBPL-BA and GBPL-4HBA cocrystals, coformers and GBPL are shown in Figure 2.3. Cocrystal solubility curves were generated from equation (2.3) with cocrystal K_{sp} values given in Table 2.3. K_{sp} values were evaluated from the linearized form of equation (2.4) from measured cocrystal solubilities at several pH values. The solubility of GBPL at 25ºC in pH 1, 3 and 5 was measured to be 0.180 ± 0.004m. Figure 2.3 indicates that cocrystal intrinsic solubilities are lower than GBPL and coformer solubilities, and range from 0.06 to 0.10 times the GBPL solubility. Intrinsic solubility is the solubility under non-ionizing conditions of cocrystal components. Measured cocrystal solubilities are shown to increase with pH and

are in excellent agreement with the predicted behavior. There is an intersection between the cocrystal and the GBPL solubility curves at a given pH value, pH_{max}. At pH_{max} the solution is saturated with both GBPL crystal and cocrystal. Below pH_{max} cocrystal is thermodynamically stable. The value of pH_{max} for these cocrystals range from 5.3 to 6.6. Parameters that determine the value of pH_{max} are discussed in detail in the next section.

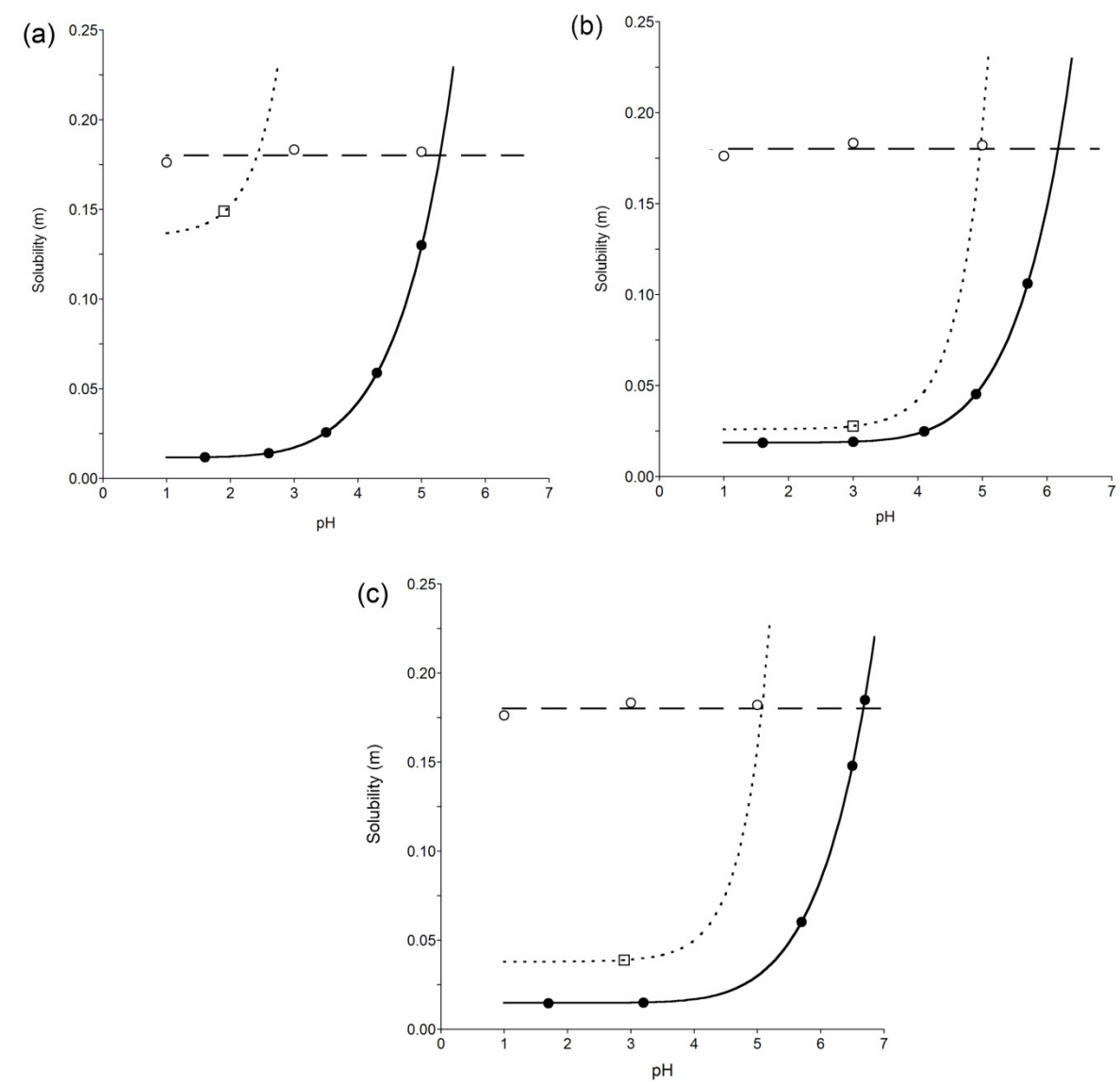

Figure 2.3: Experimental and predicted solubility-pH dependence of cocrystals expressed in terms of GBPL molal concentrations. Cocrystal and GBPL solubilities are represented by (●) and (○) respectively. Theoretical solubility (——) dependence on pH for (a) GBPL-GA (b) GBPL-BA and (c) GBPL-4HBA calculated from equation (2.3) using K_{sp} values of 1.32 x 10^{-4}, 3.43 x 10^{-4} and 2.16 x 10^{-4} m^2 and pKa values in Table 2.3. Theoretical coformer solubility-pH dependence (·····) was generated from equation (2.5) using pKa values in Table 2.3 and measured coformer solubilities shown by the symbol (□).

The coformer solubility dependence on pH, was calculated according to,

$$S_{coformer} = S_{0,coformer}\left(1+\frac{K_{a,HA}}{[H^+]}\right) \qquad (2.5)$$

From measured coformer solubility at a given pH, and reported pKa values of GA, BA and 4HBA intrinsic solubilities $\left(S_{0,coformer}\right)$ were calculated (Table 2.2 and Table 2.3). Coformer intrinsic solubilities range from 0.14 to 0.75 times the solubility of GBPL and are in good agreement with solubilities reported in the literature.[23-30]

$GBPL_2$-FA cocrystal exhibits 2:1 stoichiometry. The cocrystal solubility dependence on coformer ionization is described by:

$$S_{cc} = \sqrt[3]{\frac{K_{sp}}{4}\left(1+\frac{K_{a,H_2A}}{[H^+]}+\frac{K_{a,H_2A}K_{a,HA^-}}{[H^+]^2}\right)} \qquad (2.6)$$

where K_{a,H_2A} and K_{a,HA^-} are the ionization constants of the diprotic acidic coformer. The cocrystal K_{sp} can be calculated from the total drug $[GBPL]_T$ and the total coformer $[H_2A]_T$ solution concentrations measured in equilibrium with solid cocrystal using the following expression:

$$K_{sp} = \frac{[GBPL]_T^2\ [H_2A]_T}{\left(1+\frac{K_{a,H_2A}}{[H^+]}+\frac{K_{a,H_2A}K_{a,HA^-}}{[H^+]^2}\right)}$$

The solubility of the coformer is given by:

$$S_{coformer} = S_{0,coformer}\left(1+\frac{K_{a,H_2A}}{[H^+]}+\frac{K_{a,H_2A}K_{a,HA^-}}{[H^+]^2}\right) \qquad (2.7)$$

The predicted cocrystal and coformer (FA) solubility pH dependence was calculated from equations (2.6) and (2.7) using the cocrystal K_{sp}, coformer pK_a and measured FA

solubility (Table 2.2 and Table 2.3). Results in Figure 2.4 show that the intrinsic solubility of $GBPL_2$-FA cocrystal is 0.52 times the GBPL solubility. The predicted increase in solubility with pH is in excellent agreement with experimental behavior and shows a pH_{max} of 3.7. At the pH_{max}, the equilibrium solubility of crystalline GBPL is equal to the $GBPL_2$-FA cocrystal solubility expressed in terms of GBPL moles.

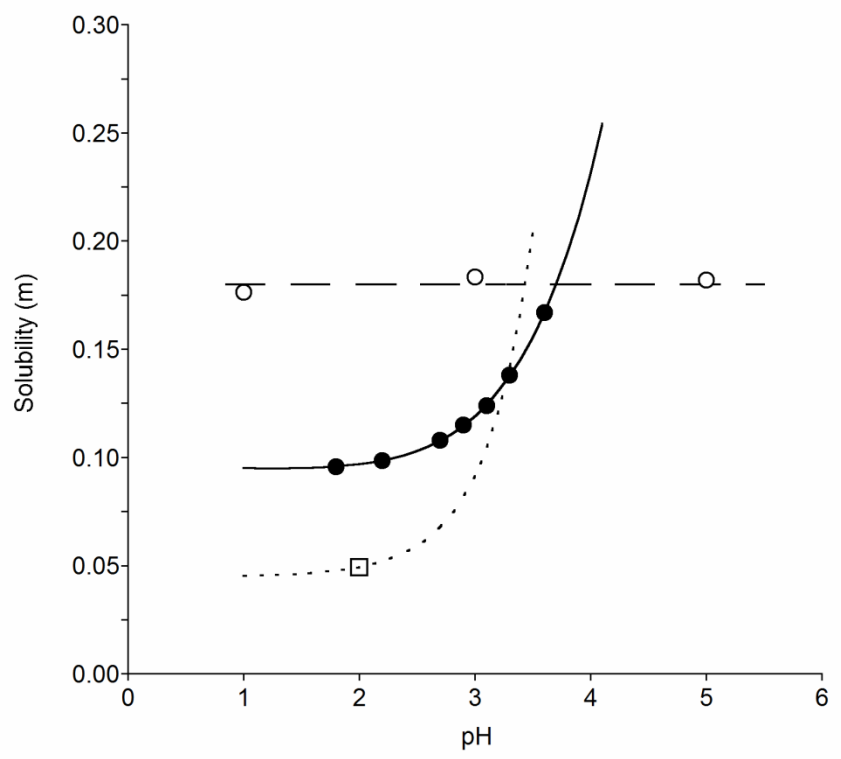

Figure 2.4: Experimental and predicted solubility-pH dependence of $GBPL_2$-FA cocrystal at 25ºC expressed in terms of GBPL molal concentration. Cocrystal and GBPL solubility are represented by (●) and (○) respectively. Theoretical solubility-pH dependence (——) was calculated from equation (2.6) using K_{sp} value of 4.13 x $10^{-4}m^3$ and the pKas listed in Table 2.3. Theoretical FA solubility-pH dependence (·····) was calculated from equation (6) using the pKas in Table 2.2 and the measured FA solubility shown by (□).

GBPL forms a 1:1 cocrystal with amphoteric coformer 4ABA. The cocrystal solubility dependence on coformer ionization is given by:

$$S_{cc} = \sqrt{K_{sp}\left(1 + \frac{K_{a,HAX}}{[H^+]} + \frac{[H^+]}{K_{a,HAXH^+}}\right)} \tag{2.8}$$

K_{a,HAX^-} and $K_{a,HAXH^+}$ are the ionization constants of the amphoteric coformer. The cocrystal K_{sp} can be calculated from the total drug $[GBPL]_T$ and the total coformer $[HAXH^+]_T$ solution concentrations measured in equilibrium with solid cocrystal using the following expression:

$$K_{sp} = \frac{[GBPL]_T \; [HAXH^+]_T}{\left(1 + \frac{K_{a,HAX}}{[H^+]} + \frac{[H^+]}{K_{a,HAXH^+}}\right)} \tag{2.9}$$

Figure 2.5 shows excellent agreement between the predicted and observed GBPL-4ABA cocrystal solubilities. Due to the amphoteric nature of 4ABA, a 'U' shaped solubility-pH profile of GBPL-4ABA cocrystal is obtained and there are two pH_{max} values given by the intersection points of the GBPL and cocrystal solubility curves. GBPL-4ABA cocrystal is the stable solid phase in the region between the two pH_{max} values of 0.8 and 6.6. GBPL-4ABA cocrystal exhibits a lower solubility relative to both GBPL and 4ABA. Cocrystal intrinsic solubility is 0.16 times that of GBPL (6.3 times less soluble).

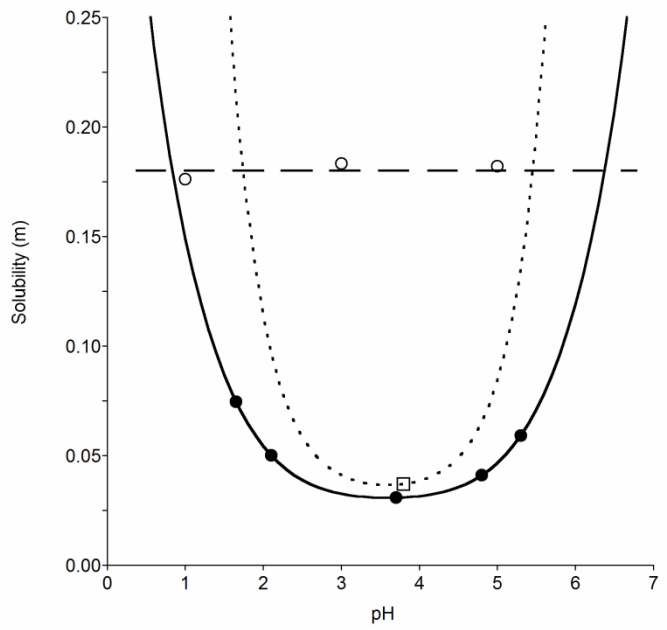

Figure 2.5: Experimental and predicted solubility-pH dependence of GBPL-4ABA cocrystal at 25ºC expressed in terms of as GBPL molal concentrations. Cocrystal and GBPL solubilities are represented by (●) and (○) respectively. Theoretical solubility dependence on pH (——) was calculated from equation (2.8) using K_{sp} value of 8.41 x 10^{-4} m^2 and the pK_a values in Table 2.3. 4ABA solubility-pH dependence (·····) was calculated from equation (2.10), values in Error! Reference source not found. and a measured 4ABA solubility shown by (□).

The coformer solubility dependence on pH was calculated from

$$S_{coformer} = S_{0,coformer}\left(1+\frac{K_{a,HAX}}{[H^+]}+\frac{[H^+]}{K_{a,HAXH^+}}\right) \qquad (2.10)$$

using the measured 4ABA solubility at a given pH and reported K_a values (Table 2.2 and Table 2.3). Cocrystal K_{sp} was evaluated from the slope of the linearized form of the solubility equations (2.3), (2.6) and (2.8), are shown in Figure 2.6. K_{sp} values are summarized in Table 2.3.

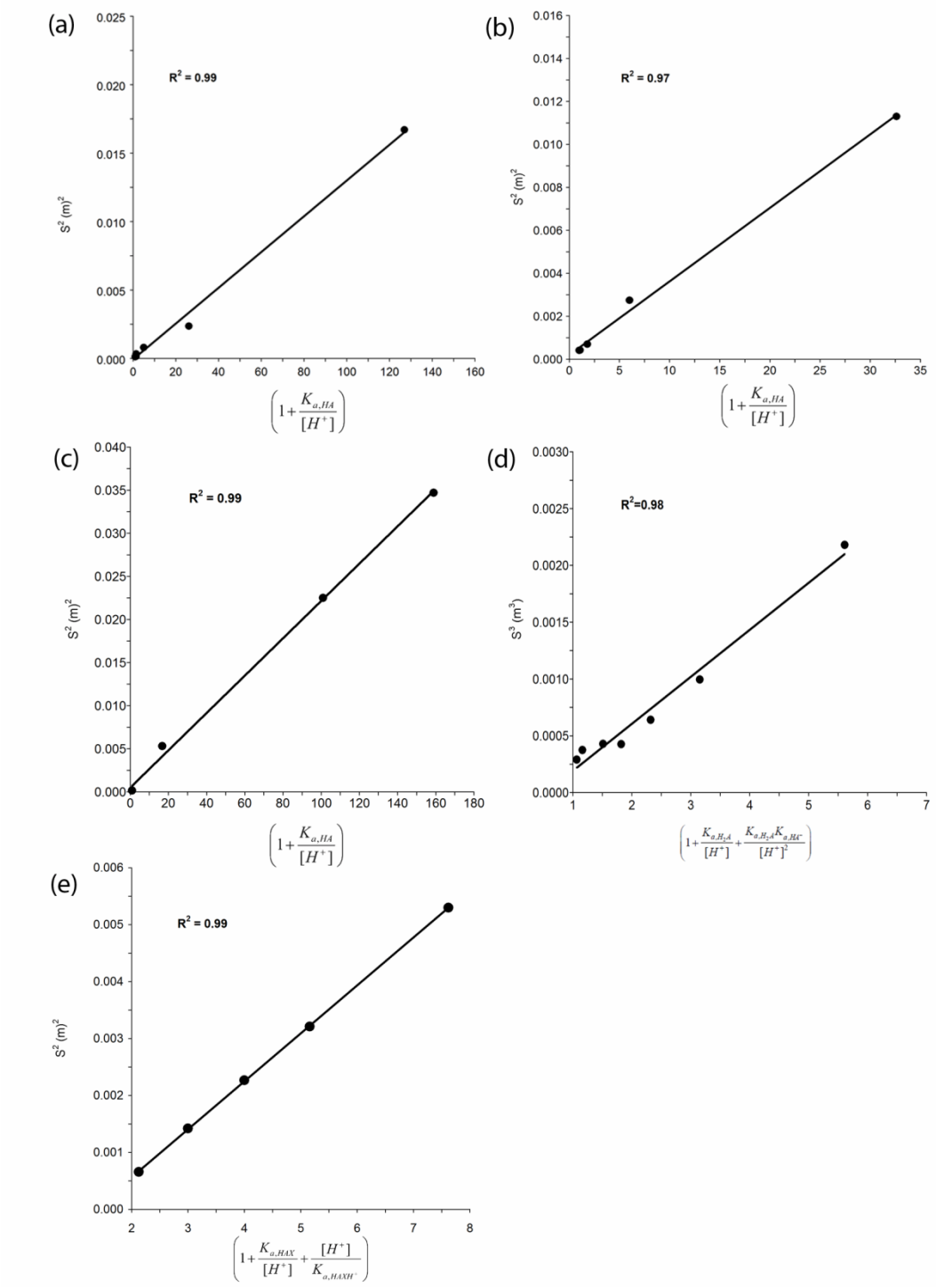

Figure 2.6: Plots used to evaluate cocrystal K_{sp} for (a) GBPL-GA (b) GBPL-BA (c) GBPL-4HBA according to equation (2.3) (d) $GBPL_2$-FUM according to equation (2.6) and (e) GBPL-4ABA according to equation (2.8).

pH_{max}

The solubility-pH dependence of an ionizable compound and its salt has been previously described by two independent curves, one where the free base (or acid) is the saturation species and the other where the salt is the equilibrium species and the point where the two saturation curves intersect is the pH_{max}.[1, 2, 12, 38, 39] pH_{max} has been referred to as pK_a^{Gibbs}, since the presence of two solid phases imparts the Gibbs phase rule constraint by forcing the pH and the solubility to be constant at pH_{max}.[12, 38] The solubility-pH dependence of GBPL cocrystals is summarized in Figure 2.7, and the mathematical basis to predict the pH_{max} dependence on K_{sp}, cocrystal component solubility and ionization behavior is derived in this section.

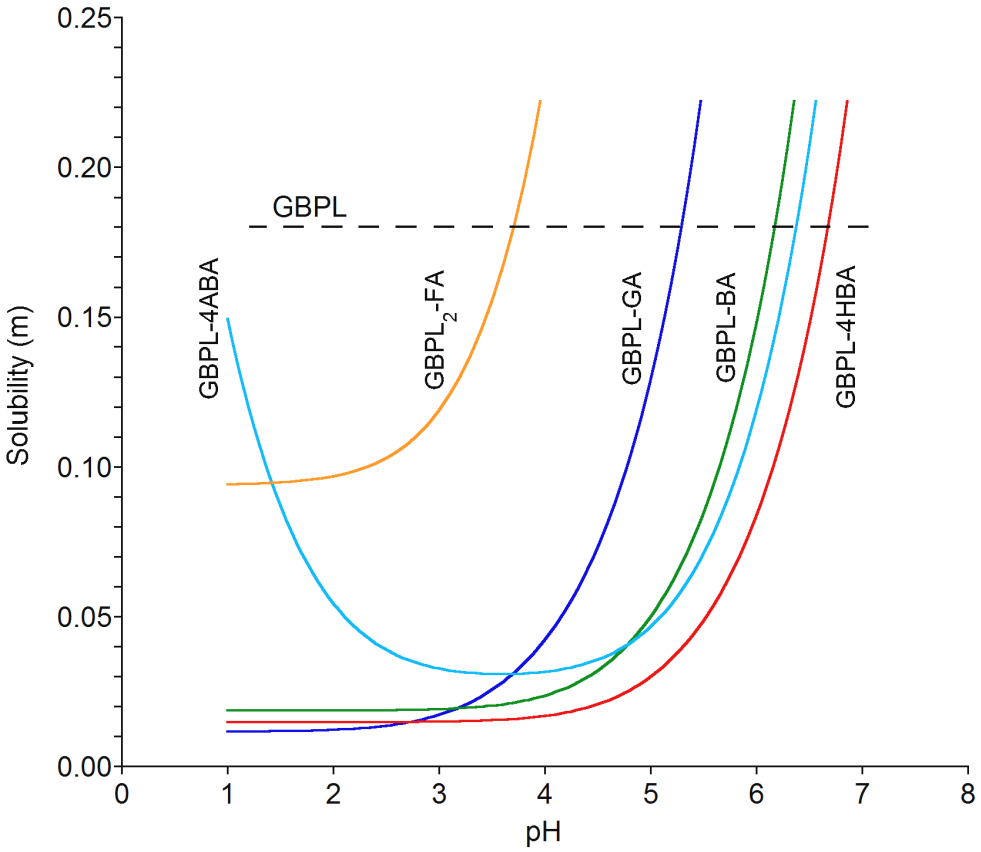

Figure 2.7: Cocrystal solubility expressed as GBPL molal concentration plotted as a function of pH. Curves were generated using models that describe cocrystal solubility-pH dependence using parameter values from Table 2.2 and Table 2.3. At $pH_{max,}$ GBPL and cocrystal is in equilibrium with a solution saturated with respect to both cocrystal and GBPL.

The pH_{max} of a 1:1 cocrystal occurs where $S_{cc} = S_{GBPL}$. For the 1:1 GBPL cocrystals with a monoprotic acidic coformer this equality leads to

$$S_{GBPL}^2 = S_{cc}^2 = K_{sp}\left(1+\frac{K_{a,HA}}{[H^+]}\right)$$

Solving for $[H^+]$ and expressing in terms of pH gives

$$pH_{max} = pK_{a,HA} + \log\left(\frac{S_{GBPL}^2}{K_{sp}} - 1\right) \qquad (2.11)$$

when $\frac{K_{a,HA}}{[H^+]} >> 1$ and $K_{sp} = S^2_{cocrystal}$, the above equation simplifies to

$$pH_{max} = pK_{a,HA} + 2\log\left(\frac{S_{GBPL}}{S_{cocrystal}}\right)$$

For the 1:1 GBPL cocrystal with an amphoteric coformer the pH_{max} is obtained from

$$S^2_{GBPL} = S^2_{cc} = K_{sp}\left(1 + \frac{K_{a,HAX}}{[H^+]} + \frac{[H^+]}{K_{a,HAXH^+}}\right)$$

Solving for $[H^+]$ results in an expression that can be used to calculate the pH_{max}

$$pH_{max} = -\log\left(\frac{K_{a,HAXH^+}}{2}\left(\left(\frac{(S_{GBPL})^2}{K_{sp}} - 1\right) \pm \sqrt{\left(1 - \frac{(S_{GBPL})^2}{K_{sp}}\right)^2 - 4\frac{K_{a,HAX}}{K_{a,HAXH^+}}}\right)\right) \qquad (2.12)$$

Equation (2.12) is the solution of a quadratic expression and thus results in two pH_{max} values.

The 2:1 cocrystal of a non-ionic compound with diprotic acidic coformer such as $GBPL_2$-FA cocrystal exhibits a pH_{max} when $2S_{cc}=S_{GBPL}$ which can be expressed as

$$pH_{max} = -\log\left(\frac{K_{a,H_2A} \pm \sqrt{K^2_{a,H_2A} - 4\left(1 - \frac{4\left(\frac{S_{GBPL}}{2}\right)^3}{K_{sp}}\right)\left(K_{a,H_2A}K_{a,HA^-}\right)}}{2\left(\frac{4\left(\frac{S_{GBPL}}{2}\right)^3}{K_{sp}} - 1\right)}\right) \qquad (2.13)$$

Equation (2.13) is obtained by setting GBPL solubility equal to the solubility of the 2:1 cocrystal of $GBPL_2$-FA (in terms of GBPL moles), and solving for $[H^+]$. This is the solution of a quadratic equation, although it yields only one real value for pH_{max}.

The pH_{max} for GBPL cocrystals (Table 2.3) were measured and calculated from cocrystal K_{sp}, coformer pK_a and GBPL solubility. The calculated pH_{max} values were confirmed experimentally for GBPL-4HBA and GBPL-4ABA cocrystals. In the case of GBPL-GA, GBPL-BA and $GBPL_2$-FA cocrystals, pH_{max} could not be accessed experimentally. This is due to self-buffering of the coformer which would not allow for independent pH adjustment.

Table 2.3: K_{sp} and pH_{max} values of GBPL cocrystals at 25ºC

Cocrystal	K_{sp} ± Std. Error m^2 or m^3 [a]	Coformer pK_a	pH_{max}
GBPL-4HBA	$(2.16 \pm 0.06)x10^{-4}$ [b]	4.4 [40, 41]	6.6 [e]
GBPL-4ABA	$(8.41 \pm 0.05)x10^{-4}$ [c]	2.4 (amine) 4.8 (acid) [42]	0.8 [f] 6.4 [f]
GBPL-BA	$(3.4 \pm 0.1)x10^{-4}$ [b]	4.2 [43]	6.2 [e]
GBPL-GA	$(1.32 \pm 0.03)x10^{-4}$ [b]	2.9 [44-46]	5.3 [e]
$GBPL_2$-FA	$(4.1 \pm 0.3)x10^{-4}$ [d]	3.0 and 4.4 [47]	3.7 [g]

(a) The unit of K_{sp} for 1:1 cocrystals is m^2 and for $GBPL_2$-FA cocrystal is m^3. (b), (c) and (d) represent K_{sp} values calculated from equations (2.3)*,* (2.6) *and* (2.8) *respectively using measured aqueous solubility values as a function of pH. Plots used to calculate K_{sp} are shown in Figure 2.6. (e), (f) and (g) represent pH_{max} calculated from equations,*(2.11)*,* (2.12) *and* (2.13) *respectively.*

pH_{max} for GBPL cocrystals with acidic coformers ranges from 3.7 to 6.6. Both K_{sp} and pK_a influence the value of pH_{max}. Larger K_{sp} and smaller pK_a values result in a lower pH_{max}. The lowest cocrystal pH_{max} values are shown to be associated with low coformer pK_a and high solubility (in terms of GBPL) as seen for the $GBPL_2$-FA (S_{cc}= $9.38x10^{-2}$ m). GBPL-GA (S_{cc}= $1.15x10^{-2}$ m) with similar pK_a and lowest cocrystal solubility in this series of cocrystal exhibits the next lowest pH_{max}.

General relationships between cocrystal K_{sp} and coformer pK_a on cocrystal pH_{max} for a 1:1 cocrystal of a non-ionizable drug and an acidic coformer, can be predicted by equation 9 as follows

1. An order of magnitude increase in K_{sp}, decreases pH_{max} by 1 unit.
2. A unit increase in coformer pK_a value, increases pH_{max} by 1 unit.
3. An order of magnitude increase in drug to cocrystal solubility ratio ($S_{Drug}/S_{Cocrystal}$), increases pH_{max} by 2 units.

The general sensitivity of cocrystal pH_{max} on these parameters is graphically demonstrated in Figure 2.8.

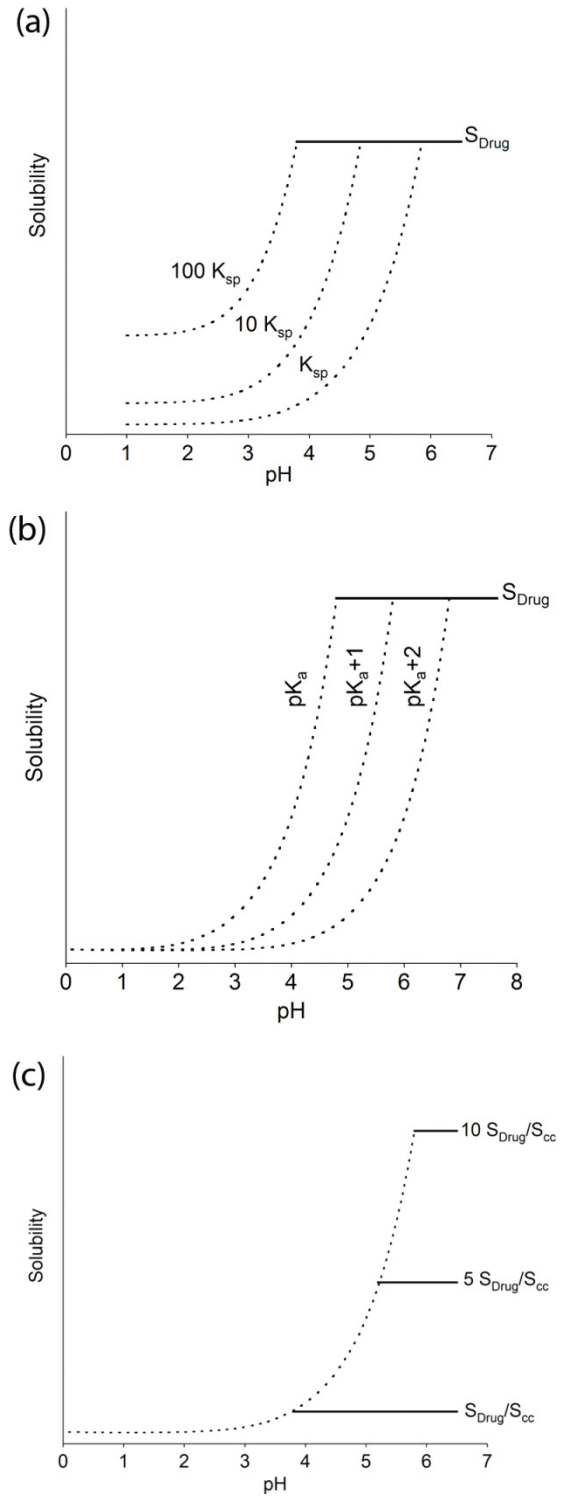

Figure 2.8: (a) increase in K_{sp} by an order of magnitude decreases the pH_{max} by 1 unit, (b) increase in pK_a by 1 unit increases the pH_{max} by 1 unit and (c) increase in the drug to cocrystal solubility ratio (S_{Drug}/S_{cc}) by an order of magnitude increases pH_{max} by 2 units.

pH_{max} expressions are useful in calculating cocrystal stability regions. Understanding cocrystal thermodynamic stability as a function of pH is useful for designing synthesis methods and understanding the *in-vitro* and *in-vivo* solubility related performance where pH is often a critical variable and may have a role in reversible transformations between cocrystal and drug.

Conclusions

Reaction crystallization method was successfully utilized to discover four cocrystals of GBPL. Cocrystallizing the highly soluble GBPL with lower solubility coformers results in cocrystals with a lower solubility than GBPL as hypothesized. Solvation was shown to be a key factor in determining cocrystal solubility. For the first time, mathematical models describing cocrystal pH_{max} are described. Mathematical models based on ionization properties and cocrystal Ksp accurately predict cocrystal solubility-pH dependence and pH_{max}. pH_{max} is of importance in estimating cocrystal solubility behavior and stability in aqueous solutions, which is critical for cocrystal synthesis and *in-vitro, in-vivo* performance. Thus the ability of cocrystals in providing varying solubility and solution concentrations to a non-ionizable compound over a wide pH range can be utilized in achieving desired pharmacokinetic behavior of a drug.

APPENDIX 1

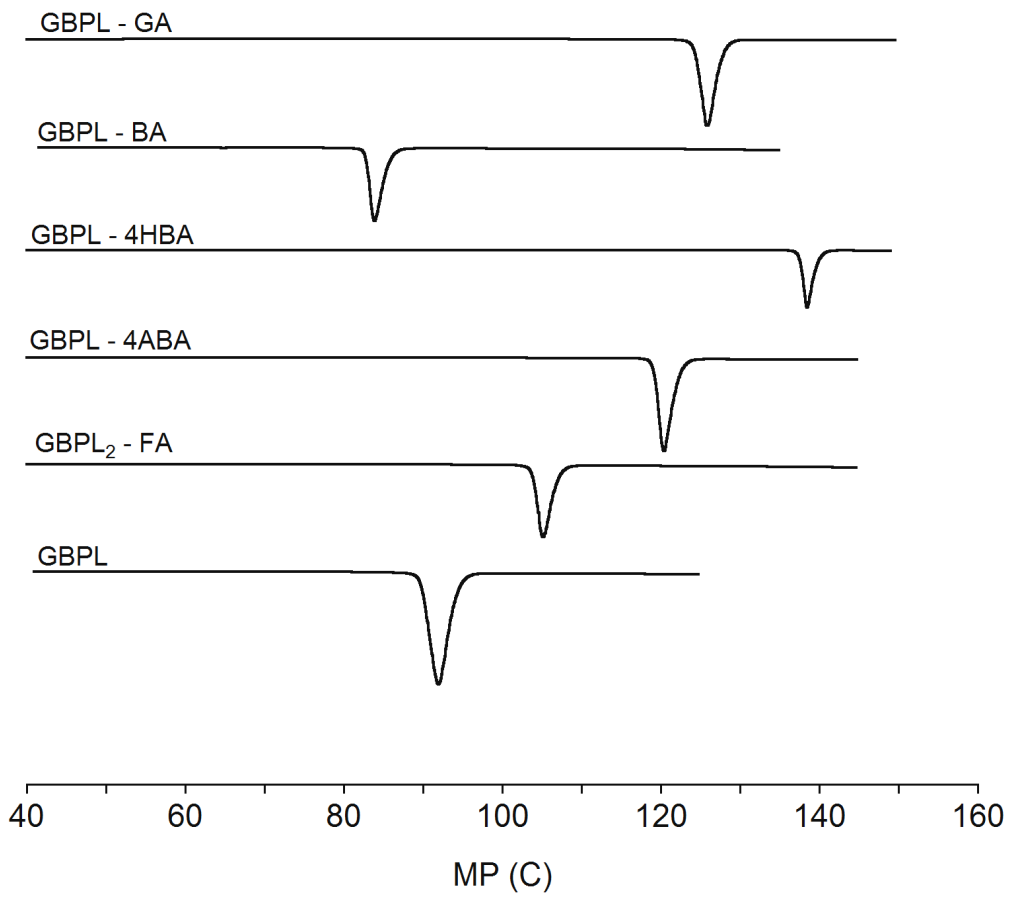

Figure A1.1: DSC thermograms of GBPL and GBPL cocrystals.

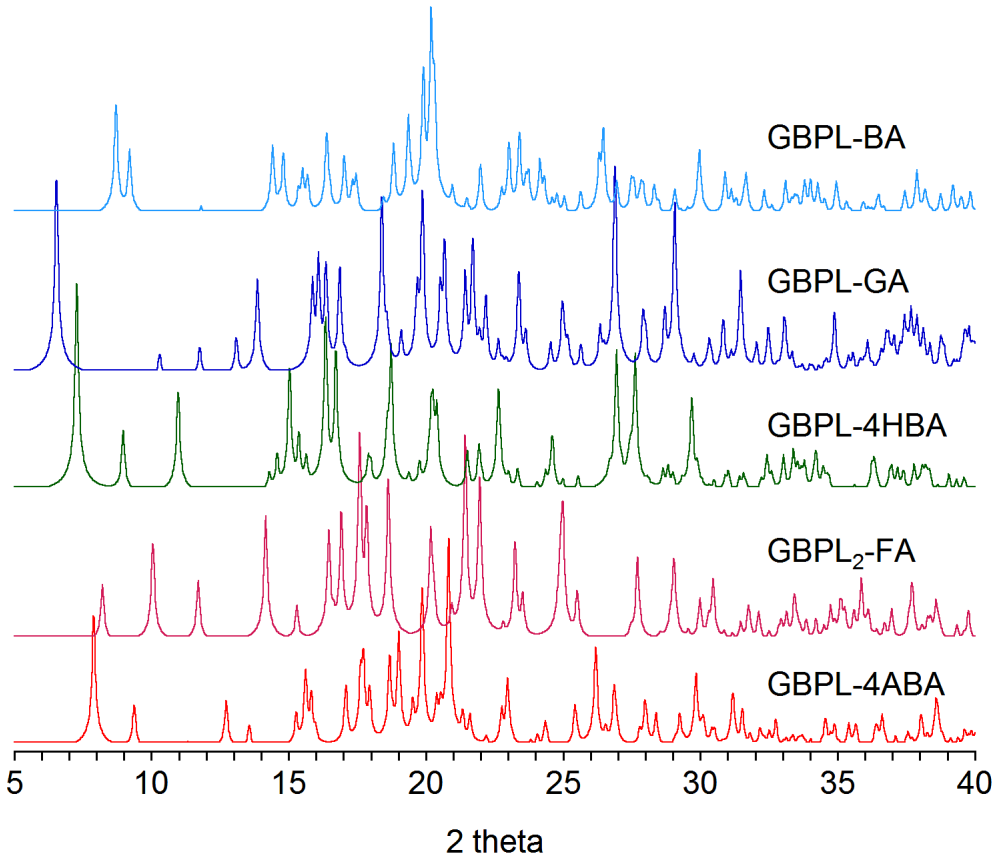

Figure A1.2: PXRD patterns of GBPL cocrystals

Table A1.1: Melting point in Kelvin, enthalpy of fusion, experimental solubility, ideal solubility and activity coefficient of GBPL and GBPL cocrystals.

Component	MP (K)	ΔH_f (kJ/mol)	ln χ_{ideal}	χ_{ideal}	Exp. Sol. (m)	-ln χ_{aq}	χ_{aq}	- log γ_{aq}
GBPL-GA	398.9	23.7	-2.4	8.90×10^{-2}	1.15×10^{-2}	-8.5	2.07×10^{-4}	-2.6
GBPL-4HBA	411.5	20.9	-2.3	9.78×10^{-2}	1.48×10^{-2}	-8.2	2.66×10^{-4}	-2.6
GBPL-4ABA	394	18.4	-1.8	1.64×10^{-1}	2.85×10^{-2}	-7.6	5.13×10^{-4}	-2.5
GBPL	365	19.0	-1.4	2.44×10^{-2}	1.80×10^{-1}	-5.7	3.23×10^{-3}	-1.9
GBPL-BA	356.9	15.7	-1.0	3.53×10^{-1}	2.07×10^{-2}	-7.9	3.73×10^{-4}	-2.9
GBPL-FA	378.3	9.9	-0.9	4.26×10^{-1}	4.69×10^{-2}	-7.1	8.45×10^{-4}	-2.7

Table A1.2: Cocrystal component melting points and the ratio of melting points of cocrystals and its components. These results are plotted in Figure A1.3 on next page.

Compound (MP)	Coformer	Coformer MP (ºC)	Cocrystal MP (ºC)	$\frac{T_f^{cc}}{T_f^{Compound}}$	$\frac{T_f^{coformer}}{T_f^{Compound}}$
AMG 517 (230ºC)	*trans*-Cinnamic Acid	133.0	204.0	0.9	0.6
	Gentisic Acid	205.0	229.0	1.0	0.9
	2 hydroxy caaproic Acid	61.0	130.0	0.6	0.3
	Glutaric Acid	97.0	153.0	0.7	0.4
	Gluycolic Acid	78.0	141.0	0.6	0.3
	Sorbic Acid	134.0	150.0	0.7	0.6
	trans-2-hexanoic	34.0	127.0	0.6	0.1
	L(+)- Lactic	46.0	138.0	0.6	0.2
	BA	122.0	146.0	0.6	0.5
GBPL (92ºC)	4HBA	219.3	146.0	1.5	2.4
	4ABA	188.9	121.0	1.3	2.1
	GA	200.0	125.9	1.4	2.2
	BA	122.8	83.9	0.9	1.3
Nicotinamide (130ºC)	R/S Mandelic Acid	130.0	89.0	0.7	1.0
	RS-Mandelic Acid	117.0	76.0	0.6	1.1
	S-Ibuprofen	50.0	82.0	1.6	2.6
	RS-Iboprofen	76.0	91.0	1.2	1.7
Carbamazepine (192ºC)	NCT	130.0	160.8	0.8	0.7
	Glutaric Acid	97.7	125.9	0.7	0.5
	Succinic Acid	188.1	188.9	1.0	1.0
	Salicylic Acid	160.9	160.1	0.8	0.8
	Saccharin	229.7	177.5	0.9	1.2

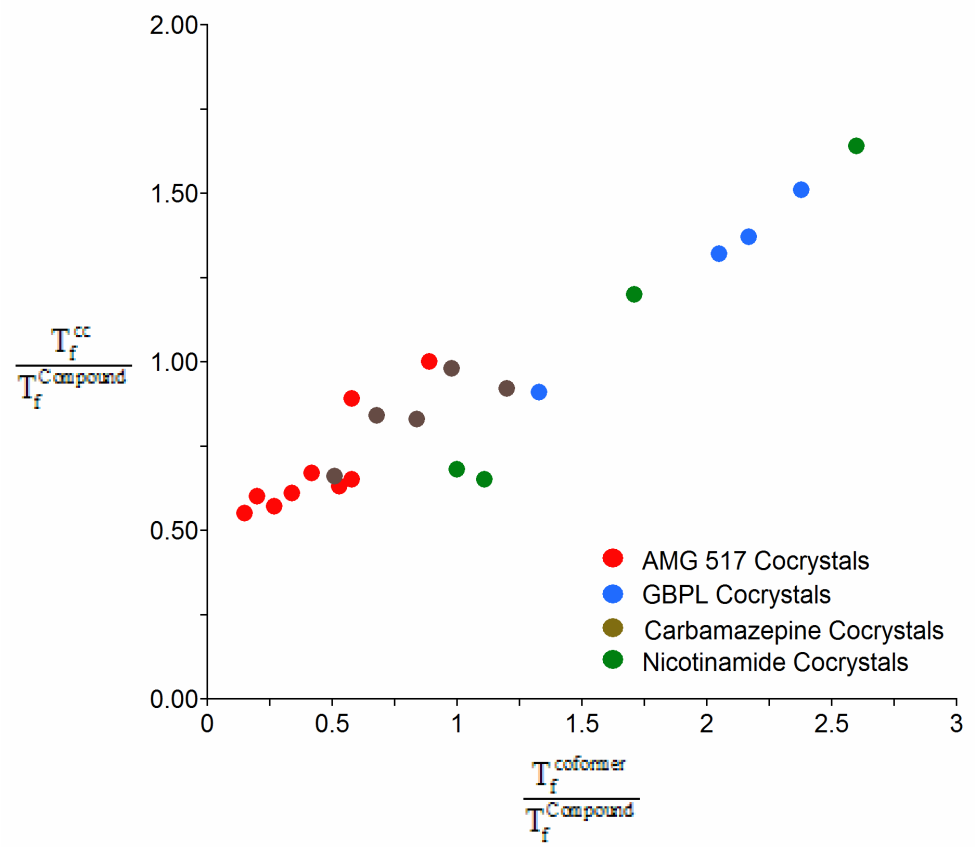

Figure A1.3: Figure plotted from the data in Table A1.2 showing the trend between the ratio of coformer and cocrystal melting point to the melting point of the compound which are AMG 517, GBPL, carbamazepine and nicotinamide.

References

1. A.T.M. Serajuddin, *Advanced Drug Delivery Reviews*, **(2007)**, 59(7), 603-616.

2. P.H. Stahl and C.G. Wermuth, *Handbook of Pharmaceutical Salts: Properties, Selection and Use*. 2002, Zürich: Wiley-VCH.

3. L.S. Reddy, S.J. Bethune, J.W. Kampf, and N. Rodríguez-Hornedo, *Crystal Growth & Design*, **(2008)**, 9(1), 378-385.

4. D.J. Good and N. Rodríguez-Hornedo, *Crystal Growth & Design*, **(2009)**, 9(5), 2252-2264.

5. S. Agharkar, S. Lindenbaum, and T. Higuchi, *J. Pharm. Sci*, **(1976)**, 65(5), 747-749.

6. S.J. Bethune, N. Huang, A. Jayasankar, and N. Rodríguez-Hornedo, *Crystal Growth & Design*, **(2009)**, 9(9), 3976-3988.

7. E. Nelson, J.G. Wagner, E.L. Knoechel, and W.E. Hamlin, *Journal of Pharmaceutical Sciences*, **(1962)**, 51(6), 509-&.

8. K.J. Paluch, L. Tajber, C.J. Elcoate, O.I. Corrigan, S.E. Lawrence, and A.M. Healy, *J. Pharm. Sci*, **(2011)**, 100(8), 3268-3283.

9. L.D. Bighley, S.M. Berge, and D.C. Monkhouse. Encyclopedia of Pharmaceutical Technology, ed. J. Swarbrick and J.C. Boylan. Vol. 13. 1996, New York, Basel, Hong Kong: Marcel Dekker. 453-499.

10. S.H. Yalkowsky, *Solubility and Solubilization in Aqueous Media*. 1999, New York: Oxford University Press, Inc.

11. Y. Miyako, N. Khalef, K. Matsuzaki, and R. Pinal, *International Journal of Pharmaceutics*, **(2010)**, 393(1-2), 48-54.

12. A. Avdeef, *Adv. Drug Del. Rev.*, **(2007)**, 59, 568-590.

13. Y. Miyako, H. Tai, K. Ikeda, R. Kume, and R. Pinal, *Drug Development and Industrial Pharmacy*, **(2008)**, 34(5), 499-505.

14. A. Bak, A. Gore, E. Yanez, M. Stanton, S. Tufekcic, R. Syed, A. Akrami, M. Rose, S. Surapaneni, T. Bostick, A. King, S. Neervannan, D. Ostovic, and A. Koparkar, *Journal of Pharmaceutical Sciences*, **(2008)**, 97(9), 3942-3956.

15. S.L. Childs and K. Hardcastle, *Crystal Growth & Design*, **(2007)**, 7(7), 1291-1304.

16. S.L. Childs, L.J. Chyall, J.T. Dunlap, V.N. Smolenskaya, B.C. Stahly, and G.P. Stahly, *J. Am. Chem. Soc.*, **(2004)**, 126, 13335-13342.

17. J.F. Remenar, M.L. Peterson, P.W. Stephens, Zhong Zhang, Y. Zimenkov, and M.B. Hickey, *Molecular Pharmaceutics*, **(2007)**, 4(3), 386-400.

18. A. Jayasankar, S.L. Reddy, S.J. Bethune, and N. Rodríguez-Hornedo, *Crystal Growth & Design*, **(2009)**, 9(2), 889-897.

19. M.L. Chency, N. Shan, E.R. Healey, M. Hanna, L. Wojtas, M.J. Zaworotko, V. Sava, S.J. Song, and J.R. Sanchez-Ramos, *Crystal Growth & Design*, 10(1), 394-405.

20. S.L. Childs, N. Rodríguez-Hornedo, L.S. Reddy, A. Jayasankar, C. Maheshwari, L. McCausland, R. Shipplett, and B.C. Stahly, *Crystengcomm*, **(2008)**, 10(7), 856-864.

21. W.A. Lagreze, R.M. Velten, and T.J. Feuerstein, *Graefe's Arch Clin Exp Opththalmol*, **(2001)**, 239, 845-849.

22. T. Jehle, W.A. Lagreze, E. Blauth, R. Knorle, P. Schnierle, C.H. Lucking, and T.J. Feuerstein, *Naunyn-Schmiedeberg's Acrh. Pharmacol*, **(2000)**, 362, 74-81.

23. J.O. Bockris, J. Bowler-Reed, and J.A. Kitchner, *Transactions of Faraday Society*, **(1951)**, 47, 184.

24. H.S. Booth and H.E. Everson, *Industrial and Engineering Chemistry*, **(1948)**, 40(8), 1491.

25. M. Eisenberg, P. Chang, and C.W. Tobias, *Aiche Journal*, **(1995)**, 1(4), 558.

26. K.A. Herzog and J. Swarbrick, *J. Pharm. Sci*, **(1971)**, 60(11), 1666-1668.

27. A.G. Mitchell and D.J. Saville, *J. Pharmacy and Pharmacology*, **(1969)**, 21(1), 28.

28. A.N. Paruta, *J. Pharm. Sci*, **(1964)**, 53(10), 1252.

29. S.H. Yalkowsky and Y. He, *Handbook of Aqueous Solubility Data*. 2006, Boca Raton, FL: CRC Press.

30. J.M. Weiss and C.R. Downs, *J. Am. Chem. Soc.*, **(1923)**, 45, 1003-1008.

31. J.A. McMahon, J.A. Bis, P. Vishweshwar, T.R. Shattock, O.L. McLaughlin, and M.J. Zaworotko, *Zeitschrift Fur Kristallographie*, **(2005)**, 220(4), 340-350.

32. D. Braga, F. Grepioni, L. Maini, K. Rubini, M. Polito, R. Brescello, L. Cotarca, M.T. Duarte, V. Andre, and M.F.M. Piedade, *New Journal of Chemistry*, **(2008)**, 32, 1788-1795.

33. N. Rodríguez-Hornedo, S.J. Nehm, K.F. Seefeldt, Y. Pagan-Torres, and C.J. Falkiewicz, *Molecular Pharmaceutics*, **(2006)**, 3(3), 362-367.

34. A. Altomare, M.C. Burla, M. Camalli, G.L. Cascarno, C. Giacovazzo, A. Guagliardi, A.G.G. Moliterni, G. Polidori, and R. Spagna, *Journal of Applied Crystallography*, **(1999)**, 1999(32), 115-119.

35. G.M. Sheldrick, *Crystallographica Section A*, **(2008)**, 64, 112-122.

36. S.N. Black, E.A. Collier, R.J. Davey, and R.J. Roberts, *J. Pharm. Sci*, **(2007)**, 96(5), 1053-1068.

37. M.K. Stanton and A. Bak, *Crystal Growth & Design*, **(2008)**, 8(10), 3856-3862.

38. A. Avdeef, *Phar. Pharmacol. Commun.*, **(1998)**, 4, 165-178.

39. S.F. Kramer and G.L. Flynn, *Journal of Pharmaceutical Sciences*, **(1972)**, 61(12), 1896-&.

40. J.-D. Zhang, Q.-Z. Zhu, S.-J. Li, and F.-M. Tao, *Chemical Physics Letters*, **(2009)**, 475(1-3), 15-18.

41. H. Miklautz, D. Keller, F.L. Holguin, and R. Woloszczak, *Anal. Bioanal. Chem.*, **(2006)**, 384, 1191-1195.

42. R.A. Robinson and A.I. Biggs, *Australian Journal of Chemistry*, **(1957)**, 10(2), 128-134.

43. D. Robinson, J.N. Smith, and R.T. Williams, *Biochemical Journal*, **(1953)**, 55(1), 151-155.

44. *The Merck Index: An Ecylopedia of Chemicals, Drugs and Biologicals*. 13th ed. 2001: Merck & Co., Inc., Whitehouse Station, NJ.

45. F.Z. Erdemgil, S. Sanli, N. Sanli, G. Ozkan, J. Barbosa, J. Guiteras, and J.L. Beltran, *Talanta*, **(2007)**, 72(2), 489-496.

46. D.L. French, K.J. Himmelstein, and J.W. Mauger, *Journal of Controlled Release*, **(1995)**, 37(3), 281-289.

47. W. German, *Philosophical Magazine*, **(1936)**, 22(149), 790.

CHAPTER 3

DO COCRYSTALS OFFER SOLUBILITY ADVANTAGE OVER SALTS?

Abstract

The purpose of this work was to determine the extent to which aqueous solubility, pH_{max}, and thermodynamic stability can be altered by cocrystals and salts of a basic drug. Lamotrigine (LAM) cocrystal with nicotinamide (NCT) and LAM salt with saccharin (SAC) were used as model compounds, while the reported data for lamotrigine-methylparaben (LAM-MP) and LAM·HCl were used to draw pH dependent solubility comparisons of LAM solid forms. Reaction crystallization was used to synthesize LAM-NCT·H2O cocrystal hydrate and LAM-SAC salt. Supersaturation was controlled by use of sodium lauryl sulfate to obtain highly pure LAM-NCT·H_2O cocrystal. Mathematical models developed by considering solid-solution equilibria were used to generate the predicted pH dependent solubility of cocrystal and salt. These models were challenged by measuring pH dependent solubility and eutectic point concentration of cocrystal components which represents the cocrystal solubility under non stoichiometric conditions where solid drug and cocrystal are in equilibrium with the solution. LAM-NCT·H_2O cocrystal and LAM-SAC salt are 30 and 5 times more soluble than LAM·H_2O respectively, while LAM-NCT·H_2O cocrystal is 6 times more soluble than LAM-SAC salt. This solubility comparison is based on the pH values at which the crystalline forms

are in their intrinsic solubility state. A pH_{max} value of 2.7 exists between LAM-NCT·H_2O cocrystal and LAM·H_2O, below which LAM-NCT·H_2O cocrystal is the stable solid phase relative to LAM·H_2O, while a pH_{max} value of 5.0 exists between LAM-SAC salt and LAM·H_2O below which LAM-SAC salt is the stable solid phase. pH_{max} is a critical thermodynamic parameter which governs cocrystal and salt stability and can be accurately calculated from the equations based on solid solution equilibria. The predicted solubility behavior calculated from the mathematical models is in excellent agreement with experimental results. The thermodynamic solubility rank order of LAM solid forms investigated in this work is, LAM-NCT·H_2O > LAM-SAC > LAM-MP, and the coformer solubility rank order is NCT > SAC > MP. Solubility of LAM·HCl salt is dependent on the Cl^- concentration in the medium due to common ion effect.

Introduction

Approximately one-third of the new chemical entities have aqueous solubilities of less than 10μg/ml[1]. Solubility often governs drug dissolution, and when bioavailability is limited by solubility, higher solubility forms may be useful to provide faster dissolution rates in the gastrointestinal tract resulting in improved bioavailability. The intended higher dissolution is often achieved via alternative solid forms such as salts, cocrystals and amorphous solids exhibiting higher solubility than the crystalline free drug. For several decades, pharmaceutical salts which are formed by charge assisted molecular bonds have been considered as the form of choice for poorly water soluble drugs[2-6]. As a result a large number of drugs are marketed as salts[7]. Cocrystals offer a choice of solid forms for drug delivery when salt formation is not possible or when non-ionic hydrogen

bonded interactions can be exploited to produce alternative crystalline forms of desirable properties, such as solubility modification.

Lamotrigine [6-(2,3-dichlorophenyl)-1,2,4-triazine-3,5-diamine] is a triazine drug that exhibits poor aqueous solubility and dissolution rate in its crystalline form. It is used for the treatment of epilepsy and psychiatric conditions such as bipolar disorder. LAM is a weakly basic compound with a pK_a of 5.7[8] and reported aqueous solubility of 0.17mg/ml[9-12]. Enhancing solubility of such poorly water soluble drugs *via* salt formation is well known, whereas several studies have demonstrated that cocrystals can provide dissolution and bioavailability advantage due to their higher solubility relative to the parent drug[3, 5, 13-15]. It has been shown that solubility of cocrystals is influenced by coformer solubility and if the constituents are ionizable then cocrystals exhibit a pH dependent solubility.[13, 15-17]

Recently, several new crystalline forms of LAM were discovered and investigated for their solubility enhancement properties[10, 11, 15]. In one case, dissolution experiments were carried out on LAM salts and cocrystals on the basis of which, solubilities of LAM crystalline forms were estimated[18]. However, solubility is a thermodynamic property and its estimation using kinetic methods may lead to inaccurate results. This is due to solution mediated phase transformation of higher solubility crystalline form to lower solubility more stable solid form. Furthermore, such phase transformations can be pH dependent as shown for salts and recently for cocrystals[16, 19-216]. Hence for an accurate determination of solubility, it is critical to understand the solution mediated phase transformation as well as the effect of solution pH on solid form stability, especially during kinetic concentration measurements.

The effect of micellar concentration on cocrystal solubility and stability have also been investigated recently, where it is shown that beyond a critical micellar concentration a higher solubility cocrystal can be stabilized. This is defined as the 'critical stabilization concentration' (CSC), beyond which the thermodynamic stabilities of cocrystal and its components are reversed. For example, a higher solubility cocrystal relative to the drug would be thermodynamically stable above the CSC and can persist in aqueous suspensions. This is due to the differential affinities of the drug and coformer to the surfactant[22]. The LAM-NCT·H_2O cocrystal investigated in this work could not be synthesized by reported methods, micellar solubilization has been utilized to synthesize this cocrystal and the existence of a CSC is investigated.

In this work we apply the principles of solution phase chemistry to address the solubility and phase stability assessment by, (i) measurement and prediction of true thermodynamic solubilities of highly soluble cocrystalline phase, from eutectic point concentrations of cocrystal components, (ii) comparison of solubility dependence on pH of several crystalline forms of LAM, (iii) importance of pH_{max} on the crystalline phase stability and, (iv) the role of micellar solubilization and CSC on the synthesis of LAM-NCT·H_2O cocrystal. All salts and cocrystals investigated in this work are of 1:1 stoichiometry.

Materials and Methods

Materials

LAM was purchased from Jai Radhe Sales, India with a purity of 99.6% w/w and was used as received. All other chemicals were purchased from Sigma-Aldrich and were used as received. PXRD and DSC analyses were performed on all materials to confirm phase purity prior to use. LAM·H_2O was prepared by suspending anhydrous LAM for a period of 24 hrs in water at 25±0.1ºC. The slurry was vacuum filtered and the solid phase was checked by PXRD and DSC.

Cocrystal and Salt Synthesis

LAM-NCT·H_2O was synthesized by reaction crystallization method (RCM). An aqueous solution of 2% w/w SLS and 3.5m NCT was prepared, to which anhydrous LAM was added and stirred for 24hrs at ambient temperature. Cocrystalline solid phase was analyzed by PXRD, DSC and HPLC to confirm crystalline form and phase purity. LAM-SAC salt was synthesized by adding stoichiometric weight fraction of anhydrous LAM to a SAC solution of known concentration. The solid phase was filtered after approximately 24hrs and confirmed by PXRD, DSC and HPLC. The saturated solution of LAM-SAC solid phase equilibrated to a pH of 3.4.

Powder X-ray Diffraction (PXRD)

PXRD patterns of solid phases were recorded with a Rigaku MiniFlex X-ray diffractometer (Danvers, MA) using Cu Kα radiation (λ = 1.5418 Å), a tube voltage of 30 kV, and a tube current of 15 mA. The intensities were measured at 2θ values from 2° to 30° with a continuous scan rate of 2.5°/min.

Thermal Analysis

Crystalline samples of 2-4 mg were analyzed by differential scanning calorimetry (DSC) using a TA instrument (Newark, DE) 2910 MDSC system equipped with a refrigerated cooling unit. DSC experiments were performed by heating the samples at a rate of 10 K/min under a dry nitrogen atmosphere. Temperature and enthalpy calibration of the instruments was achieved by using a high purity indium standard. Cocrystal samples for DSC analysis comprised of dried power isolated from slurries by vacuum filtration followed by air drying step. The isolated dried powder was characterized by PXRD before DSC analysis and HPLC for purity. The mean result of a minimum of three samples is reported for each substance.

Solubility Measurements

All solubility measurements were carried out in aqueous medium at 25º±0.1C. pH was adjusted by adding pH 2 phosphate buffer or 0.1N NaOH. Solution concentrations of both components of cocrystal and salt were measured by HPLC. Solutions were considered to have reached equilibrium when less than 5% change in concentration was detected in either component of the cocrystal or salt when measured subsequently over a period of 24-72 hours. Solid phases were characterized by PXRD and DSC to determine any phase transformation at the end of the solubility measurements. Equilibrium solubility measurement of LAM-SAC salt was made since salt was the stable phase below pH_{max}. Thermodynamic solubility of LAM-NCT·H_2O cocrystal was calculated from eutectic point concentration measurements of LAM and NCT. At the eutectic point solid LAM·H_2O and LAM-NCT·H_2O cocrystal are in equilibrium with the solution and represents cocrystal equilibrium solubility under non stoichiometric conditions[4, 23].

Determination of Eutectic Point Concentrations and K_{sp}

Eutectic point was established by the presence of two solid phases, LAM·H_2O and LAM-NCT·H_2O cocrystal in equilibrium with the solution. The presence of solid phases was confirmed by PXRD and DSC. Samples were confirmed to have two solid phases for at least 24-48hrs before isolating the solution and analyzing by HPLC for concentrations. Eutectic point was obtained from supersaturated conditions by dissolving cocrystal in saturated LAM solution containing excess solid LAM·H_2O and from undersaturation by dissolution of cocrystal. By measuring the eutectic point concentration of cocrystal components and the solution pH, the solubility product (K_{sp}) value which is defined as the product of solution concentration of cocrystal components in their un-ionized state (LAM and NCT) was determined according to equation (3.1). Similarly, K_{sp} for LAM-SAC salt was calculated by measuring the solution concentrations of $LAMH^+$ and SAC^- according to equation (3.8) with excess solid LAM-SAC salt in equilibrium with the solution.

Measurement of Micellar Solubilization Constant, (Ks)

Excess solid was equilibrated in varying concentrations of aqueous SLS solutions. Samples were maintained at 25±0.1ºC for the duration of 24hrs. Solid phases were analyzed by PXRD and the solution concentrations by HPLC.

High-Performance Liquid Chromatography (HPLC)

Purity and stoichiometry of the LAM cocrystal and salt was analyzed by HPLC before carrying out pH dependent solubility studies and eutectic measurement studies. Solution concentrations of drug and coformer were analyzed by Waters HPLC (Milford, MA)

equipped with a UV/vis spectrometer detector. A C18 Atlantis column (5 μm, 4.6 × 250 mm; Waters, Milford, MA) at ambient temperature was used to separate the drug and the coformer. An isocratic method with a water, methanol, and trifluoroacetic acid mobile phase was used with a flow rate of 1 mL/min. Sample injection volume was 20μL. Absorbance of the drug and coformer analytes was monitored between 210-300nm. Empower software from Waters Inc., was used to analyze the data. All concentrations, unless otherwise indicated are reported in molality (moles solute/kilogram solvent).

Results and Discussion

Solubility-pH dependence of salt and cocrystal forms

Solubilities of the weakly basic drug LAM, a 1:1 cocrystal form (LAM-NCT·H_2O), and a 1:1 salt form (LAM-SAC) were measured under equilibrium conditions. The solubility-pH dependence was evaluated by considering the appropriate solid solution dissociation equilibria of cocrystal, salt and the corresponding equilibrium constants (constituent ionization constant values (K_a) and solubility product (K_{sp}) of cocrystal and salt). The solubility of LAM-NCT·H_2O cocrystal, composed of a weakly basic drug and a nonionizable coformer, can be expressed as

$$S_{cocrystal} = [LAM]_T = \frac{K_{sp}}{[NCT]_T}\left(1 + \frac{[H^+]}{K_{a,BH^+}}\right) \quad (3.1)$$

K_{sp} is the cocrystal solubility product given by

$$LAM\text{-}NCT_{solid} \rightleftharpoons^{K_{sp}} LAM_{soln} + NCT_{soln}$$

$$K_{sp} = [LAM][NCT] \quad (3.2)$$

K_{a,BH^+} is the ionization constant of the conjugate acid of weakly basic LAM,

$$LAMH^+ \overset{K_a}{\rightleftharpoons} LAM + H^+ \tag{3.3}$$

$$K_{a,BH^+} = \frac{[LAM][H^+]}{[LAMH^+]} \tag{3.4}$$

Under stoichiometric solution composition, $[LAM]_T = [NCT]_T$, equation (1) becomes

$$S_{cocrystal} = \sqrt{K_{sp}\left(1 + \frac{[H^+]}{K_{a,BH^+}}\right)} \tag{3.5}$$

When $\frac{[H^+]}{K_{a,BH^+}} << 1$, i.e., at pH where LAM is mostly in its un-ionized form, equation (3.5) can be written to define the cocrystal intrinsic solubility $S_{0,cocrystal}$ as,

$$S_{0,Cocrystal} = \sqrt{K_{sp}}$$

$[LMT]_T$ is the total concentration of LAM which is the sum of ionized and un-ionized species,

$$[LMT]_T = [LAM] + [LAMH^+] \tag{3.6}$$

The solubility dependence on H^+ for lamotrigine is given by

$$S_{drug} = S_{0,drug}\left(1 + \frac{[H^+]}{K_{a,BH^+}}\right) \tag{3.7}$$

where $S_{0,drug}$ is the solubility of the unionized free base, $[LAM]_0$, or intrinsic drug solubility. Comparing equations (3.5) and (3.7) shows that cocrystal and drug solubilities differ in their pH dependence. Cocrystal solubility has a weaker dependence on $[H^+]$, which corresponds to the square root of the drug solubility dependence. For instance at $[H^+] = K_a$

$$S_{cocrystal} = \sqrt{2K_{sp}} = \sqrt{2}\, S_{0,cocrystal}$$

and

$$S_{drug} = 2S_{0,drug}$$

Likewise, the solubility of LAM-SAC salt is given by

$$S_{salt} = [LAM]_T = \frac{K_{sp}}{[SAC]_T}\left(1+\frac{K_{a,BH^+}}{[H^+]}\right)\left(1+\frac{[H^+]}{K_{a,HA}}\right) \quad (3.8)$$

where K_{sp} is the solubility product of the salt, and $K_{a,HA}$ is the acid ionization constant given by the following equilibria,

$$LAMH^+SAC^-_{solid} \overset{K_{sp}}{\rightleftharpoons} LAMH^+_{soln} + SAC^-_{soln}$$

$$K_{sp} = [LAMH^+][SAC^-] \quad (3.9)$$

$$SAC \overset{K_a}{\rightleftharpoons} SAC^- + H^+$$

$$K_{a,HA} = \frac{[SAC^-][H^+]}{[SAC]} \quad (3.10)$$

and under stoichiometric solution composition equation (3.8) can be expressed as,

$$S_{salt} = \sqrt{K_{sp}\left(1+\frac{K_{a,BH^+}}{[H^+]}\right)\left(1+\frac{[H^+]}{K_{a,HA}}\right)} \quad (3.11)$$

When $\frac{K_{a,BH^+}}{[H^+]}$ and $\frac{[H^+]}{K_{a,HA}}$ are << 1, i.e., at pH values where both LAM and SAC are largely present as ionized species then equation (3.11) can be simplified to represent the intrinsic solubility of the salt,

$$S_{0,salt} = \sqrt{K_{sp}} \quad (3.12)$$

Thus salt solubility dependence on $[H^+]$ is also weaker than the drug solubility dependence and is different from that of a cocrystal. Species without subscripts indicate

solution phase and brackets represent the solution concentration in molality unless mentioned otherwise. The analysis presented here assumes ideal behavior with concentrations replacing activities in the equilibrium constants.

Significance of Eutectic Point Concentrations and Calculation of K_{sp}

Since cocrystal and salt solubilities are highly dependent on the solution composition of their constituents, solubilities were evaluated from measurement of both cocrystal and salt constituent concentrations ([LAM] and [NCT] or [SAC]) and pH at equilibrium with solid phases according to the above equations. This is critical to ensure that solid phase purity did not inadvertently influence solubility measurements. K_{sp} of LAM-NCT·H_2O cocrystal was calculated according to equation (3.1) by measuring eutectic concentrations $[LAM]_{eu}$ and $[NCT]_{eu}$ which represents the cocrystal solubility under non-stoichiometric conditions with solid cocrystal and drug in equilibrium with the solution. This K_{sp} value was then used to calculate the stoichiometric solubility-pH dependence of the cocrystal according to equation (3.5). Analytical solution concentrations of cocrystal components at the eutectic point are given in table 3.1. The eutectic constant (K_{eu}) which is the ratio of coformer to drug eutectic concentration has shown to be useful in predicting cocrystal stoichiometric solubility. The ratio of $[NCT]_{eu}$ to $[LAM]_{eu}$ is 480. For a 1:1 cocrystal the square root of K_{eu} is equal to the solubility ratio of cocrystal to the drug.[24] For LAM-NCT·H_2O cocrystal, this solubility ratio is 30 and the square root of K_{eu} is 22. These values are reasonably close, enabling the estimation of cocrystal stoichiometric solubility from eutectic concentrations of cocrystal components. K_{sp} for LAM-SAC salt was calculated by measuring the solution concentrations of $LAMH^+$ and SAC^- according to equation (3.8) with excess solid LAM-

SAC salt in equilibrium with the solution. Equation (3.11) was used to generate the solubility pH dependence of the salt (Figure 3.1). The eutectic concentrations, K_{sp} values as well as cocrystal and salt solubilities are presented in Table 3.1.

Table 3.1: Eutectic concentration of LAM and NCT in water, K_{sp} and solubility of LAM-NCT·H_2O cocrystal and LAM-SAC salt.

Solid Phase	$[LAM]_{eu}$ (m)	$[NCT]_{eu}$ (m)	K_{sp} (m^2)	S_0 (m)
LAM-NCT·H_2O*	$(9.25 \pm 0.44) \times 10^{-4}$	$(4.43 \pm 0.07) \times 10^{-1}$	$(4.1 \pm 0.26) \times 10^{-4}$	2.02×10^{-2}
LAM-SAC**	-	-	$(1.1 \pm 0.31) \times 10^{-5}$	3.26×10^{-3}

* *The average pH of $[LAM]_{eu}$ and $[NCT]_{eu}$ concentration measurement was 8.1 ± 0.15*
** *LAM-SAC salt is thermodynamically stable below pH 5.0 enabling measurement of K_{sp} from $LAMH^+$ and SAC^- concentrations according to equation* (3.8).

Solubility Advantage and pH_{max} of Cocrystals and Salts of LAM

Figure 3.1 shows the effect of $[H^+]$ on the solubilities on LAM-NCT·H_2O cocrystal, LAM-SAC salt and LAM·H_2O. These results reveal several important features regarding the solubility and stability of cocrystal and salt forms of lamotrigine. LAM-NCT·H_2O cocrystal is 30 times more soluble than LAM·H_2O and LAM-SAC salt is 6 times more soluble than LAM·H_2O. These solubility comparisons are made using the intrinsic solubility values of solid phases given in Table 3.2 Cocrystal and salt exhibit very different solubility-pH dependence as a result of the ionization behavior of their constituents. LAM-NCT·H_2O cocrystal is the most soluble form between pH 2.7 and 7.0 and LAM-SAC salt is the least soluble form below pH 5.0. The cocrystal with a nonionizable coformer follows a pH dependent behavior determined by the ionization of the drug (pK_a 5.7) and solubility increases with pH values above pK_a. In contrast, the salt with an acidic counterion (SAC) of much lower pK_a (1.8) than the drug exhibits a U

shape curve, where salt solubility is independent of pH between 2.5 and 5.0 which was determined graphically. Above these pH values, salt solubility increases.

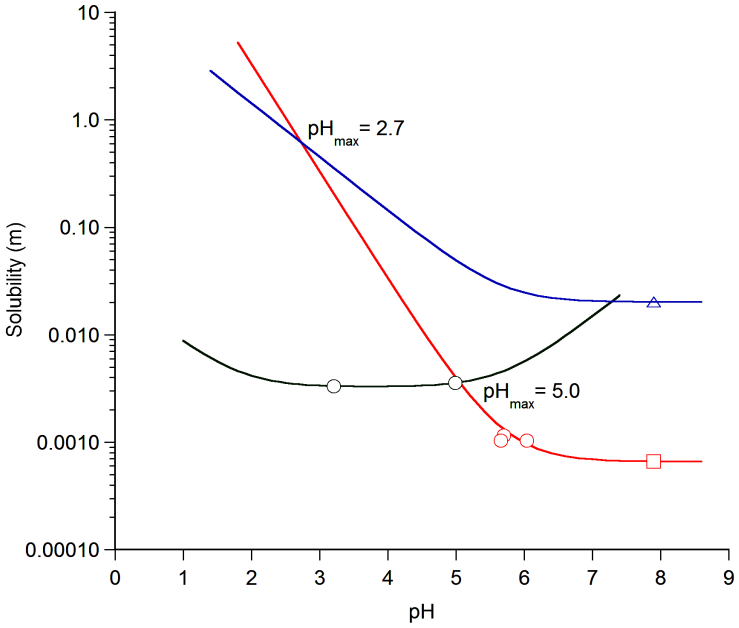

Figure 3.1: Stoichiometric solubility 2.02 x 10^{-2}(m) of LAM-NCT·H_2O cocrystal is represented by (△) and (—) represents solubility pH dependence generated using K_{sp} = 4.10x10^{-4} m^2. Green (○) represents LAM-SAC salt solubility and red (○) represent [LAM] from LAM-SAC salt transformed to LAM·H_2O. Solubility dependence on pH of LAM-SAC salt (—) and LAM·H_2O (—) were generated using salt K_{sp} = 1.1x$10^{-5}m^2$ and measured LAM·H_2O solubility of 6.6x10^{-4} m represented by (□) according to equations (3.11) and (3.7) respectively.

It is important to note that cocrystal and salt solubility curves each intersect the drug solubility curve at a specific pH value, corresponding to the pH_{max}, also referred to as Gibbs pK_a[2]. At this pH two solids (LAM·H_2O and cocrystal or salt) coexist in equilibrium with solution. The pH_{max} can be read off the graph for cocrystal at pH = 2.7 and for the salt at pH = 5.0. This means that at pH > 2.7, cocrystal is more soluble than LAM·H_2O whereas for the salt this increase in solubility over drug occurs at pH > 5.0. pH_{max} is an important parameter in solid form selection and formulation design as it

establishes the range of thermodynamic stability for salts and cocrystals as well as the pH above which either salt or cocrystal can form.

Recently, dissolution behavior of several cocrystals and salts of LAM at pH 5.5 and 1.0 was investigated and the data was used for solubility assessement[18]. We utilized the reported steady state dissolution concentrations to estimate the K_{sp} of LAM-Methylparaben (LAM-MP) cocrystal. At the steady state LAM-MP cocrystal was in equilibrium with the solution. Solubility of LAM·HCl salt was also estimated for comparison with other solid forms of LAM as well as to investigate the effect of [Cl^-] on LAM·HCl salt solubility. K_{sp} of LAM·HCl salt was calculated from reported solubility of 0.46 mg/ml at 37ºC in pH 1.2 medium[12] and the solubility at 25ºC was estimated by using a heat of solution value of 30 kJ/mol. A difference of ± 10 kJ/mol in the heat of solution changes the solubility by ± 8% and the pH_{max} by ± 1 %. Solubilities were calculated under non-ionized conditions for cocrystals (pH 8) and fully ionized conditions for salts (pH 1 for HCl and pH 4 for SAC). The importance of phase transformations is also utilized to understand the trends in the reported maximum concentration (C_{max}) achieved during the dissolution studies[18]. Table containing the values of C_{max}, steady sate concentrations, measured and estimated solubilities as well as initial and final pH of the dissolution medium is provided in the appendix.

The solubility comparison of LAM crystalline forms and the dependence of solubility on pH are extremely critical to understand the role of (i) phase transformations on dissolution behavior of solid forms, (ii) role of pH on phase stability and the observed kinetic solubility and, (iii) role of coformer solubility on cocrystal and salt solubilities. Table 3.2 summarizes the cocrystal and salt K_{sp} and solubility ($S_{0,CC/Salt}$) values, $S_{0,CC/Salt}$

relative to $S_{0,LAM\cdot H_2O}$, ratio of maximum concentration achieved during dissolution (C_{max}) with respect to $S_{0,LAM\cdot H_2O}$ solubility and pH_{max}.

Table 3.2: K_{sp}, solubility of cocrystals, salts and LAM·H_2O, solubility ratios of cocrystals and salts relative to LAM·H_2O, Ratio of maximum concentration (C_{max}) of cocrystals and salts relative to LAM·H_2O solubility and pH_{max} of solid forms.

Solid phase	K_{sp} ± Std. Dev. (m^2)	$S_{0,CC/Salt}$ (m)	$\frac{S_{0,CC/Salt}}{S_{0,LAM\cdot H_2O}}$	$\frac{C_{max}}{S_{0,LAM\cdot H_2O}}$	pH_{max}
LAM-SAC Salt	$(1.1 \pm 0.31) \times 10^{-5}$	3.3×10^{-3}	6	2.66	5.0
Anhydrous LAM	-	-	-	1.66	-
LAM-NCT·H_2O Cocrystal	$(4.1 \pm 0.27) \times 10^{-4}$	2.0×10^{-2}	30	1.36	2.7
LAM-MP Cocrystal	$(5.3 \pm 0.47) \times 10^{-7}$	7.3×10^{-4}	1.1	1.24	6.4
LAM-HCl Salt	$(6.7 \pm 0.53) \times 10^{-5}$	8.2×10^{-3}	13	-	4.6
LAM-HCl Salt*			1*	-	5.8

* *LAM-HCl salt solubility estimated in 0.1M HCl. The lowering of solubility ratio is due to common ion effect in the presence of 0.1M HCl.*

Table 3.2 shows that cocrystals can have much higher aqueous solubilities than salts and cocrystal solubility is highly pH dependent. K_{sp} increases with LAM-NCT > LAM-SAC > LAM-MP. At the pH of saturated aqueous solutions LAM-NCT·H_2O cocrystal is 30 times more soluble than LAM·H_2O, LAM-SAC salt is 6 times more soluble than LAM·H_2O and LAM-MP cocrystal has a solubility value similar to LAM·H_2O. The solubility of the hydrochloride salt will depend on the presence of Cl^- concentration. In the absence of Cl^- ion, the solubility of the salt is 13 times greater than LAM·H_2O solubility. It is noteworthy that the order of C_{max} (LAM-SAC > LAM-ANHYD > LAM-NCT·H_2O > LAM-MP) is not consistent with the equilibrium solubility order. LAM-NCT·H_2O cocrystal exhibits lower C_{max} relative to anhydrous LAM and LAM-SAC salt

in spite of its higher solubility in water (neutral pH range) due to solution mediated phase transformation of cocrystal to LAM·H_2O. Results in Table 3.2 show that within this small series of LAM cocrystals and salts there is a wide range of pH_{max} values. The pH_{max} varies by about 3 units within the cocrystals, and increases with increase in cocrystal K_{sp}. This trend is similar to that observed for salts, however, for cocrystals, pH_{max} is more sensitive on the cocrystal to drug solubility ratio (by 2 pH units) as indicated by the following equations. For a cocrystal,

$$pH_{max}^{cc} = pK_{a,BH^+} - \log\left(\frac{K_{sp}}{S_{0,drug}^2} - 1\right) \tag{3.13}$$

When $\frac{K_{sp}}{S_{0,drug}^2} >> 1$ equation (3.13) becomes,

$$pH_{max}^{cc} = pK_{a,BH^+} - \log\left(\frac{K_{sp}}{S_{0,drug}^2}\right) \tag{3.14}$$

which simplifies to

$$pH_{max}^{cc} = pK_{a,BH^+} - 2\log\left(\frac{S_{cocrystal}}{S_{0,drug}}\right) \tag{3.15}$$

when $K_{sp} = S_{cocrystal}^2$.

Similar analysis for a salt of a basic drug leads to the well-known pH_{max} relationships[14, 15].

$$pH_{max}^{salt} = pK_{a,BH^+} - \log\left(\frac{\sqrt{K_{sp}}}{S_{0,drug}}\right) \tag{3.16}$$

$$pH_{max}^{salt} = pK_{a,BH^+} - \log\left(\frac{S_{salt}}{S_{0,drug}}\right) \tag{3.17}$$

This analysis demonstrates the impact of cocrystal and salt solubilities on pH_{max} and on the corresponding thermodynamic stability regions. Thus an increase in drug solubility by a factor of 10 will result in pH_{max} values of pKa – 2 for a cocrystal and pKa – 1 for a salt. The measured pH_{max} for the LAM-SAC salt is in excellent agreement with that calculated from equation (3.17). The pH_{max} of LAM-NCT·H_2O cocrystal is calculated to be 2.7, but experimental measurement was not possible since pH could not be independently adjusted below pH 5.0 due to the self buffering effect of LAM. The LAM-SAC salt and LAM-NCT·H_2O cocrystal are also shown to attain equal solubilities at a pH value of 7.3. This solubility is about 30 times higher than the solubility of LAM·H_2O.

Figure 3.2 show the solubility ratios of both LAM-NCT·H_2O and LAM-SAC salt relative to LAM·H_2O increase with increasing pH. Cocrystal solubility reaches a maximum value and plateaus near pH 7 while the salt solubility continues to increase with pH. This result in the intersection of the cocrystal and salt pH dependent solubility curves where the two solid forms exhibit equal solubilities at pH 7.3, while below pH 7.3 cocrystal solubility is higher than that of salt relative to LAM·H_2O.

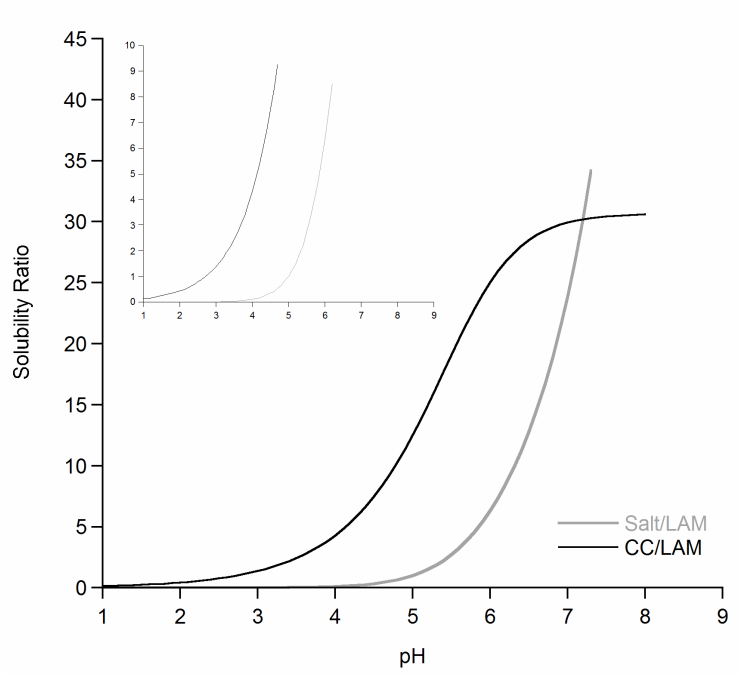

Figure 3.2: Solubility ratio of LAM-NCT·H_2O and LAM-SAC relative to LAM·H_2O as a function of pH is shown. At pH 7.3 the cocrystal and salt solubility ratios are equal. The solubility ratio difference in the lower pH range of 1-4 which is relevant to the gastric and upper GI tract environment is highlighted by the inset.

The results for LAM·H_2O are in good agreement with previous reports.[9, 11, 12] There is some discrepancy in the solubility values of the salt, with higher values measured in this work of 2 to 3 fold higher than those reported by Galcera[10] and by Cheney[18]. There is huge discrepancy, however, in the solubility values of the cocrystal, with values 30 fold higher than those reported by Cheney et al. at pH 6.2 (equilibrium pH of the dissolution medium after 250mins)[18]. Cheney et al. used kinetic methods for their solubility measurements and in this work we used equilibrium methods. The source of this large disagreement between solubility measurements appears to be the fast transformation of cocrystal to the less soluble drug or the HCl salt depending on the pH. In another recently published report, Chadha et. al., observed that LAM concentration

from LAM·H_2O and LAM-NCT·H_2O increases as the pH is lowered, however the concentration of LAM from LAM-SAC salt increased when the pH was lowered from 7 to 5 but declined as the pH was lowered below 5. This is due to the fact that LAM is more soluble than LAM-SAC salt below pH 5.0. Chadha et. al., report that LAM-NCT·H_2O transformed to LAM-H_2O and the pH at equilibrium (400mins) was 6.6, while the LAM-SAC salt was the stable phase at equilibrium pH of 4.5[25]. These results are in excellent agreement with the pH dependent solubility behavior shown in Figure 3.1 and Figure 3.3.

In contrast to the dissolution data reported in water, dissolution studies at pH 1 showed higher LAM concentration from LAM-ANHYD, LAM-NCT·H_2O and LAM-MP cocrystals relative to LAM-SAC. Dissolution in pH 1 medium results in LAM-NCT·H_2O cocrystal maintaining a higher concentration relative to LAM-ANHYD and LAM-SAC.[18] This is likely due to faster transformation of LAM to LAM·HCl due to its higher solubility relative to LAM-NCT·H_2O cocrystal at pH 1 (Figure 3.1 and Figure 3.3). LAM-SAC and LAM·HCl salts have similar solubilities in water at pH 1, i.e., in the absence of chloride ion. However due to common ion effect in 0.1M HCl solution, LAM-HCl salt has 11.4 fold lower solubility (dashed line in Figure 3.3) relative to its solubility in water. Thus, LAM·HCl salt being the thermodynamically most stable form at pH 1, all solid forms transformed to LAM·HCl salt in the presence of Cl^- during dissolution experiment carried out at pH 1[18].

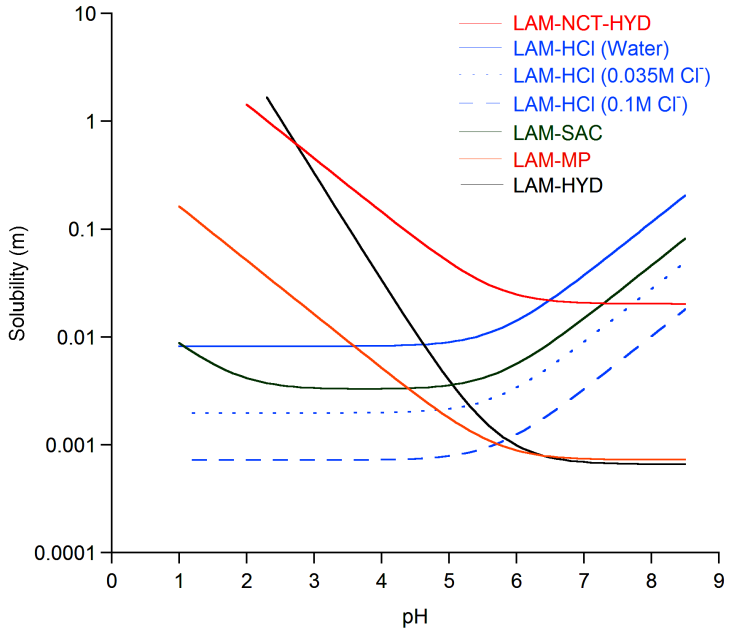

Figure 3.3: Solubility pH dependence of LAM solid forms calculated from K_{sp} values given in Table 3.2 and equations that describe the solubility pH dependence of cocrystals and salts. Common ion effect on solubility of LAM·HCl salt in 0.1M and 0.035M HCl is shown to simulate Cl^- concentration of pH 1 dissolution medium and rat gastric environment respectively.

Rate of transformation of metastable forms, pH of the GI environment and common ions present can significantly affect the bioavailability of solid forms. It has been shown that the presence of chloride ion in gastric environment suppresses the dissolution of HCl salts[26]. One of the commonly used animal models for *in-vivo* estimation of bioavailability involves administering the drug to rats. The Cl^- ion concentration in rat stomach is reported to be as high as 35mM, while pH of rat stomach ranges from 3-5 in fasted state[27]. In this pH range and in presence of 35mM Cl^- ion, LAM-HCl salt solubility is lowered by a factor of 4.2 relative to in water in the absence of Cl^- (Figure 3.3). In the report where LAM-NCT·H_2O cocrystal, LAM-SAC salt and LAM-ANHYD were dosed to Sprague-Dawley rats, the observed trend in plasma concentration was similar to that observed from dissolution studies in water (pH 5.5)[18].

These trends are due to transformation of metastable forms and do not reflect the true thermodynamic solubility of LAM crystalline forms. Table A2.1 in appendix summarizes the measured cocrystal and salt equilibrium solubilities from this work as well as, $C_{max,}$ steady state (SS) concentrations, initial and final solid phases and pH from reported dissolution data.

LAM-NCT·H_2O Synthesis and Micellar Solubilization

Cocrystal synthesis and screening methods have drawn a lot of attention in recent years. Several methods to screen cocrystals have been published such as, synthesis from slurry (reaction crystallization method), grinding of cocrystal components in a mill or with the aid of a small quantity of solvent as well as thermal methods such as cocrystallization from the melt[28-30]. Two methods are reported for the synthesis of LAM-NCT·H_2O cocrystal, (i) slurrying a 1:2 mixture of LAM and NCT in ethyl acetate, and (ii) slow evaporation of LAM and NCT solution in *n-butanol*[31]. Our attempts to synthesize LAM-NCT·H_2O cocrystal from these reported methods did not yield a cocrystalline solid phase. Several other methods reported to generate cocrystals, such as, reaction crystallization method (RCM) where LAM·H_2O was added to near saturated solutions of NCT, grinding of reactants in a ball mill, grinding with small amount of water as well as by melting of reactants were also applied. None of these attempts were successful in synthesizing the cocrystal. LAM-NCT·H_2O cocrystal could only be synthesized by RCM in the presence of 2% w/w SLS aqueous solution. Further investigation was carried out to understand the role of SLS on the solubilization of LAM-NCT·H_2O cocrystal and its components.

Recently the role of surfactants in stabilizing cocrystals against solution mediated transformation has been reported where stabilization of the cocrystal is achieved via the differential solubilization of cocrystal components in micellar solution. It is shown that above a critical surfactant concentration, cocrystal is the thermodynamically stable solid phase relative to its components. This critical surfactant concentration is referred as the 'critical stabilization concentration' (CSC)[22, 32]. Since LAM-NCT·H_2O cocrystal could only be synthesized from 2% w/w SLS solution, the solubility of LAM·H_2O and LAM-NCT·H_2O cocrystal was measured as a function of micellar concentration to evaluate if SLS could be used to stabilize the cocrystal. The stoichiometric solubility of cocrystal in SLS solution was estimated in a similar fashion as estimated in water, i.e., by measuring the eutectic concentration of LAM and NCT in SLS solution. Table 3.3 show the values of measured eutectic concentrations of LAM and NCT and cocrystal solubility in SLS solution according to equation (3.27).

Table 3.3: Eutectic concentration of cocrystal components, LAM·H_2O and cocrystal solubility in 2% w/w SLS solution

$[LAM]_{eu}^{SLS}$ (m)	$[NCT]_{eu}^{SLS}$ (m)	$S_{LAM\cdot H_2O}^{SLS}$ (m)	S_{cc}^{SLS} (m)
$(5.6 \pm 0.16) \times 10^{-3}$	$(5.1 \pm 0.06) \times 10^{-1}$	$(4.9 \pm 0.24) \times 10^{-3}$	5.2×10^{-2}

The effect of differential solubilization on cocrystal solubility is modeled from the homogenous and heterogeneous reaction equilibria that describe cocrystal solubility product behavior and ionization of cocrystal components[16, 17, 23]. The relevant equilibria for a 1:1 cocrystal (LAM-NCT·H_2O), in surfactant solutions of micellar concentration [M] are,

$$LAM-NCT \rightleftharpoons LAM_{aq} + NCT_{aq} \qquad K_{sp} = [LAM]_{aq}[NCT]_{aq} \tag{3.18}$$

$$LAM_{aq} + M \overset{K_s^{LAM}}{\rightleftharpoons} LAM_m \qquad K_s^{LAM} = \frac{[LAM]_m}{[LAM]_{aq}][M]} \tag{3.19}$$

$$NCT_{aq} + M \overset{K_s^{NCT}}{\rightleftharpoons} NCT_m \qquad K_s^{NCT} = \frac{[NCT]_m}{[NCT]_{aq}[M]} \tag{3.20}$$

$$LAMH^+_{aq} \rightleftharpoons LAM + H^+ \qquad K_{a,LAMH^+} = \frac{[LAM_{aq}][H^+]}{[LAMH^+_{aq}]} \tag{3.21}$$

$$LAMH^+_{aq} + M \overset{K_s^{LAMH^+}}{\rightleftharpoons} LAMH^+{}_m \qquad K_s^{LAMH^+} = \frac{[LAMH^+]_m}{[LAMH^+]_m[M]} \tag{3.22}$$

$$[M] = [C_{surf}] - [CMC]$$

The subscript aq and m denotes species in the aqueous and micellar phases respectively. C_{surf} is the total concentration of the surfactant, CMC is the critical micellar concentration, which is reported to be 8mM for SLS in water[33]. The micellar surfactant concentration [M] is the total surfactant concentration minus the CMC. K_s^{LAM} and K_s^{NCT} are the equilibrium constants for the solubilization of LAM and NCT respectively. Activities are replaced by concentrations as a first approximation applicable to dilute solutions. The total solubility of cocrystal, $S_{CC,Total} = S_{aq} + S_m$ is derived by considering the above equilibria and mass balance on LAM and NCT,

$$LAM_T = [LAM]_{aq} + [LAM]_m + [LAMH^+] + [LAMH^+]_m \tag{3.23}$$

$$NCT_T = [NCT]_{aq} + [NCT]_m \tag{3.24}$$

From the above equilibria and equations (3.23) and (3.24), the solubility of cocrystal as a function of micellar concentration can be represented as,

$$[LMT]_T = \frac{K_{sp}}{[NCT]_T}\left(1+K_s^{NCT}[M]\right)\left(1+\frac{[H^+]}{K_{a,LAMH^+}}+K_s^{LAM}[M]+\frac{[H^+]}{K_{a,LAMH^+}}K_s^{LAMH^+}[M]\right) \quad (3.25)$$

Under stoichiometric conditions, equation (3.25) can be expressed as,

$$S_{CC} = \sqrt{K_{sp}\left(1+K_s^{NCT}[M]\right)\left(1+\frac{[H^+]}{K_{a,LAMH^+}}+K_s^{LAM}[M]+\frac{[H^+]}{K_{a,LAMH^+}}K_s^{LAMH^+}[M]\right)} \quad (3.26)$$

The CMC is assumed to be constant in the concentrations and solubilization ranges reported here. It is common for $K_s^{LAM} >> K_s^{LAMH^+}$ as the micellar solubilization negligibly affects the total solubility of the ionized species, unless high concentration of ionized species are present[34-36]. Under these conditions, equation (3.26) can be simplified to,

$$S_{CC} = \sqrt{K_{sp}\left(1+K_s^{NCT}[M]\right)\left(1+K_s^{LAM}[M]+\frac{[H^+]}{K_{a,LAMH^+}}\right)} \quad (3.27)$$

Equation (3.27) applies to cocrystal solubility in solutions of stoichiometric concentrations (equimolar concentration of cocrystal components) and shows that cocrystal solubility increases with increasing K_{sp}, component micellar solubilization constants (K_s^{LAM} and K_s^{NCT}) and ionization of weakly basic drug LAM. From the unionized aqueous solubility of LAM ($[LAM]_0$) and using the equilibria shown, the total drug concentration ($[LAM]_{Total}$) as a function of micellar concentration [M] can be calculated by,

$$[LAM]_{Total} = [LAM]_0\left(1+K_s^{LAM}[M]+\frac{[H^+]}{K_{a,LAMH^+}}+K_s^{LAMH^+}[M]\frac{[H^+]}{K_{a,LAMH^+}}\right) \quad (3.28)$$

Since the micellar solubilization of LAM·H_2O was measured under non-ionizing conditions (pH 7.9), $[LAM]_{Total}$ can be approximated by,

$$[\mathrm{LAM}]_{\mathrm{Total}} = [\mathrm{LAM}]_0 \left(1 + \mathrm{K_s^{LAM}}[\mathrm{M}]\right) \tag{3.29}$$

The solubilization constant K_s and ionization constant K_a values are often reported in the literature and cocrystal solubility can be easily calculated from a single measurement of cocrystal K_{sp} and solution pH. However, solubility of LAM·H_2O and NCT as a function of SLS concentration is not reported to the best of our knowledge, therefore K_s was experimentally measured for both LAM·H_2O and NCT. From the equilibria shown for partitioning of LAM (or NCT) in a micelle, the total drug in solution is given by,

$$[\mathrm{LAM}]_{\mathrm{T}} = [\mathrm{LAM}]_{\mathrm{aq}} + [\mathrm{LAM}]_{\mathrm{m}} \tag{3.30}$$

Substituting the equilibrium constants in to equation (3.30) gives,

$$[\mathrm{LMT}]_{\mathrm{T}} = \mathrm{LAM}_{\mathrm{aq}}(1 + \mathrm{K_s^{LAM}}[\mathrm{M}]) \tag{3.31}$$

$$\frac{\mathrm{LAM_T} - \mathrm{LAM_{aq}}}{\mathrm{LAM_{aq}}} = \mathrm{K_s^{LAM}}[\mathrm{M}] \tag{3.32}$$

Likewise for NCT,

$$\frac{\mathrm{NCT_T} - \mathrm{NCT_{aq}}}{\mathrm{NCT_{aq}}} = \mathrm{K_s^{NCT}}[\mathrm{M}] \tag{3.33}$$

K_s for LAM·H_2O and NCT were calculated from the slope according to equation (3.32) and (3.33) by plotting total LAM and NCT concentrations against micellar concentrations. All measurements were carried out at pH 7.9 where LAM·H_2O and NCT are in their non-ionized state, the data is summarized in Table 3.4.

Table 3.4: LAM and NCT solubility as a function of micellar concentration used to calculate the solubilization constant (K_s) of LAM and NCT according to equations (3.32) and (3.33).

$[M]^1$ (m)	$[LAM]_T$ (m)	$[M]^2$ (m)	$[NCT]_T$ (m)
9.0×10^{-3}	1.8×10^{-3}	9.7×10^{-3}	4.21
2.6×10^{-2}	2.9×10^{-3}	3.4×10^{-2}	4.28
5.0×10^{-2}	4.2×10^{-3}	6.0×10^{-2}	4.33
6.0×10^{-2}	4.7×10^{-3}	7.7×10^{-2}	4.36

Superscripts 1 and 2 represents the micellar concentrations at which $[LAM]_T$ and $[NCT]_T$ were measured respectively.

Figure 3.4 shows the plots used to calculate the value of K_s for LAM and NCT according to equations (3.32) and (3.33) by using aqueous solubility values of cocrystal components ($[LMT]_{aq} = 6.6 \times 10^{-4}$ (m) and $[NCT]_{aq} = 4.2$ (m)). The calculated K_s values for LAM·H_2O and NCT are $88.4 m^{-1}$ and $0.5 m^{-1}$ respectively. These results are in agreement with the literature findings suggesting that micellar solubilization is larger for compounds that are more hydrophobic relative to those that are hydrophilic[37, 38].

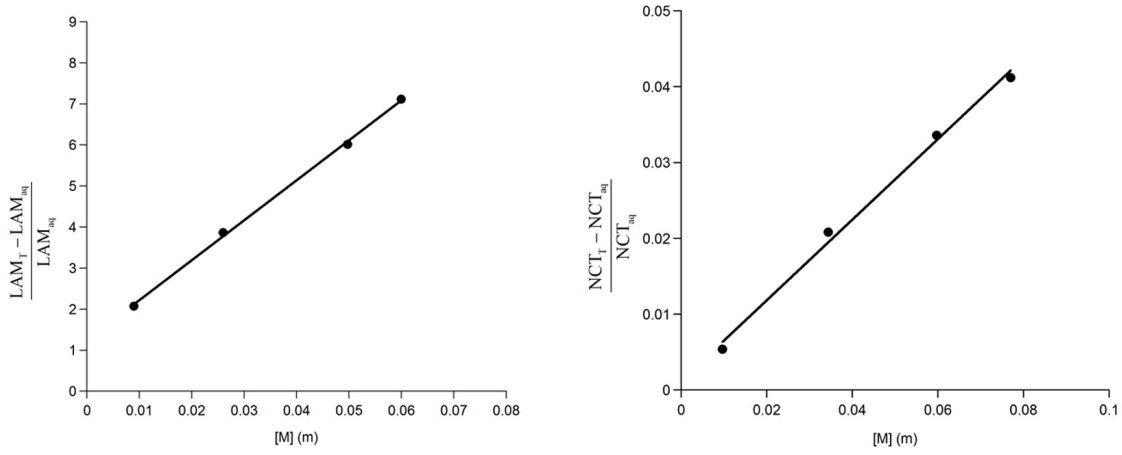

Figure 3.4: $\frac{LAM_T - LAM_{aq}}{LAM_{aq}}$ for LAM and $\frac{NCT_T - NCT_{aq}}{NCT_{aq}}$ for NCT plotted as a function of micellar concentration for LAM·H_2O and NCT. Subscript T and aq represents the total concentration in SLS solution and aqueous solubility respectively of LAM·H_2O and NCT. Slope represents the micellar solubilization capacity (K_s) of LAM·H_2O and NCT by SLS. pH of solutions were in the range of 7.9 – 9.2.

A more rigorous analysis to evaluate the parameters that govern the CSC would be useful not only to establish confidence in the existence of CSC but also to understand the conditions under which a CSC would be present and its magnitude. The mathematical expression that describes the CSC for a cocrystal of a monoprotic base and a non-ionic coformer is given by equation (3.34), which is derived by setting equations (3.27) and (3.28) equal to each other, a thermodynamically defined condition for CSC**.**

$$CSC = \frac{\frac{K_{sp}}{S_{0,LAM}{}^2} - \left(1 + \frac{[H^+]}{K_{a,LAMH^+}}\right)}{K_s^{NCT}\left(\frac{K_s^{LAM}}{K_s^{NCT}} - \frac{K_{sp}}{S_{0,LAM}{}^2}\right)} + CMC \qquad (3.34)$$

When, $K_{sp} = S_{cc}^2$, the above equation can be written as,

$$CSC = \frac{\left(\frac{S_{cc}}{S_{0,LAM}}\right)^2 - \left(1 + \frac{[H^+]}{K_{a,LAMH^+}}\right)}{K_s^{NCT}\left(\frac{K_s^{LAM}}{K_s^{NCT}}\right) - \left(\frac{S_{cc}}{S_{0,LAM}}\right)^2} + CMC \qquad (3.35)$$

Inputting the values for the parameters in equation (3.35) does not yield a positive value, thus mathematically confirming that there is no CSC between cocrystal and LAM·H_2O. Equation (3.35) indicates that a CSC will only exist if both, numerator and denominator are positive. Thus the higher the solubilization constant of the drug (K_s^{LAM}), or the lower the S_{cc} is, the lower the value of CSC will be. Similarly, for a weakly basic drug (LAM), at high pH values ($H^+ << K_{a,LAMH^+}$) i.e., if $\left(1 + \frac{[H^+]}{K_{a,LAMH^+}}\right) < \left(\frac{S_{cc}}{S_{0,LAM}}\right)^2$, then a CSC will exist as long as the denominator is positive i.e., $\left(\frac{K_s^{LAM}}{K_s^{NCT}}\right) > \left(\frac{S_{cc}}{S_{0,LAM}}\right)^2$. From the values of S_{cc} (K_{sp}), $S_{0,LAM}$, K_s^{LAM} and K_s^{NCT} for LAM-NCT·H_2O cocrystal and its components, $\frac{K_s^{LAM}}{K_s^{NCT}}$ and $\left(\frac{S_{cc}}{S_{0,LAM}}\right)^2$ were determined to be 166.0 and 941.2 respectively suggesting that for a cocrystal that is about 30 times more soluble than the drug, the solubilization constant (K_s^{LAM}) is not high enough to yield a positive value for equation (3.35). Figure 3.5 shows the solubility dependence of LAM-NCT·H_2O cocrystal and LAM·H_2O as a function of total surfactant concentration by using equations (3.27) and (3.28). The figure shows that the two solubility curves do not intersect in the range of surfactant concentrations studied. These results are in good agreement with the predicted behavior by the above mathematical analysis.

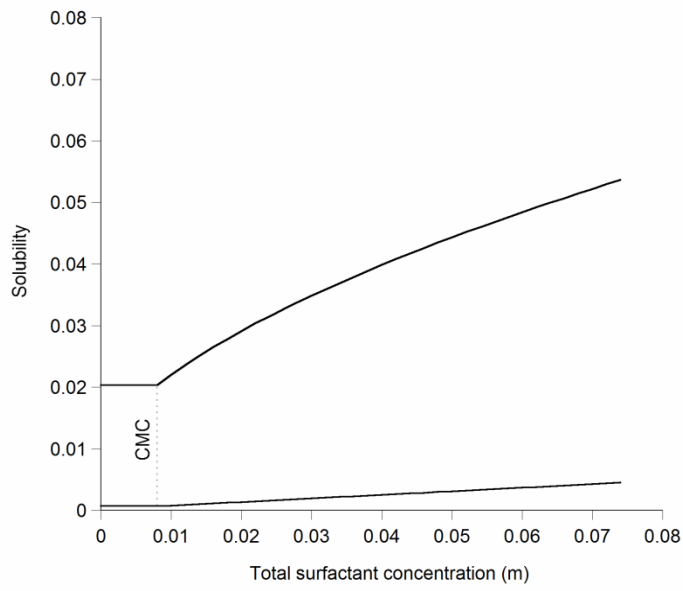

Figure 3.5: Effect of micellar solubilization on LAM·H_2O and LAM-NCT·H_2O cocrystal solubility. Equations (3.27) and (3.28) were used to generate LAM-NCT·H_2O and LAM·H_2O cocrystal solubility as a function of total SLS concentration at pH 7.9.

The usefulness of solubilization constants is not limited to the determination of CSC alone. An important estimation that can be made from the value of micellar concentration and solubilization constants is that of cocrystal solubility in surfactant solutions. For example, equations (3.27) and (3.28) indicate that cocrystal and drug solubilities exhibit different dependencies on micellar concentration. In the case of cocrystal, solubility increases proportionally to $\sqrt{[M]}$ while drug solubility increases proportionally to [M]. Assuming that ionization of drug and coformer solubilization by surfactant is negligible, then for a 1:1 cocrystal LAM-NCT·H_2O,

$$\frac{S_{CC,T}}{S_{CC,aq}} = \sqrt{\frac{S_{LAM,T}}{S_{0,LAM}}} \tag{3.36}$$

According to equation (3.36), if in a given concentration of surfactant, if the solubility of a drug increases by 10 fold relative to its aqueous solubility, then the cocrystal solubility increases by $\sqrt{10}$ fold relative to its aqueous solubility. This relationship is experimentally confirmed for LAM-NCT·H_2O cocrystal.

The solubility values presented in Table 3.2 and Table 3.3 show that the increase in cocrystal solubility in SLS relative to the increase in LAM·H_2O solubility in SLS is consistent with equation (3.36) i.e., $\sqrt{\frac{S_{LAM,T}}{S_{0,LAM}}} = \sqrt{7.4} \approx \frac{S_{CC,T}}{S_{CC,aq}} = 2.6$. Thus from the known solubilities of the drug in water and surfactant, cocrystal solubility in surfactants can be estimated. The knowledge of CSC remains crucial as it can have an influence on rational selection of additives to modulate cocrystal and drug solubilities. Additives with different solubilization capacities of cocrystal components impart thermodynamic stability to cocrystal phases when exposed to a solvent. As discussed earlier using the example of pH dependent solubility studies, the dissolution test conditions can have a huge impact on the true solubility advantage of a particular solid form. Surfactants are common constituent of dissolution media and therefore may influence the dissolution behavior of cocrystals. If cocrystals are thermodynamically stable at the concentration of surfactant present in the dissolution medium (i.e., if there is a CSC), then the cocrystal thermodynamic solubility in the absence or at other surfactant concentrations may not be apparent leading to poor judgment of true solubility advantage. This can have implications, such as erroneous bioavailability prediction or phase transformations during processing.

With respect to LAM-NCT·H_2O cocrystal synthesis, although a CSC does not exist, other mechanisms could be the driving force in cocrystal formation in 2% w/w SLS aqueous solution. The degree of supersaturation is a key factor that has an influence on cocrystallization. In a study with carbamazepine-nicotinamide (CBZ-NCT) cocrystal, cocrystallization reaction time was reduced from 3hrs to 3mins, when NCT concentration was increased in cocrystallization medium. The supersaturation of CBZ-NCT increased with NCT concentration and thus increased the transformation rate for cocrystal.[27]

A direct measurement of LAM in NCT and 2% w/w SLS solution was not possible due to conversion of LAM to cocrystal in surfactant solutions above the eutectic point. Figure 3.6 shows LAM concentration supersaturated with respect to the cocrystal in 3.5m NCT solution represented by A1 and A2 in water and 2% SLS respectively. A1 and A2 were estimated from $K_{1:1}$ which was calculated by measuring the LAM concentration in NCT solutions shown by open circles (○). Complexation constant (K11) was calculated to be 1.46 according to equation (3.37).

$$K_{1:1} = \frac{\text{Slope}}{\text{Intercept}(1-\text{Slope})} \tag{3.37}$$

$$K_{1:1} = \frac{S_t^{LAM\cdot H_2 0} - S_0}{S_0^{LAM\cdot H_2 0}(L_t^{NCT} - S_t^{LAM\cdot H_2 0} + S_0)} \tag{3.38}$$

From the value of $K_{1:1}$, and LMT $S_0^{LAM\cdot H_2 0}$ values of 6.60 x 10^{-4} (m) and 4.86 x 10^{-3} (m) in water and 2% SLS shown by the solid diamond (◆), S_t^{LAM} was estimated at 3.5m NCT concentration (L_t^{NCT}) in water and 2% SLS solution (represented by A1 and A2) according to equation (3.38).

Table 3.5: LAM·H_20 solubility in NCT solutions used to determine $K_{1:1}$ according to equation (3.37). pH of all measurements were in the range of 7.9 – 8.1.

[NCT] (m)	[LAM] ± Std. Dev. (m)
-	$(6.60 \pm 0.13) \times 10^{-4}$
0.25	$(8.36 \pm 0.40) \times 10^{-4}$
0.50	$(1.06 \pm 0.08) \times 10^{-3}$
1.00	$(1.56 \pm 0.16) \times 10^{-3}$
1.50	$(2.01 \pm 0.03) \times 10^{-3}$

From the values of LAM concentration at A1, A2, and at equilibrium with cocrystal in water and 2% w/w SLS solution, the calculated σ1 and σ2 values are 33.3 and 36.9 respectively. Although the increase in supersaturation is not large in 2% w/w SLS solution, the critical supersaturation value required to crystallize the cocrystal may exist between the values of σ1 and σ2. Figure 3.6 indicates that cocrystal is the thermodynamically stable phase in water beyond the eutectic point. This was confirmed by phase transformation studies where the cocrystal converts to LAM·H_2O in solutions of NCT below the eutectic point, whereas the cocrystal is the stable phase in NCT solutions above the eutectic NCT concentration. However, the eutectic concentration in water could only be measured upon cocrystal synthesis from 2% w/w SLS solutions.

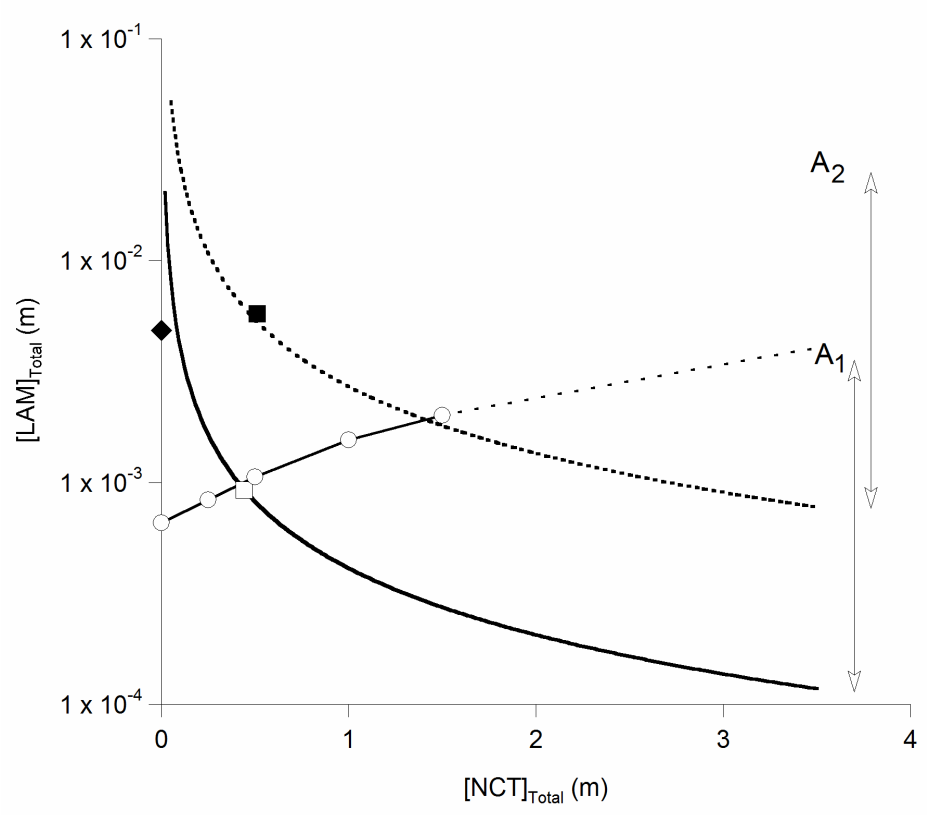

Figure 3.6: Solubility of LAM-NCT·H_2O cocrystal in water (solid line) and 2% w/w SLS (dotted line) generated from K_{sp} = 4.10x$10^{-4}m^2$ according to equations (3.5) and (3.27) and pH 7.9. (○) represents LAM concentration in NCT aqueous solutions in equilibrium with LAM·H_2O solid phase, (□) represent eutectic concentration in water, (◆) represent LAM·H_2O solubility in 2% w/w SLS aqueous solution, (■) represent eutectic concentration in 2% w/w SLS aqueous solution, A1 and A2 represents the LAM concentrations in 3.5m NCT solution in water and 2% w/w SLS aqueous solutions respectively, estimated using a measured K11 value of 1.46.

Other mechanisms could be responsible for cocrystallization in the presence of surfactants. It is well known that the rate of a chemical reaction is very sensitive to the nature of the reaction environment. Many chemical reactions exhibit faster reaction rates in the presence of micellar surfactants, especially where one reactant is hydrophilic while the other is hydrophobic. Several mechanisms have been proposed where surfactants

provide an interface for a chemical interaction between reactants of vastly different polarities. For example, the palisades region of the micelle provides a transition zone between the polar and non-polar regions. This gradient in polarity serves as a convenient area of intermediate polarity suitable for increased reactant interactions. Another way micelles can facilitate reactions and reaction rates is by solubilizing a reactant with poor solubility, in effect increasing the concentration of reactant. In the case of LAM-NCT·H_2O cocrystal, although the degree of supersaturation of LAM-NCT·H_2O in 2% w/w SLS is not very large relative to its value in water, a higher concentration of LAM (7.4 fold increase in LAM·H_2O solubility) in SLS solution may facilitate a chemical reaction. Thus the ability of a micellar system to solubilize a reactant can affect its action as a catalyst in a reaction[39-41]. The role of micellar catalysis to aide cocrystallization is a subject of further research.

Conclusion

These results indicate that cocrystals can have much higher solubilities than salts. Lamotrigine-nicotinamide cocrystal hydrate (LAM-NCT·H_2O) is 30 times more soluble while lamotrigine-saccharin (LAM-SAC) salt is 5 times more soluble than LAM. The order of solubilities is LAM-NCT·H_2O > LAM-SAC > LAM-MP, while the solubility of LAM·HCl salt is highly dependent on the Cl^- concentration in the solution. Coformer solubility is a huge factor in the solubility of cocrystals and salts. NCT solubility is over 5000 times higher than LAM solubility while SAC and methylparaben (MP) solubilities are 27 and 24 times higher respectively. As a consequence, LAM-NCT·H_2O is the most soluble form thermodynamically. The results presented here are consistent with previously published reports where it's shown that cocrystal equilibrium solubility is influenced by coformer solubility[4]. pH dependent solubility studies indicate that LAM-NCT·H_2O is the most soluble form between pH 3.0 and 7.0 and LAM-SAC is least soluble form below pH 5.0. In the presence of 0.1M HCl, LAM·HCl salt has the lowest solubility and all solid forms of LAM would therefore transform to the HCl salt. The eutectic concentration measurement is of critical importance in the estimation of cocrystal's true thermodynamic solubility. LAM-NCT cocrystal hydrated could only be synthesized by reaction crystallization method and in the presence of 2% SLS. The supersaturation states A1 and A2 are similar with respect to cocrystal solubility in water and 2% SLS, however LAM solubility is 8 fold higher in the presence of 2% SLS and therefore could facilitate cocrystal formation by providing higher concentration of reactant in the solution.

APPENDIX 2

Table A2.1: Cocrystal and salt solubilities, C_{max}, steady state (SS) concentrations, initial and final solid phases and corresponding pH from reported dissolution data

	Molal Solubility (pH)	Conc. from Dissolution[12]		Solid Phase[12]		pH[11, 12]	
		C_{max} (m)	SS (m)	Initial	Final	Initial	Final
LAM-NCT·H_2O	2.0×10^{-2} (8.0)[(a)]	9.4×10^{-4}	6.6×10^{-4}	LAM-NCT·H_2O	LAM·H_2O	5.5	6.2
LAM-ANHYD	6.6×10^{-4} (7.9)[(a)]	1.1×10^{-3}	6.8×10^{-4}	LAM-ANHYD	LAM·H_2O	5.5	6.9
LAM-SAC	3.3×10^{-3} (3.7)[(a)]	1.8×10^{-3}	1.8×10^{-3}	LAM-SAC	LAM-SAC	5.5	5.1
LAM-MP	7.9×10^{-4} (8.3)[(b)]	8.8×10^{-4}	7.9×10^{-4}	LAM-MP	LAM-MP	5.5	6.3
LAM·HCl	1.1×10^{-2} (1.2)[(c)]	-	-	LAM-ANHYD[(c)]	LAM·HCl[(c)]	1.2[(c)]	Not Reported

(a) Experimentally measured solubility in this work, (b) Steady state concentration from dissolution data reported in reference 12 was used to calculate the K_{sp} of LAM-MP cocrystal,[12] (c) Estimated solubility of LAM·HCl salt from reported LAM solubility in reference 11, assuming that in reference 11 the starting phase (LAM) transformed to LAM·HCl at pH 1.2. This assumption is based on the studies of Cheney et. al. where all solid forms of LAM transformed to LAM·HCl salt during dissolution in pH 1 medium.

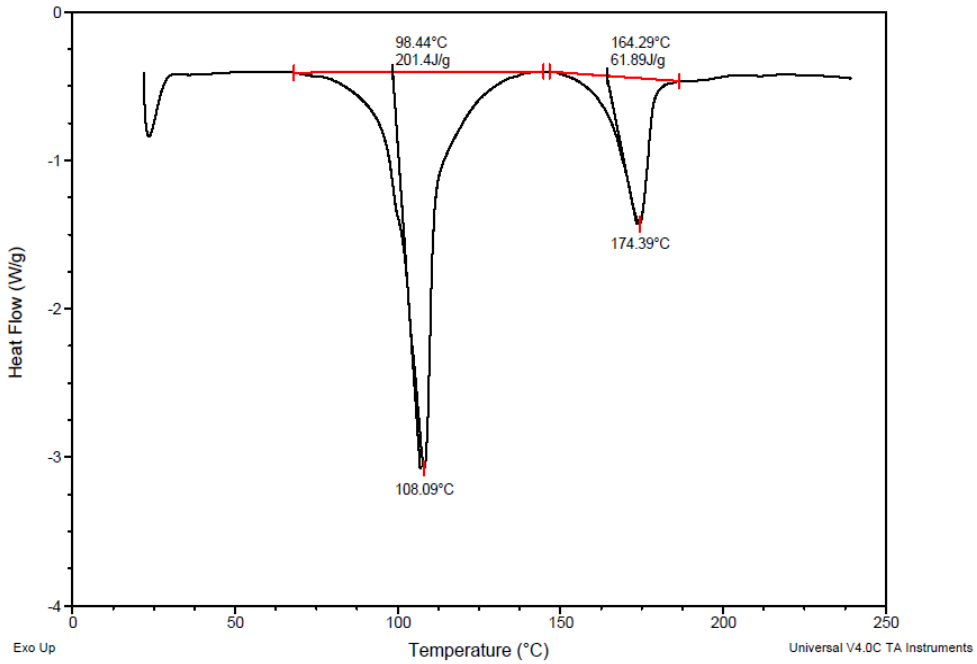

Figure A2.1: DSC thermogram of LAM-NCT·H2O cocrystal

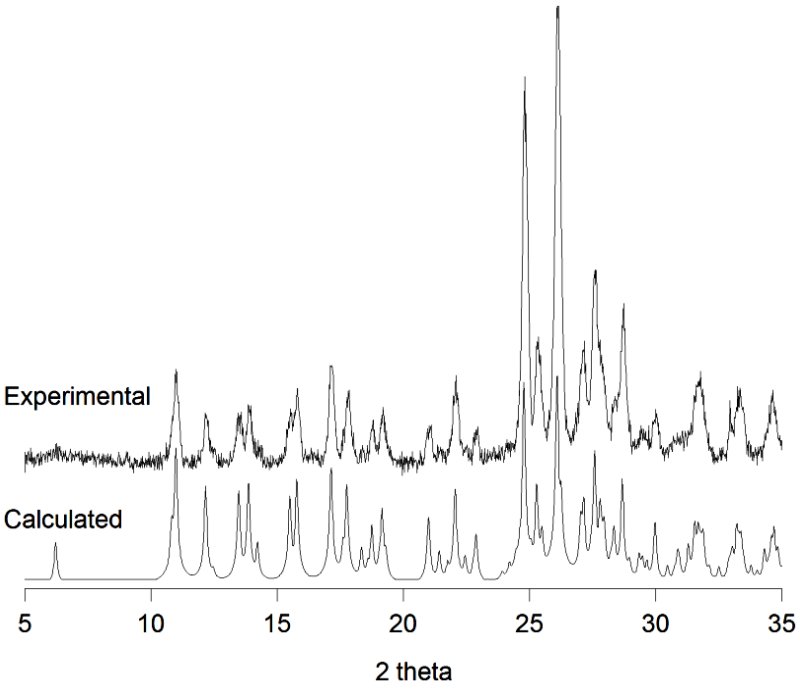

Figure A2.2: Calculated and experimental PXRD pattern of LAM-NCT·H2O cocrystal

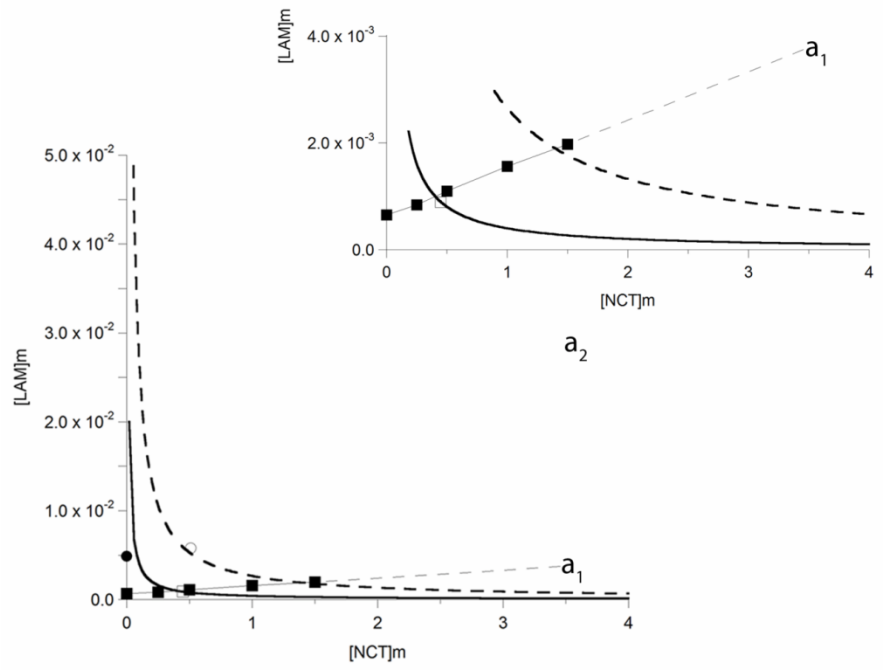

Figure A2.3: Solubility of LAM-NCT·H_2O cocrystal in water (solid line) and 2% w/w SLS (dotted line) generated from K_{sp} = 4.10x$10^{-4}m^2$ according to equations (3.5) and (3.27) and pH 7.9. (○) represents LAM concentration in NCT aqueous solutions in equilibrium with LAM·H_2O solid phase, (□) represent eutectic concentration in water, (◆) represent LAM·H_2O solubility in 2% w/w SLS aqueous solution, (■) represent eutectic concentration in 2% w/w SLS aqueous solution, A1 and A2 represents the LAM concentrations in 3.5m NCT solution in water and 2% w/w SLS aqueous solutions respectively, estimated using a measured K11 value of 1.36. σ1 and σ2 are the LAM concentrations in supersaturated state with respect to the equilibrium LAM concentration.

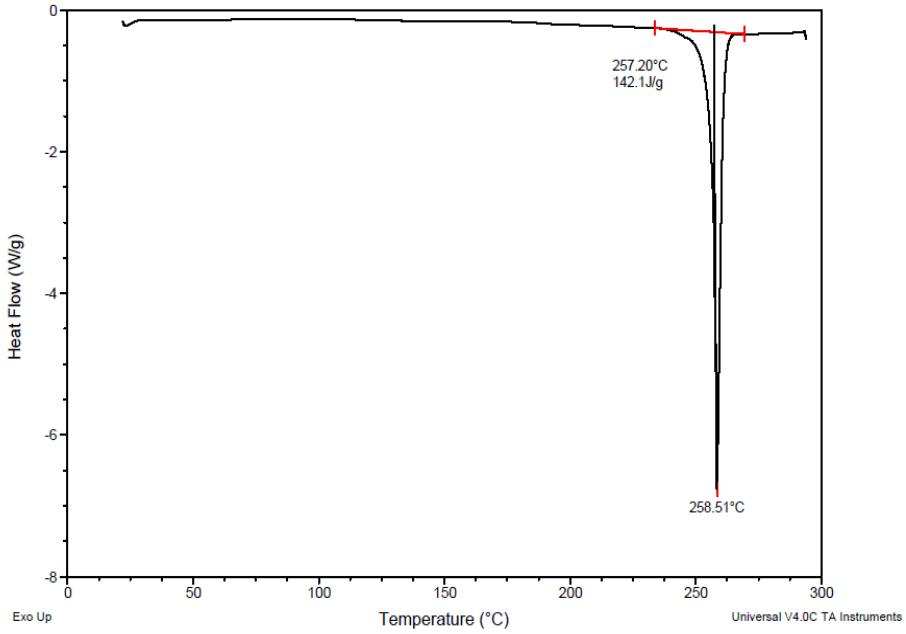

Figure A2.4: DSC thermogram of LAM-SAC salt

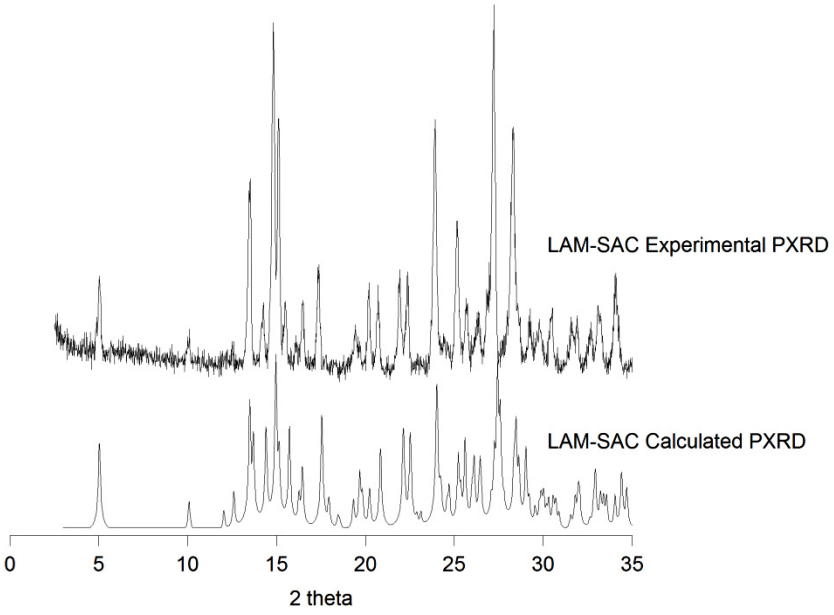

Figure A2.5: Calculated and experimental PXRD pattern of LAM-SAC salt

pH_{max} for a cocrystal of a weakly basic drug and non-ionic coformer:

At pH_{max} the drug solubility = Cocrystal solubility

$$S_{drug} = S_{0,drug}\left(1+\frac{[H^+]}{K_{a,BH^+}}\right) = S_{cocrystal} = \sqrt{K_{sp}\left(1+\frac{[H^+]}{K_{a,BH^+}}\right)}$$

$$S_{0,drug}\left(1+\frac{[H^+]}{K_{a,BH^+}}\right) = \sqrt{K_{sp}\left(1+\frac{[H^+]}{K_{a,BH^+}}\right)}$$

$$\frac{S_{0,drug}^2}{K_{sp}} = \frac{1}{\left(1+\frac{H^+}{K_{a,BH^+}}\right)};\ K_{sp} = S_{cc}^2$$

$$\frac{S_{cc}^2}{S_{0,drug}^2} = 1+\frac{H^+}{K_{a,BH^+}}, \text{ when } H^+ >> K_{a,BH^+} \text{ that is when the drug is largely ionized}$$

$$\frac{S_{cc}^2}{S_{0,drug}^2} = \frac{H^+}{K_{a,BH^+}}, \text{ taking log on both sides}$$

$$\log H^+ - \log K_{a,BH^+} = 2\log\left(\frac{S_{cc}}{S_{0,drug}}\right); \text{ at } pH_{max} \text{ this equation can be written as,}$$

$$pH_{max} = pK_{a,BH^+} - 2\log\frac{S_{cc}}{S_{0,drug}}$$

References

1. Lipinski, C. A., Lombardo, F., B.W., D. & Feeney, P. J. Drug Del. Rev. 23, 3-25 (1997).
2. Avdeef, A. Solubility of Sparingly-Soluble ionizable drugs. Adv. Drug Del. Rev. 59, 568-590 (2007).
3. Bak, A. et al. The co-crystal approach to improve the exposure of a water-insoluble compound: AMG 517 sorbic acid co-crystal characterization and pharmacokinetics. Journal of Pharmaceutical Sciences 97, 3942-3956 (2008).
4. Good, D. J. & Rodriguez-Hornedo, N. Solubility Advantage of Pharmaceutical Cocrystals. Crystal Growth & Design 9, 2252-2264 (2009).
5. McNamara, D. P. et al. Use of a glutaric acid cocrystal to improve oral bioavailability of a low solubility API. Pharmaceutical Research 23, 1888-1897 (2006).
6. Stahl, P. H. & Wermuth, C. G. Handbook of Pharmaceutical Salts: Properties, Selection and Use (Wiley-VCH, Zürich, 2002).
7. Lipinski, C. H. Poor Aqueous Solubility - An Industry Wide Problem in Drug Discovery. Am. Ph. Rev. 5, 82 (2002).
8. O'Neil, M. J., Smith, A. & Heckelman, P. E. The Merck Index (New Jersey, 2001).
9. Soltanpour, S., W. E. Acree, J. & Joubyan, A. Solubility of 5-(2-Chlorophenyl)-7-nitro-1,3-dihydro-1,4-benzodiazepin-2-one, 7-Chloro-1-phenyl-3H 1,4-benzodiazepin-2-one, and 6-(2,3-Dichlorophenyl)-1,2,4,-triazine-3,5-diamine in the Mixtures of Poly(ethylene glycol) 600, Ethanol and Water at a Temperature of 298.2K. J. Chem. Eng. Data 55, 1727-1731 (2010).
10. Galcera, J. & Molins, E. Effect of the Counterion on the Solubility of Isostructural Pharmaceutical Lamortigine Salts. Crystal Growth & Design 9, 327-334 (2009).
11. Budavari, S., Kineary, J., O'Neil, M. J., Smith, A. & Heckelman, P. E. The Merck Index (1996).
12. Floyd, A. G. & Jain, S. (ed. Office, U. S. P.) (Glaxo Wellcome Inc.,, USA, 1999).
13. Remenar, J. F. et al. Crystal Engineering of Novel Cocrystal of a Triazole Drug with 1,4-Dicarboxylic Acid. J. Am. Chem. Soc. 125, 8456-8457 (2003).
14. Remenar, J. F. et al. Celecoxib:Nicotinamide Dissociation: Using Excipients to Capture the Cocrystal's Potential. Mol. Pharm. 4, 386-400 (2007).
15. Cheny, M. L. et al. Coformer Selection in Pharmaceutical Cocrystal Development: A Case Study of a Meloxicam Aspirin Cocrystal That Exhibits Enhanced Solubility and Pharmacokinetics. J. Pharm. Sci 100, 2172-2181 (2011).

16. Maheshwari, C. et al. Tailoring Aqueous Solubility of a Highly Soluble Compound via Cocrystallization: Effect of Coformer Ionization, pH_{max} and Solute-Solvent Interactions. CrytEngComm 14, 4801-4811 (2011).

17. Bethune, S. J., Huang, N., Jayasankar, A. & Rodriguez-Hornedo, N. Understanding and Predicting the Effect of Cocrystal Components and pH on Cocrystal Solubility. Crystal Growth & Design 9, 3976-3988 (2009).

18. Cheny, M. L. et al. Effects of Crystal Form on Solubility and Pharmacokinetics: A Crystal Engineering Case Study of Lamotrigine. Crystal Growth & Design 10, 394-405 (2010).

19. Kramer, S. F. & Flynn, G. F. Solubility of Organic Hydrochloride. J. Pharm. Sci 61, 1896-1904 (1972).

20. Bogardus, J. B. & Blackwood, R. K. Dissolution Rates of Doxycycline Free Base and Hydrochloride Salts. Journal of Pharmaceutical Sciences 68, 1183-1184 (1979).

21. Serajuddin, A. T. M. & Puddipedi, M. Salt-selection strategies (eds. Stahl, P. H. & Wermuth, C. G.) (Wiley-VCH, Weinheim, 2002).

22. Huang, N. & Rodriguez-Hornedo, N. Engineering cocrystal thermodynamic stability and eutectic points by micellar solubilization and ionization. CrstEngComm. (2011).

23. Nehm, S. J., Rodriguez-Spong, B. & Rodriguez-Hornedo, N. Phase solubility diagrams of cocrystals are explained by solubility product and solution complexation. Crystal Growth & Design 6, 592-600 (2006).

24. Good, D. J. & Rodriguez-Hornedo, N. Cocrystal Eutectic Constants and Prediction of Solubility Behavior. Crystal Growth & Design 10, 1028-1032 (2010).

25. Chadha, R. et al. Multicomponent solids of lamotrigine with some selected coformers and their characterization by thermoanalytical, spectroscopic and X-ray diffraction methods. CrytEngComm 13, 6271-6284 (2011).

26. Miyazaki, S., Oshiba, M. & Nadai, T. Precaution of Use of Hydrochloride Salts in Pharmaceutical Formulation. J. Pharm. Sci 70, 594-596 (1981).

27. Nickelsen, M. G., Nweke, A., Frank E. Scully, J. & Ringhand, H. P. Reactions of Aqueous Chlorine in Vitro in Stomach Fluid from the Rat: Chlorination of Tyrosine. Chem. Res. Toxicol. 4, 94-101 (1991).

28. Lu, E., Rodriguez-Hornedo, N. & Suryanarayanan, R. A rapid thermal method for cocrystal screening. CrstEngComm. 10, 665-668 (2008).

29. Rodriguez-Hornedo, N., Nehm, S. J., Seefeldt, K. F., Pagan-Torres, Y. & Falkiewicz, C. J. Reaction crystallization of pharmaceutical molecular complexes. Molecular Pharmaceutics 3, 362-367 (2006).

30. Trask, A. V., Haynes, D. A., Motherwell, W. D. S. & Jones, W. Screening for crystalline salts via mechanochemistry. Chemical Communications, 51-53 (2006).

31. Chency, M. L. et al. Effects of Crystal Form on Solubility and Pharmacokinetics: A Crystal Engineering Case Study of Lamotrigine. Crystal Growth & Design 10, 394-405.

32. Huang, N. & Rodriguez-Hornedo, N. Effect of Micelliar Solubilization on Cocrystal Solubility and Stability. Crystal Growth & Design 10, 2050-2053 (2010).

33. Rodríguez-Hornedo, N. & Murphy, D. Surfactant Facilitated Crystallization of Dihydrate Carbamazepine During Dissolution of Anhydrous Polymorph. J. Pharm. Sci 93, 449-460 (2004).

34. He, Y. & Yalkowsky, S. H. Solubilization of monovalent weak electrolytes by micellization or complexation. Int. J. Pharm. 324, 15-20 (2006).

35. Jain, A., Ran, Y. Q. & Yalkowsky, S. H. Effect of pH-sodium lauryl sulfate combination on solubilization of PG-300995 (an anti HIV agent): A technical note. AAPS PharmSci Tech. 5, 65-67 (2004).

36. Li, P., Tabibi, S. E. & Yalkowsky, S. H. Combined effect of complexation and pH on solubilization. J. Pharm. Sci 87, 1535-1537 (1998).

37. Mithani, S. D., Bakatselou, V., TenHoor, C. N. & Dressman, J. B. Estimation of the Increase in Solubility of Drugs as a Function of Bile Salt Concentration. Pharmaceutical Research 12, 163-167 (1996).

38. Alvarez-Nunez, F. A. & Yalkowsky, S. H. Relationship between Polysorbate 80 solubilization descriptors and octanol - water partition coefficients of drugs. Int. J. Pharm. 200, 217-222 (2000).

39. Myers, D. Surfactant Science and Technology (John Wiley & Sons, Inc, New Jersey, 2006).

40. Nozaki, K., Yoshida, M. & Takaya, H. Reaction rate enhancement by addition of anionic surfactant SDS in the ruthenium catalyzed hydrogen transfer from a 1,4-diol to 4-phenyl-3-buten-2-one. J. OrganoMet Chem. 473, 253-256 (1994).

41. Bunton, C. A. Reaction Kinetics in Aqueous Surfactant Solutions. Cataly. Rev. 20, 1-56 (1979).

CHAPTER 4

FACTORS THAT INFLUENCE THE SPONTANEOUS FORMATION OF PHARMACEUTICAL COCRYSTALS BY SIMPLY MIXING SOLID REACTANTS

Abstract

The purpose of this study was to investigate whether cocrystals form by simply mixing pure solid components without the need to comill. The effects of moisture and temperature during storage were studied in binary mixtures where pure components were exposed to different levels of mechanical stress: (a) two components unmilled, (b) one component milled, or (3) two components individually milled. Equimolar mixtures of anhydrous monoclinic form III carbamazepine (CBZ) with form I nicotinamide (NCT) or saccharin (SAC) were stored at 25°C-75%RH, 45°C-0%RH and 45°C-75%RH. Transformation to cocrystal was monitored by FTIR and XRPD. Results show that conversion to cocrystal occurs even when components are not mechanically stressed at all storage conditions within 3 months except for unmilled CBZ/SAC at 25°C-75%RH. Free energy calculations from solubilities and equilibrium constants confirm that transformation from reactants to cocrystal is thermodynamically favorable. Increasing temperature and relative humidity as well as mechanical activation by individually milling reactants enhances cocrystal formation. CBZ-NCT cocrystal forms faster than

CBZ-SAC at all storage conditions. A metastable CBZ-SAC polymorph was detected in mixtures of individually milled CBZ and SAC.

Introduction

The ability to alter molecular interactions, composition, and structure in materials of pharmaceutical relevance using crystal engineering principles and strategies has led to the discovery of a large number of pharmaceutical cocrystals[1-6]. Cocrystals modify the physicochemical and pharmaceutical properties of drugs and are therefore being pursued as solid-state forms for drug development[7-12]. Most studies have focused on cocrystal design and synthesis[13-20]. However, the spontaneous formation of cocrystals under conditions relevant to pharmaceutical processing or storage has not received much attention.

Conversion to cocrystals in mixtures of solid reactants has been shown to occur by solution, vapor, melt or solid phase mediated processes.[14, 21-30] Cocrystal formation in the solid state during comilling has been shown to be amorphous phase mediated and can proceed during storage after brief Comilling.[29] Water present in hydrated reactants as well as water vapor during storage facilitates conversion to cocrystal.[22, 29] Sorption of water and organic solvents is also known to induce transformation to cocrystal by a solution mediated pathway, where reactant particles take up vapor molecules and dissolve to generate supersaturation with respect to cocrystal.[22, 31]

Anticipating conversions to cocrystal is important for pharmaceutical product development and performance. In the current study, we examine spontaneous cocrystal formation by simply mixing pure solid reactants without the need to comill, and under

conditions where cocrystal formation is not melt or solution mediated. The effects of moisture and temperature during storage were studied in binary mixtures where solid reactants were exposed to different levels of mechanical stress: (a) two reactants unmilled, (b) one reactant milled, or (3) two reactants individually milled. Transformation of equimolar reactant mixtures of anhydrous monoclinic form III carbamazepine (CBZ) with form I nicotinamide (NCT) or saccharin (SAC) to cocrystal was investigated. The free energy of cocrystal formation determines the thermodynamic stability of cocrystal and was calculated from solubility and K_{sp} values.[21, 32]

Materials and Methods

Anhydrous monoclinic carbamazepine form III (CBZ), nicotinamide form I (NCT) and saccharin (SAC) were purchased from Sigma Aldrich and were used as received. CBZ-NCT and CBZ-SAC cocrystals were prepared as described previously.[21, 23, 29] Solid phases were characterized by ATR-FTIR and XRPD.

Milling of reactants

CBZ, NCT and SAC were milled individually at room temperature using the 5100 SPEX CentriPrep (Metuchen, NJ) ball mill. About 500mg of reactant was milled for 30min in a 3114 stainless steel vial using two stainless steel beads (0.25inch in diameter). The milled reactants were characterized by XRPD for changes in crystallinity.

Sample preparation

Cocrystal formation was monitored during storage in four types of mixtures: (A) mixtures of individually milled reactants, (B) mixtures of unmilled reactants, (C) mixtures of one milled and one unmilled reactant, and (D) mixtures of milled-annealed

reactants. Unmilled reactants were sieved and the particle size used was in the range of 63 -106μm. Annealing of reactants was carried out at 60°C for 24 hrs immediately after milling.

Mixtures of about 500 mg were prepared by mixing CBZ and NCT or SAC in 1:1 molar ratio in a stainless steel vial using a vortex mixer. Mixtures were characterized by FTIR and XRPD prior to storage. Mixtures A and B were stored in desiccators equilibrated at 25°C-75%RH, 45°C-0%RH, and 45°C-75%RH. Mixtures C and D were stored at 25°C-75%RH. Cocrystal formation in all mixtures was monitored by FTIR and XRPD. RH in desiccators was maintained at 0% with phosphorous pentoxide and at 75% with saturated sodium chloride solution.

Attenuated Total Reflection Fourier Transform infra-red spectroscopy (ATR-FTIR)

Vertex 70 (Bruker Optic Inc, Billerica, MA) equipped with a DTGS detector and a single bounce ATR accessory with ZnSe crystal (Pike Tech, Madison, WI) was used for collecting the infra-red spectra of samples. The spectra were collected in the 4000-600 cm^{-1} range with 4cm^{-1} resolution. Each spectrum was an average of 64 co-added scans.

Quantification of CBZ-NCT cocrystal formation during storage by FTIR was carried out according to a previously published procedure for CBZ-SAC cocrystal [29]. Mixtures containing CBZ and NCT in 1:1 molar ratio, and 0%, 20%, 50%, 80% or 100% (w/w) CBZ-NCT cocrystal were used as calibration standards. Mixtures with 10%, 50% and 90% cocrystal were used as validation standards. The total mass of each standard was 500 mg. Cocrystal used in the standards was prepared from solution as described previously [21, 23]. CBZ, NCT, and cocrystal were individually milled for 2 minutes to minimize particle size differences. The reactants and cocrystal were then mixed in the

desired proportions to prepare the standards. Mixing was carried out in a stainless steel vial using a vortex mixer. The standards were characterized by FTIR. Triplicate spectra collected for each standard were compared to confirm homogeneity. If the standards were not homogenous, further mixing of components was carried out until homogeneity was achieved. FTIR spectra of the homogenous standards were then used to develop a calibration curve using the partial least square method (Quant software, Bruker Optic Inc, Billerica, MA). Calibration was performed by selecting the regions 3475-3435 cm^{-1}, 3370-3348 cm^{-1}, 1705-1645 cm^{-1} and 1600-1570 cm^{-1} that contain characteristic peaks of the reactants and the cocrystal. The calibration curve was validated by using validation standards. The R^2 values for the calibration and validation were 0.99.

X-Ray powder diffraction (XRPD)

XRPD patterns were collected in reflection mode, on a Rigaku miniflex diffractometer (Danvers, MA) using Cu Kα radiation (λ = 1.54Å), a tube voltage of 30kV, and a tube current of 15mA. Data was collected at a scan rate of 2.5°/min over a 2θ range of 2° to 40°.

Differential scanning calorimetry (DSC)

Thermal analysis of samples was carried out on a TA 2590 DSC (TA instruments, New Castle, DE) calibrated using indium and n-dodecane for temperature and cell constants. 6-8 mg sample was crimped in aluminum pans and heated at 10°C/min from 0 to 180°C. Samples were continuously purged with nitrogen at 50 ml/min.

Moisture sorption

Moisture uptake studies were performed using the SGA-100 symmetrical gravimetric analyzer (VTI Corp. Hialeah, FL). The instrument uses a Cahn microbalance (CI electronics, Wiltshire, U.K.) to monitor the sample weight and a chilled dew point analyzer (Edgetech, Milford, MA) to detect and control humidity in the sample chamber. Temperature is controlled to within 0.01°C and the instrument RH resolution is ±1%. About 20mg of milled or unmilled NCT was dried at 60°C for 60 min. Moisture uptake of dried samples was then measured at 25°C-75% and 45°C-75%RH. Equilibrium was considered to have been achieved when the sample weight change was less than 0.05%.

Results

FTIR spectra of crystalline reactants and cocrystals

The crystal structure of CBZ cocrystals with NCT or SAC is characterized by carboxamide homodimer that is present in CBZ as shown in Figure 4.1 (graphics were generated using X-Seed software).[33-37] NCT crystals exhibit an amide-pyridine heterodimer whereas SAC crystals exhibit a carboxamide homodimer, but these are not retained in the cocrystals. In the CBZ-NCT cocrystal the anti -NH of CBZ hydrogen bonds with the carbonyl oxygen of NCT, while in the CBZ-SAC cocrystal the anti -NH of CBZ hydrogen bonds with the sulfonyl group of SAC[16]. These differences in hydrogen bonds are reflected in the IR spectra of these materials (Figure 4.2 and Figure 4.3).

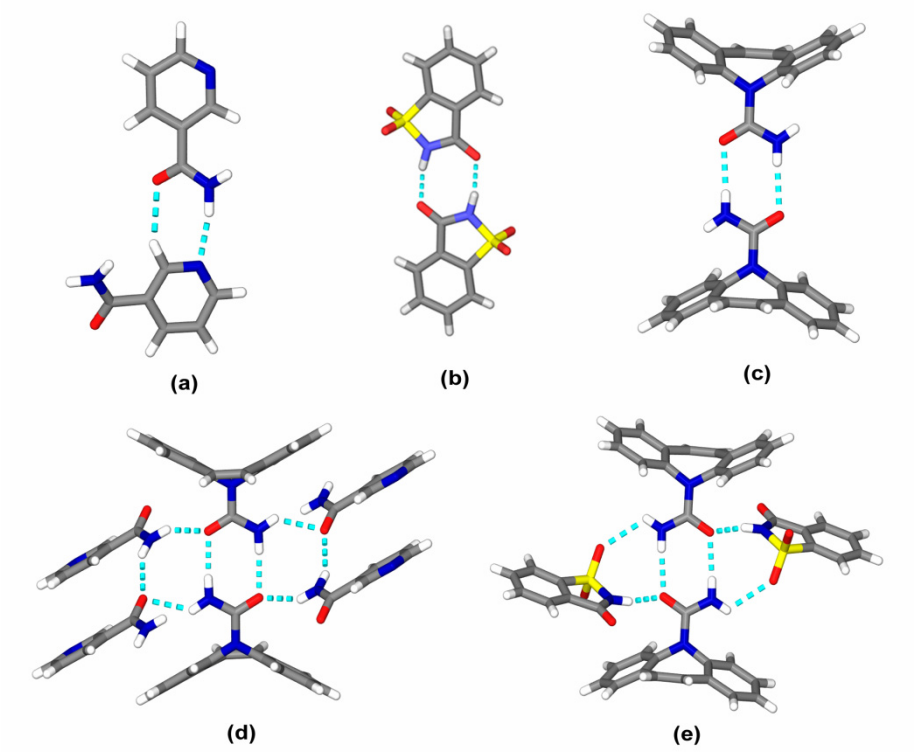

Figure 4.1: Hydrogen bonding in (a) NCT (b) SAC (c) CBZ (d) CBZ-NCT cocrystal and (e) CBZ-SAC cocrystal.

Figure 4.2 shows the IR spectra of CBZ, NCT and CBZ-NCT cocrystal. The peaks at 3464 and 3157cm^{-1} in the CBZ spectrum correspond to the free anti -NH and hydrogen bonded syn -NH respectively. A peak corresponding to the carbonyl stretch is observed at 1674cm^{-1}. The spectrum of NCT similarly shows peaks corresponding to amide -NH (3360 and 3151cm^{-1}) and C=O (1674cm^{-1}) functional groups. CBZ-NCT cocrystal spectrum shows peaks corresponding to the amide at 3445 and 3388cm^{-1} and carbonyl at 1681 and 1656cm^{-1}. These differences in the IR spectra of CBZ, NCT and the cocrystal were used to monitor transformations in reactant mixtures.

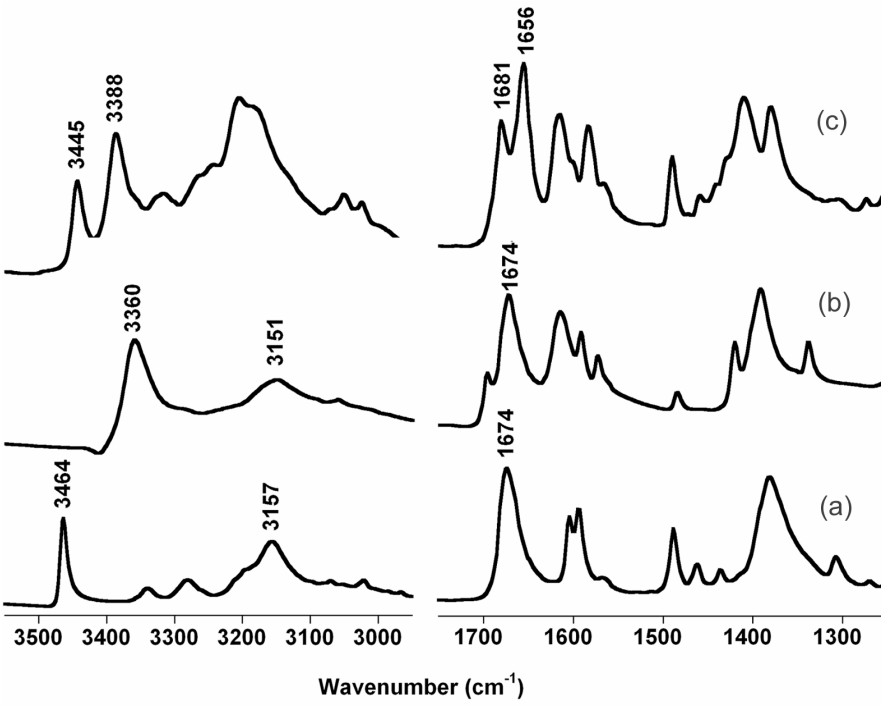

Figure 4.2: FTIR spectra of (a) CBZ (b) NCT and (c) CBZ-NCT cocrystal.

IR spectra of CBZ, SAC and CBZ-SAC are shown in Figure 4.3. Analysis of CBZ-SAC spectrum has already been reported.[29] The spectrum of SAC shows peaks corresponding to -NH and C=O stretch of the secondary amide at 3093 and 1715 cm^{-1}, respectively. Peaks corresponding to the asymmetric and symmetric stretching of -SO_2

group in SAC are observed at 1332 and 1175cm^{-1}. The cocrystal spectrum shows peaks corresponding to the amide at 3498cm^{-1}, carbonyl at 1724 and 1643 cm^{-1} and -SO_2 at 1327 and 1175 cm^{-1}, due to interactions between CBZ and SAC.

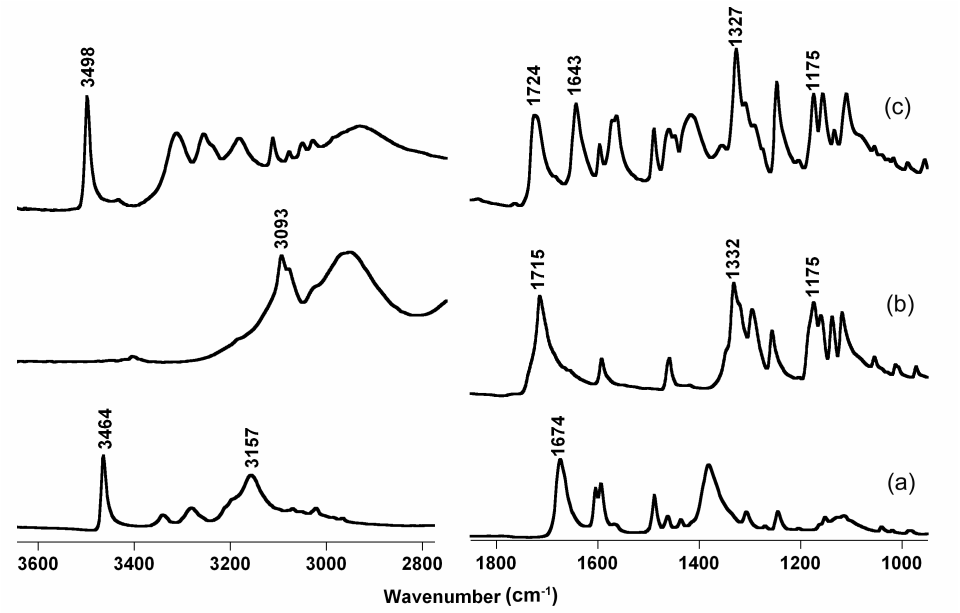

Figure 4.3: FTIR spectra of (a) CBZ (b) SAC and (c) CBZ-SAC cocrystal.

Effect of mechanical activation and storage conditions on CBZ-NCT cocrystal formation

Figure 4.4 shows the FTIR spectrum of CBZ/NCT mixture prepared from individually milled reactants and stored at 25°C-75%RH. Peaks at 3445, 3388, 1681 and 1656cm^{-1} in the spectrum of mixture at day 12 indicate cocrystal formation. XRPD confirming cocrystal formation is shown in Figure 4.5.

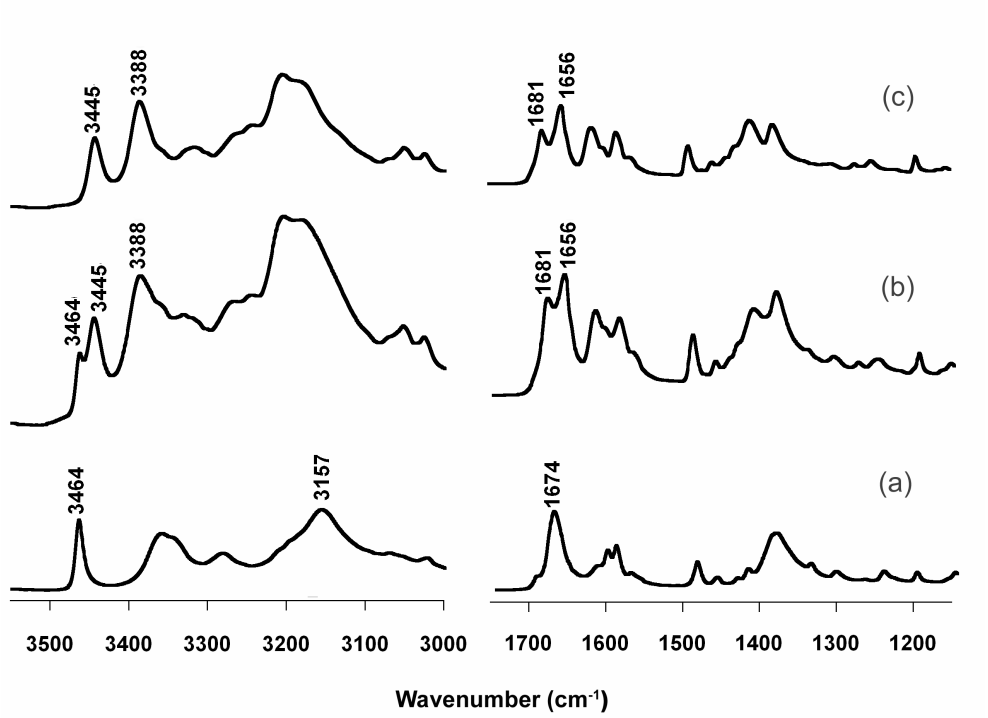

Figure 4.4: FTIR spectra showing cocrystal formation in mixtures of individually milled CBZ and NCT during storage at 25°C-75%RH. Mixture (a) before storage, and (b) at day 12; (c) CBZ-NCT cocrystal reference.

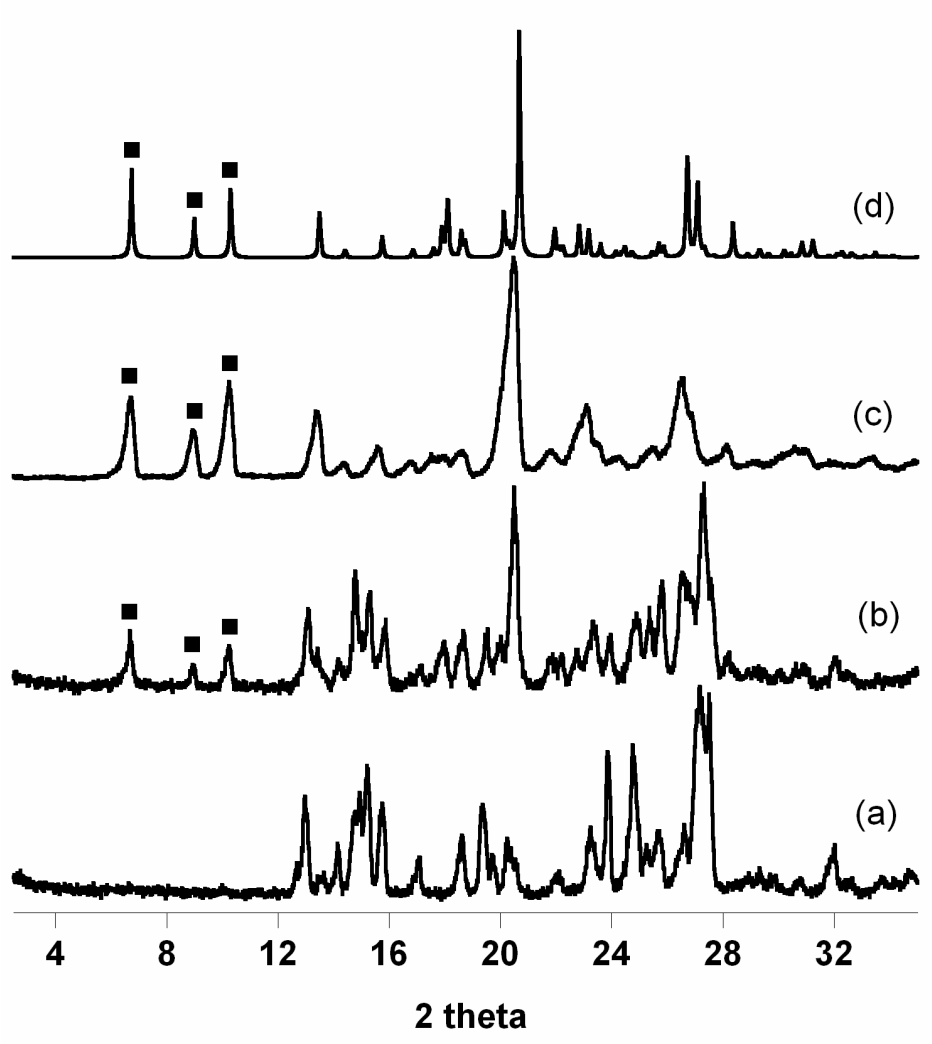

Figure 4.5: XRPD patterns showing cocrystal formation in mixtures of individually milled CBZ and NCT stored at 25°C-75%RH. Peaks used to follow the cocrystal formation are indicated by (■). Mixture (a) before storage and (b) at day 12; (c) CBZ-NCT cocrystal prepared from solution; (d) Calculated from CBZ-NCT crystal structure.

Cocrystal was also formed in mixtures of unmilled reactants (Figure 4.6), though at a slower rate than that of milled reactants e.g., 80 days versus 12 days. Higher XRPD peak intensities of cocrystal at higher temperature and RH suggest that storage conditions affect the rate of cocrystal formation.

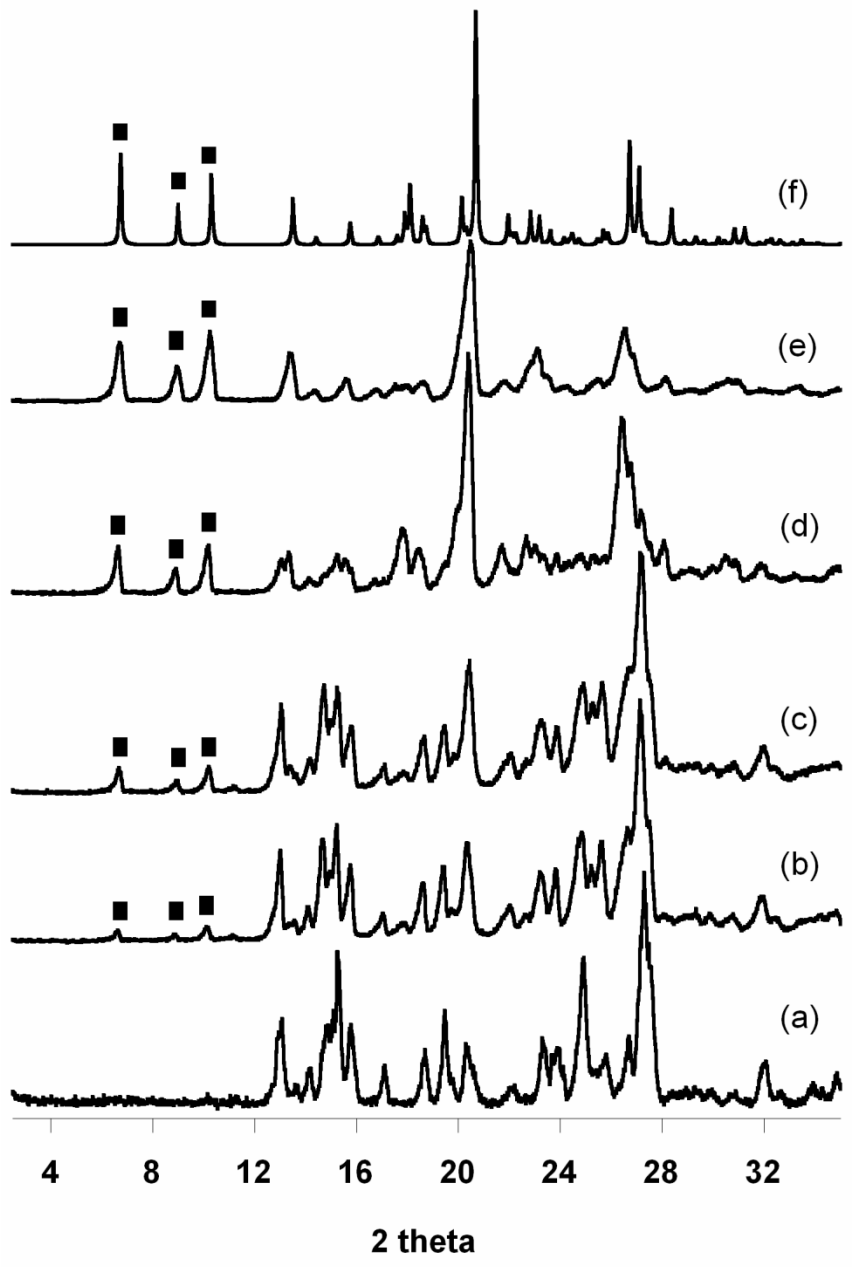

Figure 4.6: XRPD patterns showing the effect of storage conditions on CBZ/NCT mixtures prepared from unmilled reactants. Peaks used to follow the cocrystal formation are indicated by (■). Mixtures (a) before storage; and after storage for 80 days at (b) 25°C-75%RH, (c) 45°C-0%RH, (d) 45°C-75%RH; (e) CBZ-NCT cocrystal from solution; (f) Calculated from CBZ-NCT crystal structure.

Cocrystal formation during storage was quantified using ATR-FTIR. Figure 4.7 shows the rate of cocrystal formation in mixtures of unmilled reactants and mixtures of individually milled reactants stored at three conditions (a) 25°C-75%RH (b) 45°C-0%RH and (c) 45°C-75%RH. These results show cocrystal formation with both unmilled and milled reactants. Mechanical activation of reactants by milling as well as high temperature and RH increases cocrystal formation rates.

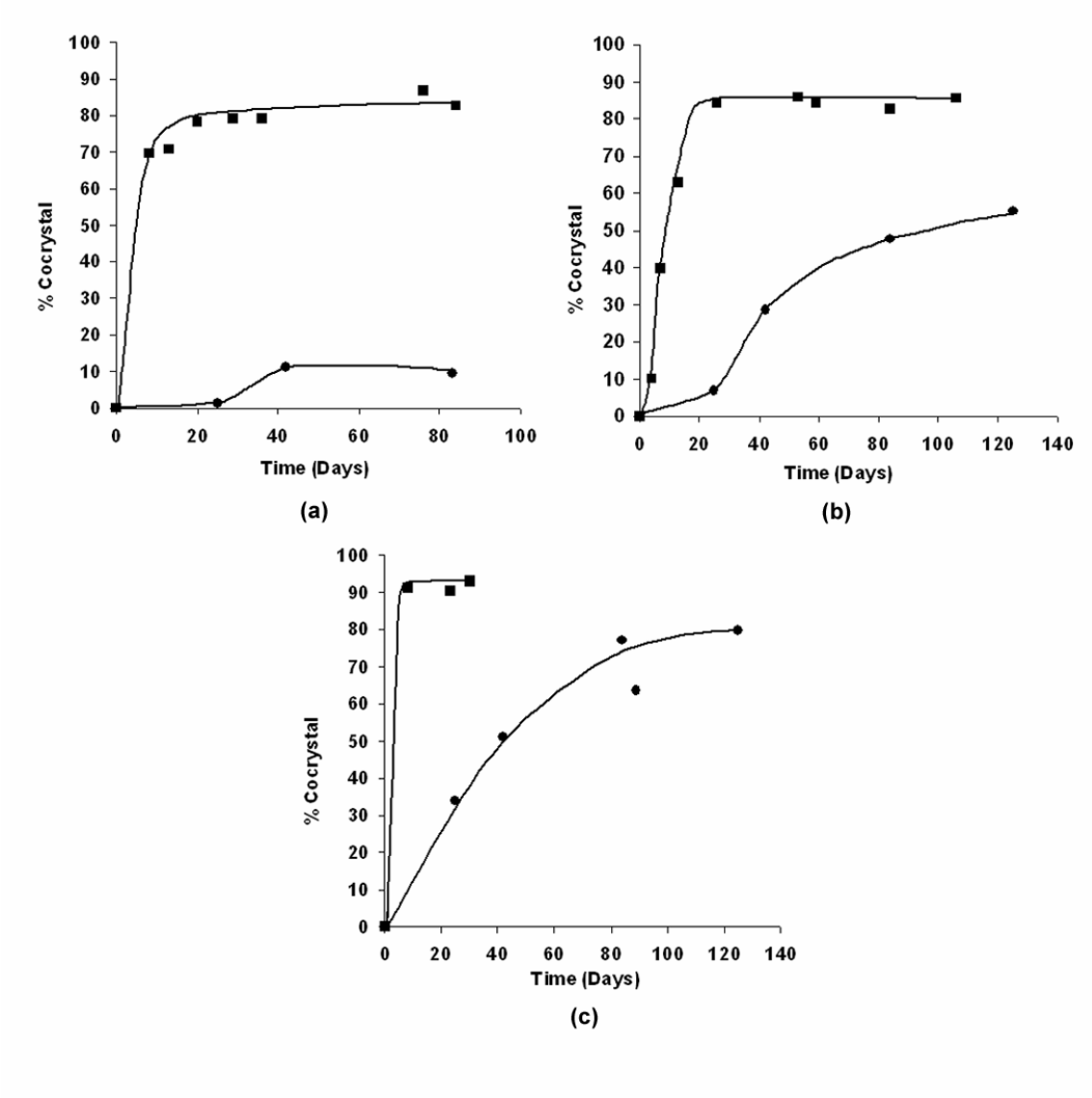

Figure 4.7: CBZ-NCT cocrystal formation in mixtures of milled reactants (■) and mixtures of unmilled reactants (●) stored at (a) 25°C-75%RH, (b) 45°C-0%RH and (c) 45°C-75%RH.

The effect of milling only one reactant, CBZ or NCT, on cocrystal formation during storage was also investigated. Results show that milling CBZ enhances cocrystal formation while milling NCT did not have a measurable effect up to 15 days of storage (Fig. 8). These results were in agreement with IR analysis (IR not shown).

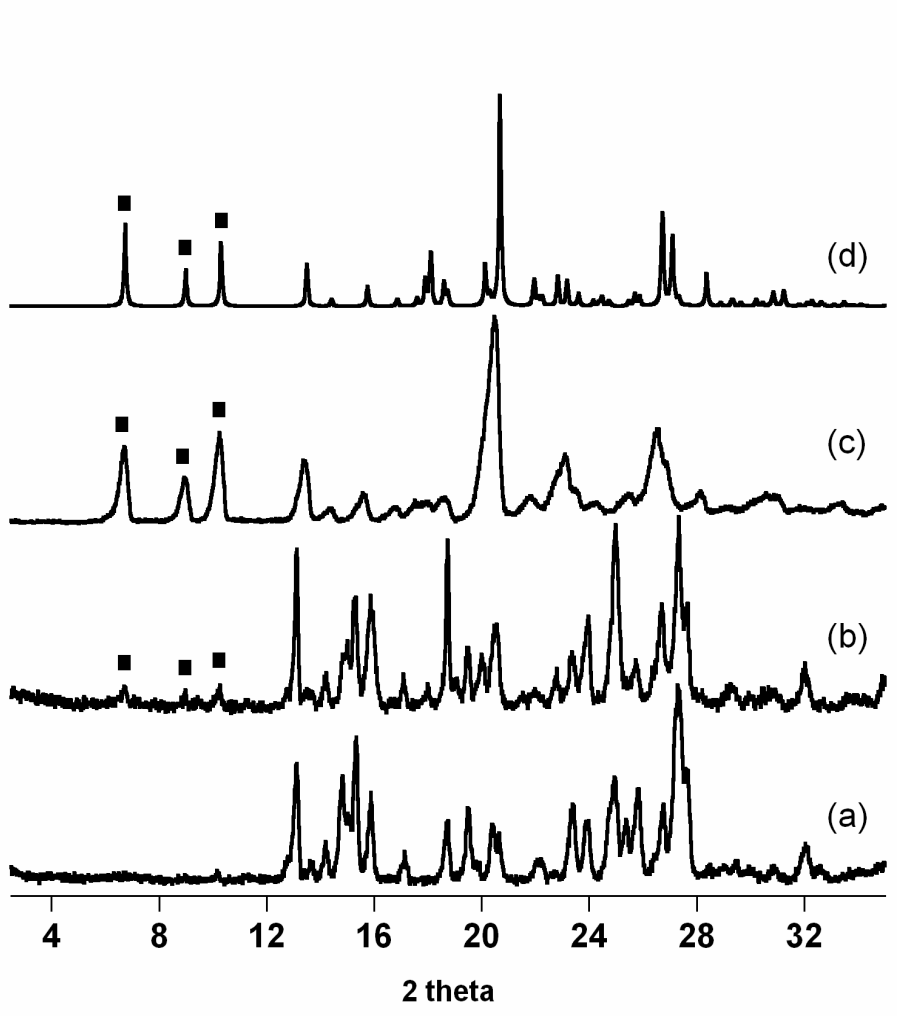

Figure 4.8: XRPD showing the effect of milling only one component on cocrystal formation in mixtures during storage at 25°C-75%RH at day 15 (a) milled NCT-unmilled CBZ, (b) milled CBZ-unmilled NCT; (c) CBZ-NCT cocrystal from solution; (d) Calculated from CBZ-NCT crystal structure.

The role of mechanical activation on cocrystal formation was investigated in mixtures of milled-annealed reactants and mixtures of milled-unannealed reactants. IR spectra and XRPD patterns in Figure 4.9 and Figure 4.10 respectively show that annealing reactants decreases the rate of cocrystal formation.

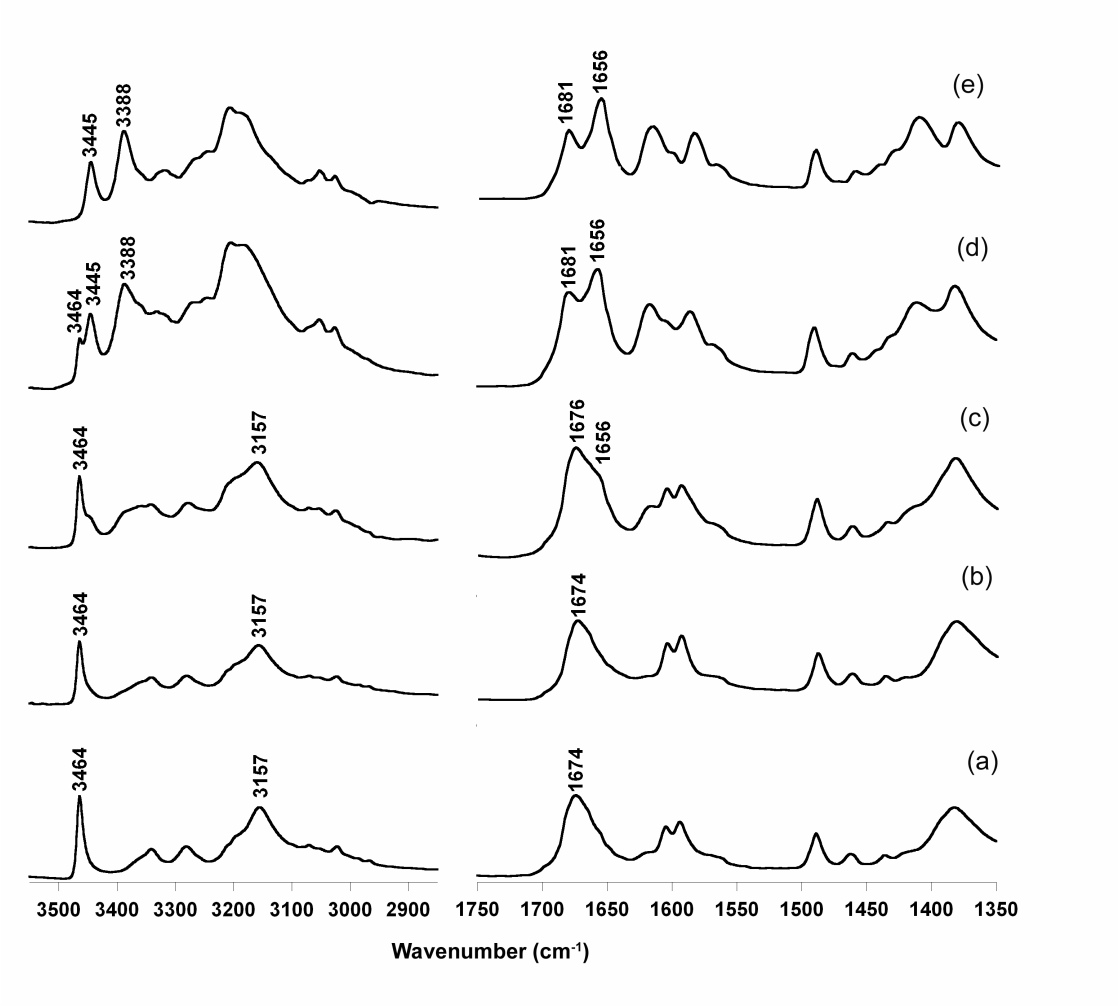

Figure 4.9: FTIR spectra showing the effect of annealing reactants on CBZ-NCT cocrystal formation during storage at 25°C-75%RH. Mixtures of (a) milled reactants at day 0, (b) milled-annealed reactants at day 0, (c) milled-annealed reactants at day 12, (d) milled-unannealed reactants at day 12; (e) CBZ-NCT cocrystal reference.

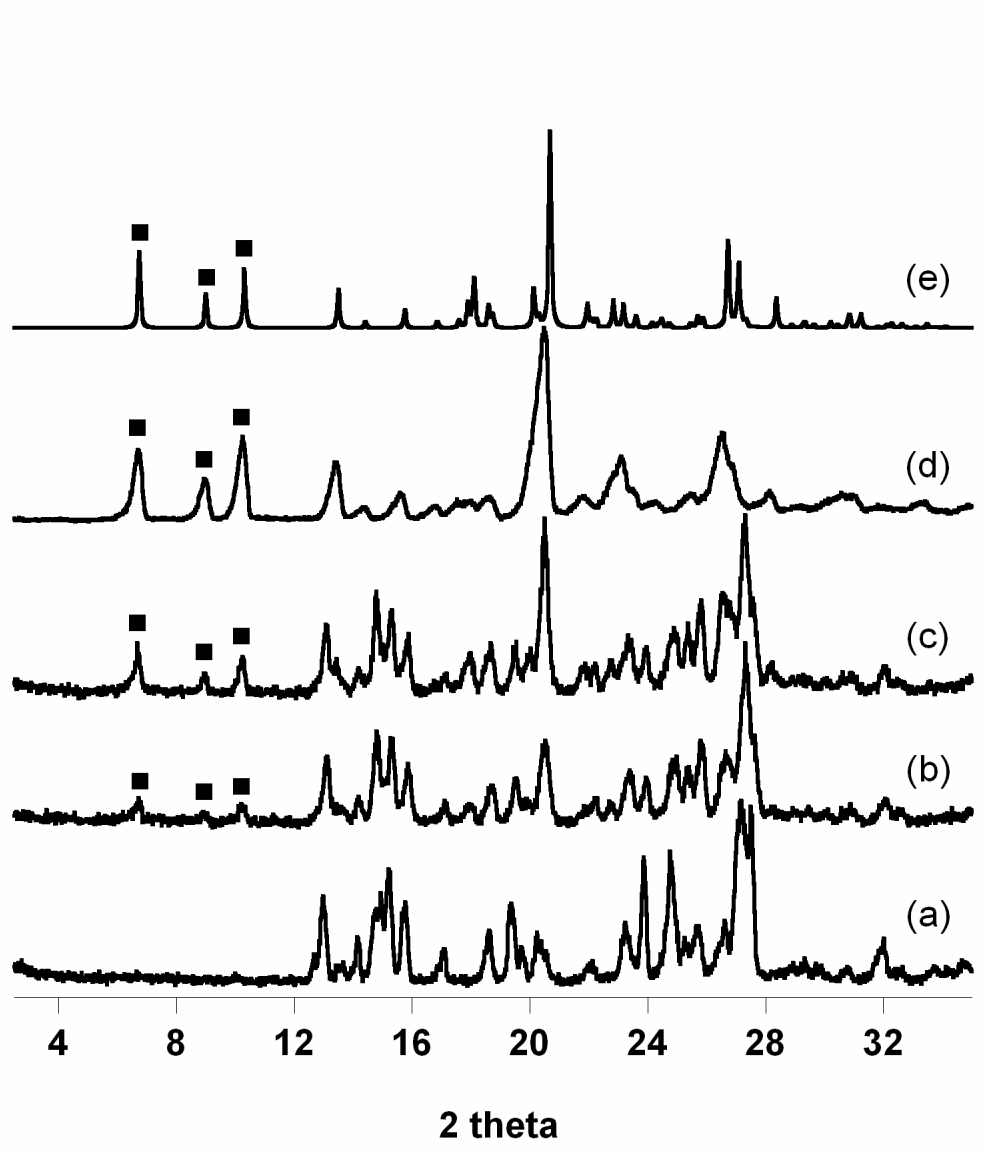

Figure 4.10: XRPD patterns showing the effect of annealing reactants on cocrystal formation at 25°C-75%RH. Mixtures of (a) milled reactants at day 0, (b) milled-annealed reactants at day 12, (c) milled-unannealed reactants at day 12; (d) CBZ-NCT cocrystal from solution; (e) Calculated from CBZ-NCT crystal structure.

Effect of Mechanical Activation and Storage Conditions on CBZ-SAC Cocrystal Formation

Cocrystal formation during storage was also monitored in mixtures of unmilled and mixtures of individually milled CBZ and SAC at 25°C-75%RH, 45°C-0%RH and

45°C-75%RH. FTIR spectra of individually milled reactant mixtures during storage show new peaks at 3440 and 1650cm^{-1} suggesting different intermolecular interactions and perhaps a new phase (Figure 4.11). Peaks corresponding to cocrystal are also observed. XRPD patterns in Figure 4.12 show peaks at 2 theta values of 5.2, 11.3 and 23.0 indicating the formation of a new crystalline phase. The XRPD patterns also show low intensity peaks at 2 theta values of 7.2, 14.2 and 28.4 characteristic of CBZ-SAC cocrystal. Transformation of the new phase to cocrystal was observed after seeding the mixed phase with CBZ-SAC cocrystal prepared from solution. This transformation indicates that the new phase is less stable than the cocrystal prepared from solution. The IR spectra and XRPD patterns suggest that this new form is different from a polymorph of CBZ-SAC cocrystal recently reported.[38] In the case of unmilled reactant mixtures the stable cocrystal was formed and the metastable form was not observed (Table 4.1).

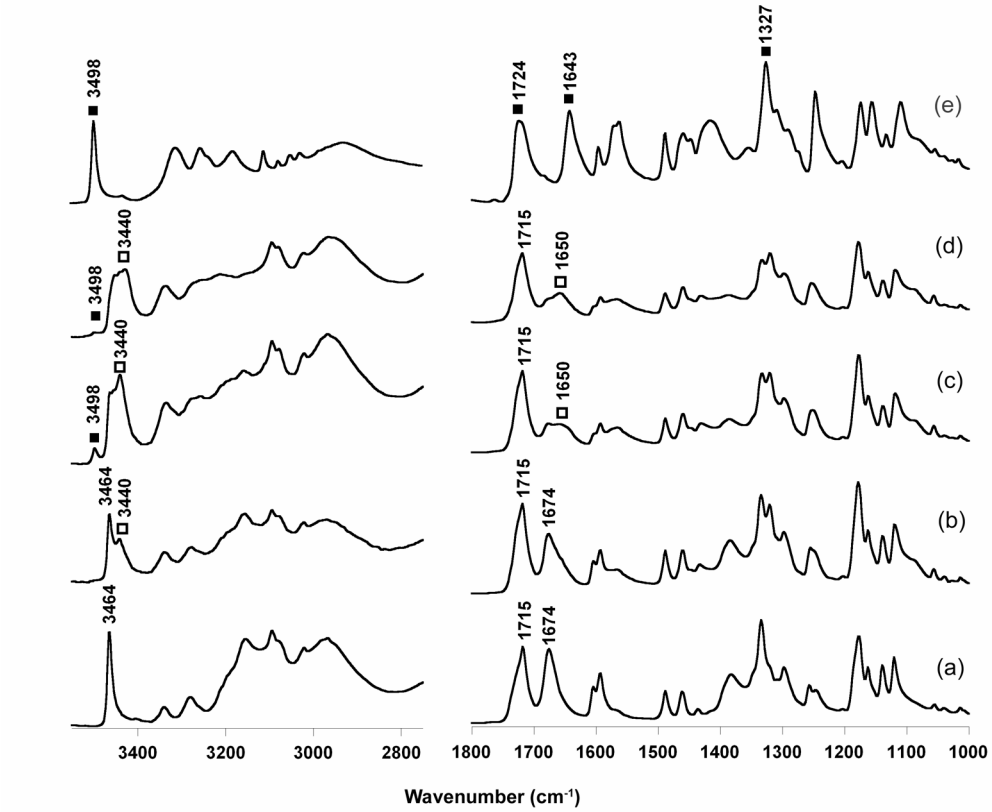

Figure 4.11: FTIR spectra showing the effect of storage condition on CBZ/SAC mixtures prepared with milled reactants. Peaks used to follow the cocrystal formation are indicated by (■) and of new phase are indicated by (□). Mixtures (a) before storage; and after storage for 80 days at (b) 25°C-75%RH, (c) 45°C-0%RH, (d) 45°C-75%RH; (e) CBZ-NCT cocrystal reference.

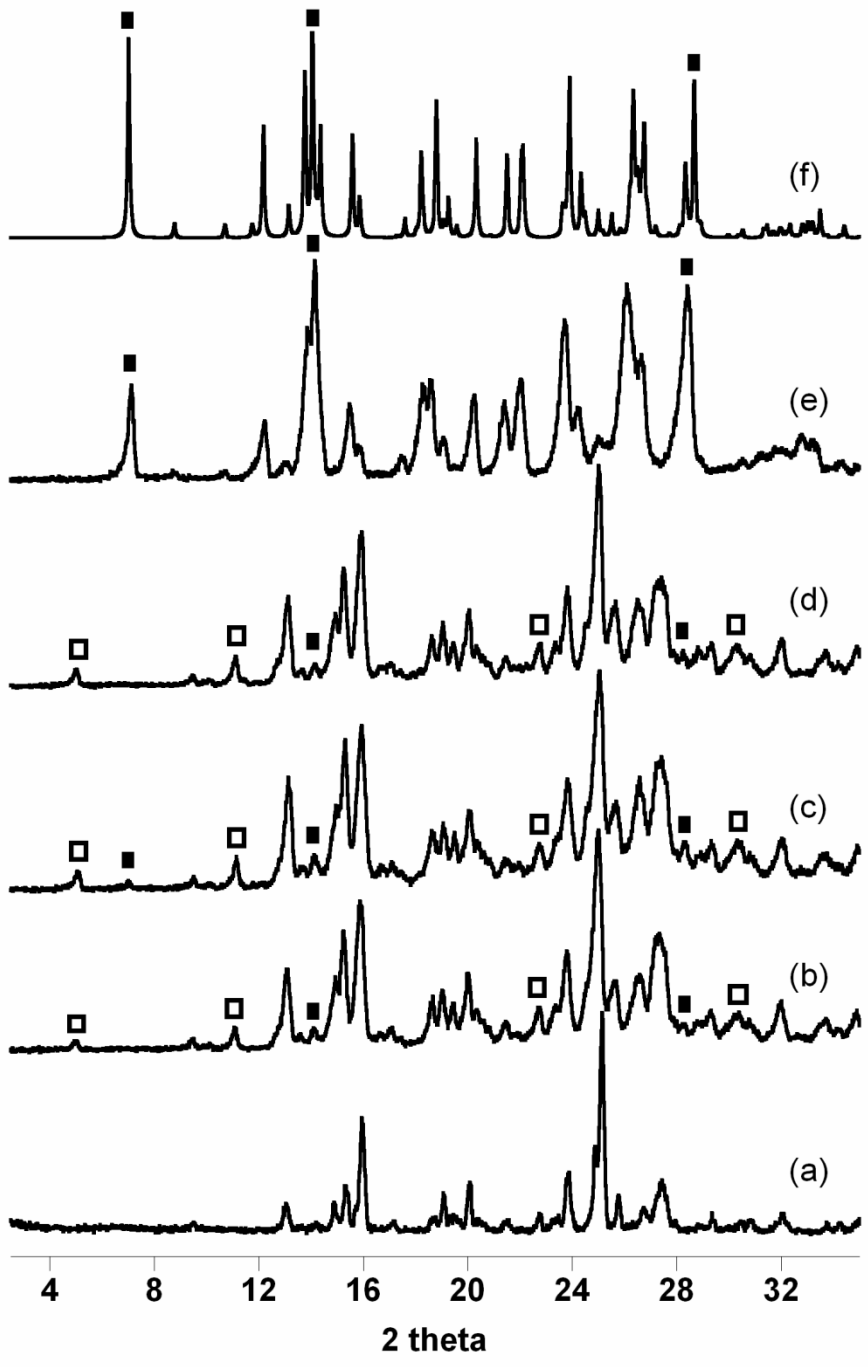

Figure 4.12: XRPD showing the effect of storage conditions on CBZ/SAC mixtures prepared with milled reactants. Peaks used to follow the cocrystal formation are indicated by (■) and of new phase are indicated by (□). Mixture (a) before storage; and after storage for 80 days at (b) 25°C-75%RH, (c) 45°C-0%RH, (d) 45°C-75%RH; (e) CBZ-NCT cocrystal from solution; (f) Calculated from CBZ-SAC crystal structure.

The effect of milling only one reactant was investigated for CBZ/SAC mixtures as well. The mixture behaved similar to the unmilled reactants. Table 4.1 summarizes cocrystal formation in mixtures of CBZ/NCT and CBZ/SAC during 3 months of storage. Under all storage conditions studied, CBZ-NCT cocrystal formation was faster than CBZ-SAC. Mechanical activation of reactants as well as higher temperatures and relative humidities enhanced cocrystal formation.

Table 4.1: Summary of results for cocrystal formation in mixtures during storage

Mixture Type	Storage Condition	Cocrystal formed (1 month)	Cocrystal formed (2 months)	Cocrystal formed (3 months)
CBZ/NCT *Individually milled reactants*	25°C-75%RH	+	+	+
	45°C-0%RH	+	+	+
	45°C-75%RH	+	+	+
CBZ/SAC *Individually milled reactants*	25°C-75%RH	-	+, *	+, *
	45°C-0%RH	-	+, *	+, *
	45°C-75%RH	*	*	+, *
CBZ/NCT *Unmilled reactants*	25°C-75%RH	-	+	+
	45°C-0%RH	-	+	+
	45°C-75%RH	+	+	+
CBZ/SAC *Unmilled reactants*	25°C-75%RH	-	-	-
	45°C-0%RH	-	-	+
	45°C-75%RH	-	+	+

(-) No cocrystal formed, (+) cocrystal formed and (∗) new cocrystal polymorph.

Discussion

Spontaneous cocrystal formation without milling reactants indicates that cocrystal is the thermodynamically stable phase. The requirement for spontaneity is a negative free energy change. The free energies for cocrystal formation can be evaluated from solubilities or equilibrium constants by a method similar to that described for solvates.[39, 40] The free energies for CBZ-NCT and CBZ-SAC cocrystal formation from the reactant mixtures in the solid-state were calculated to be -4.8 kJ/mol and -5.1 kJ/mol, at 25°C according to the thermodynamic cycle illustrated in Table 4.2. K_{sp} and solubility values in terms of concentrations measured in ethanol were used to calculate free energies. For a more rigorous calculation activities should be considered, however, solution complexation under these conditions is negligible and K_{sp} describes the experimental solubility behavior. [21] These negative free energies confirm the spontaneity of the process. While the free energies of formation are comparable for the two cocrystals, rates of formation for CBZ-NCT were faster than for CBZ-SAC, suggesting that factors other than thermodynamics such as diffusivities, molecular mobility, molecular interactions, solid surface interactions, influence the rate of crystallization [41-46].

Table 4.2: Chemical equilibria considered for free energy calculations

Equation #	Equilibrium reaction	Free energy of reaction
4.1	$A_{(solid)} \rightleftharpoons A_{(soln)}$	$\Delta G° = -RT \ln(K) = -RT(\ln S_A)$
4.2	$B_{(solid)} \rightleftharpoons B_{(soln)}$	$\Delta G° = -RT \ln(K) = -RT(\ln S_B)$
4.3	$A_{(soln)} + B_{(soln)} \rightleftharpoons AB_{(solid)}$	$\Delta G° = -RT \ln(1/K_{sp})$
	Adding equations 4.1, 4.2 and 4.3 yields	
4.4	$A_{(solid)} + B_{(solid)} \rightleftharpoons AB_{(solid)}$	$\Delta G° = -RT \ln\left[\frac{S_A S_B}{K_{sp}}\right]$

S_A and S_B are the solubilities of the drug and ligand in the solvent. K_{sp} is the solubility product of the cocrystal. The solubility in concentration units (M) are: CBZ(III)=0.108, NCT(I)=0.841 and SAC=0.189; The K_{sp} values in concentration units (M^2) are: CBZ-NCT=0.0129 and CBZ-SAC=0.0026. All measurements were carried out at 25°C.[21, 32]

Cocrystal formation rates increased with higher relative humidities and temperatures. It is important to note that cocrystal formation occurs in unmilled reactants at room temperature. Previous studies have shown that vapor sorption of reactants can lead to deliquescence and generate the supersaturation necessary for cocrystal Formation.[22, 31] This has been shown for CBZ/NCT mixtures at high RH (98%) where moisture sorption occurs due to deliquescence of NCT.[22] Results of the present study show low moisture uptake of NCT (< 0.3%) at 25°C-75%RH and 45°C-75%RH and suggest that cocrystal formation is not deliquescence-mediated under these conditions. The deliquescence relative humidity of NCT at 25°C and 45° is above 85%. Furthermore, CBZ, SAC, CBZ-SAC and CBZ-NCT do not deliquesce under these conditions[22] . Thus low levels of moisture uptake can facilitate conversions to cocrystal.

Eutectic melt-mediated cocrystal formation at room temperature has been reported for benzophenone and diphenylamine.[27] Similar behavior has been shown for

cocrystals of CBZ with carboxylic acids at temperatures above 85°C[14]. Thermal analysis of 1:1 CBZ/NCT and CBZ/SAC mixtures did not show an endothermic event corresponding to a melt below 85°C and therefore cocrystal formation is not melt-mediated under these conditions. Solid-vapor interactions due to sublimation of reactants have also been shown to form cocrystals.[25] While it is not clear the extent to which sublimation plays a role in our studies, physical contact between the reactants was necessary for cocrystal formation.

Solid state mediated cocrystal formation has been reported to occur by disorder or amorphous phases generated by comilling or melt quenching.[29, 47] Cocrystal formation from amorphous phases has been shown for CBZ-SAC, CBZ-NCT, as well as for some cholic acid complexes.[29, 47, 48] Rates of cocrystal formation were also shown to increase with increasing temperature and relative humidities during storage. In the present study, individually milling reactants increased cocrystal formation rates during storage. Faster cocrystal formation rates may be due to disorder and higher surface areas generated by milling reactants. Disordered regions were not detectable by XRPD or DSC, however annealing reactants prior to mixing slowed the rate of cocrystal formation. Small percentage of disorder created by milling, as little as 2%, has been shown to increase reactivity as in the chemical degradation of metoclopramide by Maillard reaction, while annealing decreased reactivity.[49]

Mechanical activation of only one component in reactant mixtures also affects cocrystal formation rates. CBZ-NCT cocrystal formation is faster in mixtures of milled CBZ/unmilled NCT relative to mixtures of unmilled CBZ/milled NCT. Milling either reactant did not form CBZ-SAC cocrystal up to 30 days of storage. This behavior may

be associated with the molecular mobility and glass transition temperature of reactants and is currently under investigation.

Conclusion

Conversion of solid reactants to cocrystal occurs spontaneously even when reactants are not mechanically stressed. Free energy calculations indicate that transformation of solid reactants to cocrystal is favorable under ambient conditions. Our results show that low levels of moisture uptake and temperatures encountered during pharmaceutical processing and storage produce cocrystals. Mechanical activation of individual reactants increases the kinetics of cocrystal formation in binary mixtures of reactants. These findings have important implications in formulation development, process design and product performance.

References

1. S. L. Childs, K. Hardcastle, *Cryst. Growth Des.,* 2007**, 7,** 1291-1304.

2. S. L. Childs, N. Rodríguez-Hornedo, L. S. Reddy, A. Jayasankar, C. Maheshwari, L. M. Mccausland, R. Shipplett, B. Stahly, *CrystEngComm,* 2008**, 10,** 856-864.

3. M. R. Caira, *Mol. Pharm.,* 2007**, 4,** 310-316.

4. Ö. Almarsson, M. Zaworotko, *ChemComm,* 2004**,** 1889-1896.

5. N. Shan, M. Zaworotko, *Drug Discovery Today,* 2008**, 13,** 440-446.

6. M. J. Zaworotko, *Cryst. Growth Des.,* 2007**, 7,** 4-9.

7. P. Vishweshwar, J. R. Mcmahon, J. A. Bis, M. J. Zaworotko, *J. Pharm. Sci.,* 2006**, 95,** 499-516.

8. A. V. Trask, S. W. D. Motherwell, W. Jones, *Cryst. Growth Des.,* 2005**, 5,** 1013-1021.

9. A. V. Trask, S. W. D. Motherwell, W. Jones, *Int. J. Pharm.,* 2006**, 320,** 114-123.

10. D. P. Mcnamara, S. L. Childs, J. Giordano, A. Iarriccio, J. Cassidy, M. S. Shet, R. Mannion, E. O. Donnell, A. Park, *Pharm. Res.,* 2006**, 23,** 1888-1897.

11. J. F. Remenar, M. L. Peterson, P. W. Stephens, Z. Zhang, Y. Zimenkov, M. B. Hickey, *Mol. Pharm.,* 2007**, 4,** 386-400.

12. A. Bak, A. Gore, E. Yanez, M. Stanton, S. Tufekcic, R. Syed, A. Akrami, M. Rose, S. Surapaneni, T. Bostick, A. King, S. Neervannan, D. Ostovic, A. Koparkar, *J. Pharm. Sci.,* 2007.

13. S. Karki, T. Friscic, W. Jones, W. D. Motherwell, *Mol. Pharm.,* 2007**, 4,** 347-354.

14. E. Lu, N. Rodríguez-Hornedo, R. Suryanarayanan, *CrystEngComm,* 2008**, 10,** 665-668.

15. M. C. Etter, *J. Phys. Chem.,* 1991**, 95,** 4601-4610.

16. S. G. Fleischman, S. S. Kuduva, J. A. Mcmahon, B. Moulton, R. D. B. Walsh, N. Rodríguez-Hornedo, M. J. Zaworotko, *Cryst. Growth Des.,* 2003**, 3,** 909-919.

17. G. R. Desiraju, *J. Mol. Struc.,* 2003**, 656,** 5-15.

18. N. Shan, F. Toda, W. Jones, *ChemComm,* 2002**,** 2372-2373.

19. V. R. Pedireddi, W. Jones, A. P. Chorlton, R. Docherty, *Tetra. Lett.,* 1998**, 39,** 5409-5412.

20. A. Nangia, G. R. Desiraju, *Des. Org. Solids,* 1998**, 198,** 57-95.

21. S. J. Nehm, B. Rodríguez-Spong, N. Rodríguez-Hornedo, *Cryst. Growth Des.,* 2005**, 6,** 592-600.

22. A. Jayasankar, D. Good, N. Rodríguez-Hornedo, *Mol. Pharm.,* 2007**, 4,** 360-372.

23. N. Rodríguez-Hornedo, S. J. Nehm, K. F. Seefeldt, Y. Pagan-Torres, C. J. Falkiewez, *Mol. Pharm.,* 2006**, 3,** 362-367.

24. S. Limmatvapirat, E. Yonemochi, T. Oguchi, K. Yamamoto, *J. Incl. Mol. Recog. Chem.,* 1998**, 31,** 367-379.

25. C. C. Mattheus, J. Baas, A. Meetsma, J. L. D. Boer, C. Kloc, T. Siegrist, T. T. M. Palstra, *Acta. Crystallogr.,* 2002**, 58,** 1229-1231.

26. S. Limmatvapirat, E. Yonemochi, T. Oguchi, K. Yamamoto, *Chem. Phar. Bull.,* 1997**, 45,** 1358-1362.

27. K. Chadwick, R. Davey, W. Cross, *CrystEngComm,* 2007**, 9,** 732-734.

28. D. J. Berry, C. C. Seaton, W. Clegg, R. W. Harrington, S. J. Coles, P. N. Horton, M. B. Hursthouse, R. Storey, W. Jones, T. Friscic, N. Blagden, *Cryst. Growth Des.,* 2008**, 8,** 1697-1712.

29. A. Jayasankar, A. Somwangthanaroj, Z. J. Shao, N. Rodríguez-Hornedo, *Pharm. Res.,* 2006**, 23,** 2381-2392.

30. J. Sangster, *J. Phy. Chem. Ref. Data,* 1999**, 28,** 889-930.

31. D. Braga, S. L. Giaffreda, F. Grepioni, M. R. Chierotti, R. Gobetto, G. Palladino, M. Polito, *CrystEngComm,* 2007**, 9,** 879-881.

32. D. Good, N. Rodríguez-Hornedo, *Cryst. Growth Des.,* 2009, *Vol. 9 (5), 2252-2264*.

33. J. L. Wardell, J. N. Low, C. Glidewell, *Acta. Crystallogr.,* 2005**, E61,** 1944.

34. J. P. Reboul, B. Cristau, J. C. Soyfer, J. P. Astier, *Acta Crystallogr.,* 1981**, B37,** 1844.

35. C. B. Aakeroy, A. M. Beatty, B. A. Helfrich, M. Nieuwenhuyzen, *Cryst. Growth Des.,* 2003**, 3,** 519.

36. J. L. Atwood, L. J. Barbour, *Cryst. Growth Des.,* 2003**, 3,** 378.

37. L. J. Barbour, *J. Supramol. Chem.,* 2001**, 1,** 189-191.

38. W. W. Porter, S. C. Elie, A. J. Matzger, *Cryst. Growth Des.,* 2008**, 8,** 14-16.

39. S. Ghosh, D. J. W. Grant, *Int. J. Pharm.,* 1995**, 114,** 185-196.

40. S. J. Bethune, N. Rodríguez-Hornedo, *Manuscript in preparation*.

41. D. Murphy, F. Rodríguez-Cintron, B. Langevin, R. C. Kelly, N. Rodríguez-Hornedo, *Int. J. Pharm.,* 2002**, 246,** 121-134.

42. J. Bernstein, R. J. Davey, J.-O. Henck, *Angew. Chem. Int. Ed.,* 1999**, 38,** 3440-3461.

43. V. Andronis, G. Zografi, *J. NonCrystall. Solids,* 2000**, 271,** 236-248.

44. N. Rodríguez-Hornedo, *Cocrystals: Design, Properties and Formation Mechanisms; In: Encyclopedia of Pharmaceutical Technology; 3rd Ed.,* 2007**, DOI: 10.1081/E-EPT-120041485,** 615-635.

45. C.-H. Gu, V. Young, D. J. W. Grant, *J. Pharm. Sci,* 2001**, 90,** 1878-1890.

46. N. Rodríguez-Hornedo, R. C. Kelly, B. D. Sinclair, J. M. Miller, *Crystallization: General Principles and Significance on Product Development; In: Encyclopedia of Pharmaceutical Technology; 3rd Ed.,* 2006**,** 834-857.

47. K. Seefeldt, J. Miller, F. Alvarez-Nunez, N. Rodríguez-Hornedo, *J. Pharm. Sci.,* 2007**, 96,** 1147-1158.

48. T. Oguchi, Y. Tozuka, T. Hanawa, M. Mizutani, N. Sasaki, S. Limmatvapirat, K. Yamamoto, *Chem. Pharm. Bull.,* 2002**, 50,** 887-891.

49. Z. Qiu, J. G. Stowell, W. Cao, K. R. Morris, S. R. Byrn, M. T. Carvajal, *J. Pharm. Sci.,* 2005**, 94,** 2568-2580.

CHAPTER 5

FREE ENERGY CALCULATIONS FOR COCRYSTAL FORMATION FROM ITS REACTANTS IN THE SOLID STATE

Abstract

The purpose of this work is to present mathematical models that describe cocrystal thermodynamic stability and the driving force for cocrystal formation from its components in the solid state, from directly measurable and derived thermodynamic parameters. Based on the thermal properties of cocrystal reactants, thermodynamic cycles were developed and used to express the Gibbs free energy of formation. The Gibbs free energy of formation for several cocrystals was calculated from melting point (MP), heat of fusion (ΔH_f), entropy of fusion (ΔS_f) and from the heat capacity (ΔC_p) difference of the solid and liquid state of the components. Cocrystals with MP between the two components or with lower MP than either component were analyzed using the derived equations. Standard and modulated differential scanning calorimetry (DSC) was used for measuring the thermodynamic quantities. The Gibbs free energy of formation ($\Delta G^{o}_{T_f^A}$) at the melting point of the lower melting component, A, changes as a function of the difference in melting point between the higher melting component and the cocrystal ($\Delta T = T_f^B - T_f^C$). Greater values of ΔT, as well as when cocrystal melts

below the melting temperature of component A, result in small $\Delta G^{o}_{T_f^A}$ values, suggesting that solid to solid transition of pure crystalline components into cocrystals is not thermodynamically favored. Cocrystals with a smaller value of ($\Delta T = T_f^B - T_f^C$) usually resulted in large negative values of $\Delta G^{o}_{T_f^A}$ suggesting that the spontaneous cocrystal formation from pure crystalline components is thermodynamically favorable. This has important implications for assessing thermodynamic stability in pharmaceutical formulations containing a cocrystal and/or its components.

Introduction

In recent years, pharmaceutical cocrystals have become an emerging class of crystal forms that is considered during the early phase of drug development.[1-3] Cocrystals are attractive alternative solid forms as they have the ability to alter the physico-chemical properties of the active, leading to desirable biopharmaceutical outcome. There are several reports that describe the solute-solvent interactions such as complexation, aqueous solubility, solubility dependence on pH, micellar solubilization behavior, dissolution behavior and bioavailability advantages of cocrystals.[2, 4-10] Since the application of cocrystals as possible pharmaceutical solid forms is still emerging, a lot of research is directed towards the discovery of new cocrystals. Several reports have been published on the methods that were successfully applied to discover new cocrystals. Some of the most commonly reported techniques to synthesize cocrystals are grinding of the cocrystal reactants in a mill, grinding of reactants with the aid of solvent, reaction crystallization method and thermal methods such as cocrystallization from melt.[11-15] Although these methods are employed when a deliberate attempt is made with the

intention to discover new cocrystals, there is evidence showing that cocrystal formation can occur inadvertently from solutions of cocrystal constituents, mixtures with deliquescent additives and from eutectic melts.[3, 5, 16] In one instance, spontaneous cocrystallization from reactants has been documented where the cocrystal components when stored as physical mixtures converted to cocrystals without external energy input. It was observed in this study that the transformation was truly a solid to solid conversion of reactants to cocrystals, as no other mechanisms such as eutectic melt, water adsorption by reactants or amorphous phase mediated cocrystallization were determined to be responsible for cocrystal formation.[17] This spontaneous formation of cocrystals from its constituent reactants is the result of differences in the energetics between the cocrystal and its reactants in the solid state resulting in the negative free energy of formation (ΔG_f^o). However, there is no mathematical treatment available to calculate ΔG_f^o of formation for cocrystals from its reactants using the thermodynamic properties of the solid reactants.

The thermodynamic driving force for racemic compounds from its enantiomers has been previously described, where a binary phase diagram generated from fusion data has been used to describe the nature of racemic compound, racemic conglomerate or a pseudo-racemate.[18, 19] In the case of racemic compounds the thermodynamic driving force for the formation of racemates is provided due to the differences in thermodynamic properties of the racemates and enantiomers. Likewise, the differences in the thermodynamic properties of cocrystal and its components can be used to understand the driving force for the formation of cocrystals from solid reactants. This type of investigation has been carried out previously for chiral organic compounds as well as

chiral pharmaceuticals.[20, 21] Although some studies on the thermodynamics of cocrystal formation have been reported,[22, 23] an investigation of this nature where the thermodynamic driving force for a solid to solid cocrystal transformation is studied has not been reported to the best of our knowledge. Cocrystals differ from racemates in their chemical composition, such that unlike racemates, the constituents of cocrystals are often entities of different chemical class with widely different fusion properties. Due to this difference, the thermodynamic cycles developed by Jacques et. al., to calculate the free energy of formation of racemates cannot be applied to cocrystals. The specific aim of this work is therefore to, (i) Investigate the thermal properties of cocrystal and its components to generate a binary phase diagram, (ii) Categorize cocrystals in groups based on it thermal properties relative to their components and, (ii) Develop thermodynamic cycles that are useful in calculating the driving force for cocrystal formation from its components. Cocrystal of carbamazepine (CBZ) and nicotinamide (NCT) is used as the model system to generate the temperature-composition phase diagram. Similar to racemic compounds, a binary phase diagram can be used to predict the stability of the cocrystals. However, unlike racemic compounds melting point alone is not sufficient to predict the cocrystal stability, rather the magnitude of the difference in the melting point of the cocrystal and its components will govern the relative stability of the phases. This is discussed in detail in this chapter.

Several cocrystals are selected for investigation in this work and theoretical models to calculate the free energy of formation are developed for two categories of cocrystals, (i) cocrystals with melting point in between the melting point of its constituents and, (ii) cocrystals with melting point lower than melting point of its

constituents. The binary phase diagrams of these two types of cocrystals are shown in Figure 5.1.

Theoretical

The stability of a cocrystal can be defined by the molar Gibbs free energy change (ΔG^o) for the reaction where solid to solid transformation corresponding to the crystals of the two reactants A and B occur to yield cocrystal AB. The reaction can be depicted as,

$$A_s + B_s \rightarrow AB_s \qquad (5.1)$$

The subscript 's' refers to the crystalline solid state of the cocrystal and its reactants. For spontaneous cocrystal formation the free energy change associated with this reaction must be negative. The Gibbs free energy of formation ΔG_f^o can be expressed as a function of the corresponding molar enthalpy of formation ΔH_f^0 and the molar entropy of formation ΔS_f^0.

$$\Delta G_f^o = \Delta H_f^0 - T\Delta S_f^0 \qquad (5.2)$$

The thermodynamic quantities in equation (5.2) can be determined from calorimetric data. Two types of cocrystal systems are discussed, (a) cocrystal melting point is in between the melting point of its reactants, ($T_f^A < T_f^C < T_f^B$) and, (b) cocrystal melting point is lower than the melting point of both its reactants ($T_f^C < T_f^A < T_f^B$). These two types of systems are shown in Figure 5.2 and Figure 5.3 for cocrystals of 1:1 stoichiometry. Superscripts A, B and C refer to cocrystal constituents and cocrystal respectively.

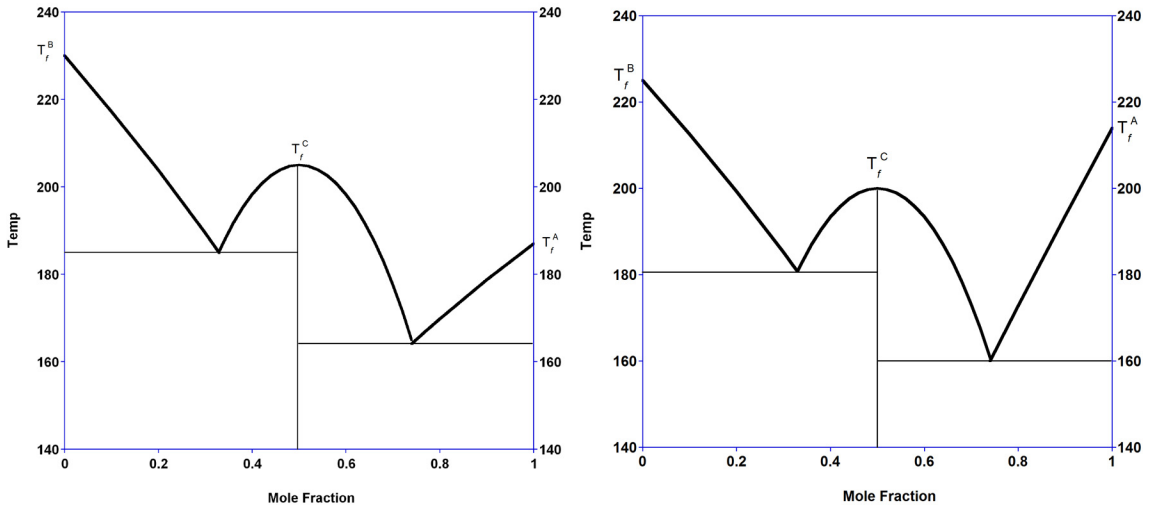

Figure 5.1: Theoretical phase diagrams of cocrystals; (a) Cocrystal melting point between the melting point of its components; (b) cocrystal melting point lower than the melting point of its components. T_f^A, T_f^B and T_f^C are the melting points of cocrystal constituents A and B and cocrystal respectively.

Jacques et al. developed an approach based on the differences in the thermodynamic quantities between racemic compounds and their corresponding racemate to calculate the enthalpy and entropy of formation, from which free energy of formation can be calculated.[20] In our work the thermodynamic cycles (TDC) are developed for cocrystals, which unlike racemic compounds have components that are chemically different and have different melting temperatures and melting enthalpies. Figure 5.2 and Figure 5.3 show TDCs for cocrystals classified into two different categories shown in Figure 5.1.

When the reaction shown by equation (5.1) occurs at the melting point of the species that has the lowest melting point (reactant B in this case), and assuming that the

cocrystal reactants are completely immiscible in the solid state i.e., $\Delta H_S^m = 0$ and the enthalpy of mixing in the liquid state is ΔH_l^m, equations can be derived to calculate the free energy of cocrystal formation. For a random mixture of compounds in the liquid state, i.e., when the entropy of mixing is ideal, ΔS_l^m can be expressed as,

$$\Delta S_l^m = -R(\chi_A \ln \chi_A + \chi_B \ln \chi_B)$$

For a 1:1 cocrystal the ideal entropy of mixing value will be,

$$\Delta S_l^m = R \ln 2 = 5.76 Jmol^{-1}K^{-1} \qquad (5.3)$$

Using the TDC shown in Figure 5.2, enthalpy and entropy of formation expressions were derived which were then used to define the expression for the Gibbs free energy of formation (ΔG_f^o) formation of cocrystals.

Case 1 ($T_f^A < T_f^C < T_f^B$):

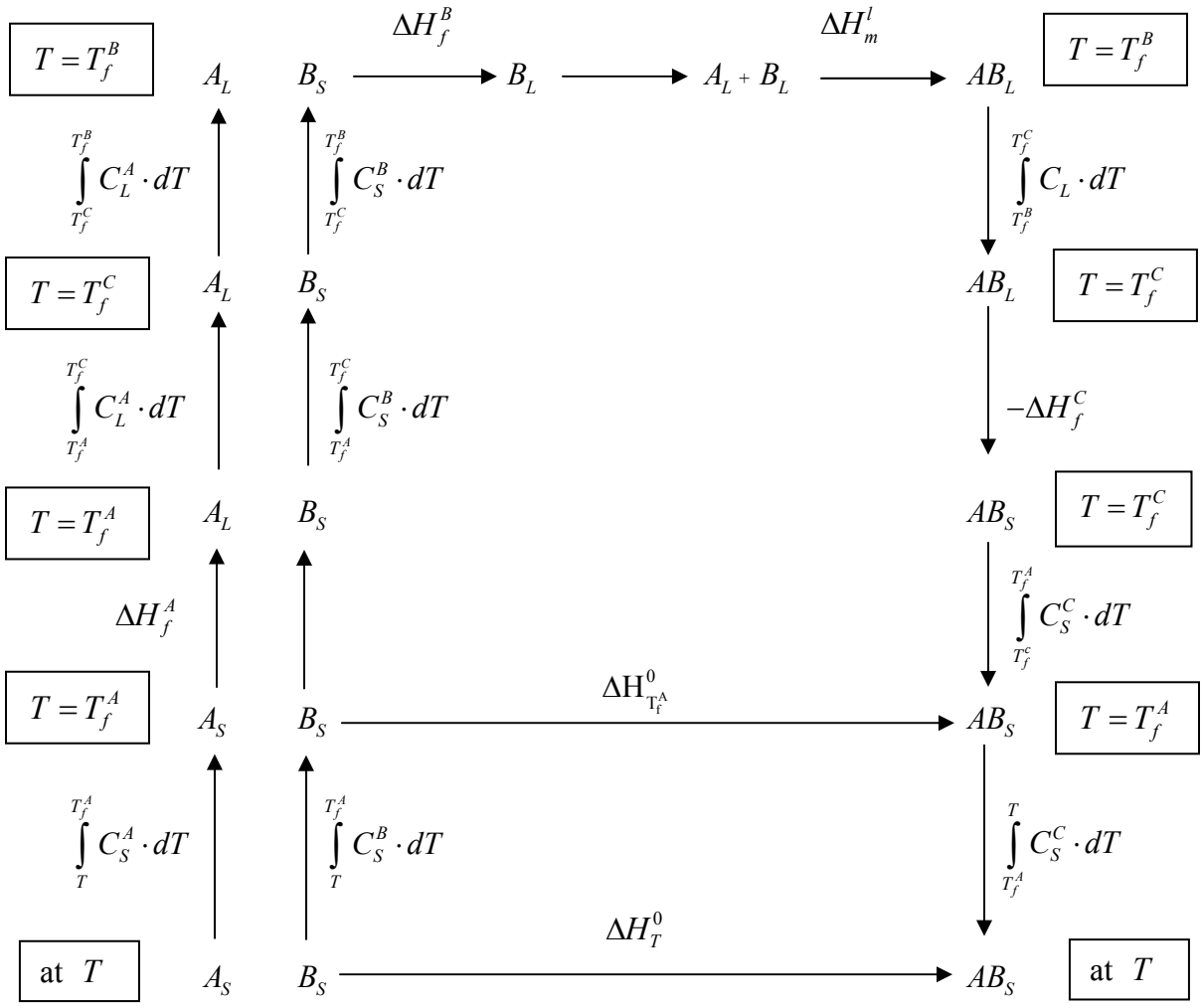

Figure 5.2: The enthalpy changes during various steps of a TDC involving cocrystal reactants A, B and cocrystal C, when cocrystal melting point is between its constituents. ΔH_f, C_s, C_L and T_f represent the enthalpy of fusion, heat capacity of the solid and liquid and fusion temperature respectively. Subscripts l and s denote the liquid and solid phases. ΔH^m and ΔH^o denote the enthalpy of mixing and the enthalpy of formation respectively.

From the TDC shown in Figure 5.2 enthalpy of formation at fusion temperature of lowest melting component is given by,

$$\Delta H^{0}_{T_f^A} = C_S^B(T_f^A - T_f^B) + C_L(T_f^C - T_f^B) + C_S^C(T_f^A - T_f^C) + \Delta H_f^A + \Delta H_f^B - \Delta H_f^C + \Delta H_l^m \qquad (5.4)$$

Entropy of formation ($\Delta S^{0}_{T_f^A}$) is given by,

$$\Delta S^{0}_{T_f^A} = (C_S^B - C_S^C)(\ln \frac{T_f^C}{T_f^A}) + (C_L - C_S^B)(\ln \frac{T_f^C}{T_f^B}) + \Delta S_f^A + \Delta S_f^B - \Delta S_f^C + R \ln 2 \qquad (5.5)$$

Assuming that the contribution of heat capacity terms in equations (5.4) and (5.5) are negligible, and substituting the enthalpy and entropy of formation in equation (5.2) gives the expression to calculate the free energy of formation $\Delta G^{0}_{T_f^A}$,

$$\Delta G^{0}_{T_f^A} = \Delta S_f^B(T_f^B - T_f^A) - \Delta S_f^C(T_f^C - T_f^A) - T_f^A R \ln 2 + \Delta H_l^m \qquad (5.6)$$

Equation (5.6) can be further simplified by applying Walden's rule and taking average entropies of fusion of component A and cocrystal,

$$\Delta G^{0}_{T_f^A} = \Delta S(T_f^B - T_f^C) - T_f^A R \ln 2 + \Delta H_l^m \qquad (5.7)$$

Equations (5.6) and (5.7) can be used to calculate the free energy of formation of cocrystal at the fusion temperature of the lower melting species. Equation (5.7) indicates that the difference between the melting temperature of the higher melting component (B) and cocrystal will influence the sign as well as magnitude of ΔG_f^o of formation. The entropy of mixing term always favors cocrystal formation while the enthalpy of mixing can be negative, positive or zero. The heat of mixing depends on the molecular interactions between the cocrystal components. The value of ΔH_l^m is negative when there is bond formation in the reactant melt, positive if the mixture is not ideal and no molecular interaction occurs, while a $\Delta H_{mix} = 0$ implies that the mixture behaves ideally

in the liquid state. In the case of cocrystal formation, the value of ΔH_l^{mix} must be negative due to interactions between the cocrystal components. These interactions are most likely due to the hydrogen bond formation between the reactants. Table 5.1 contains the thermal data for cocrystals that have melting point in between the melting point of its components.

Case 2 ($T_f^C < T_f^A < T_f^B$):

In the case when the cocrystal fusion temperature is below the fusion temperature of both its components, the TDC shown in Figure 5.3 can be used to derive the relevant equations to calculate the free energy as shown.

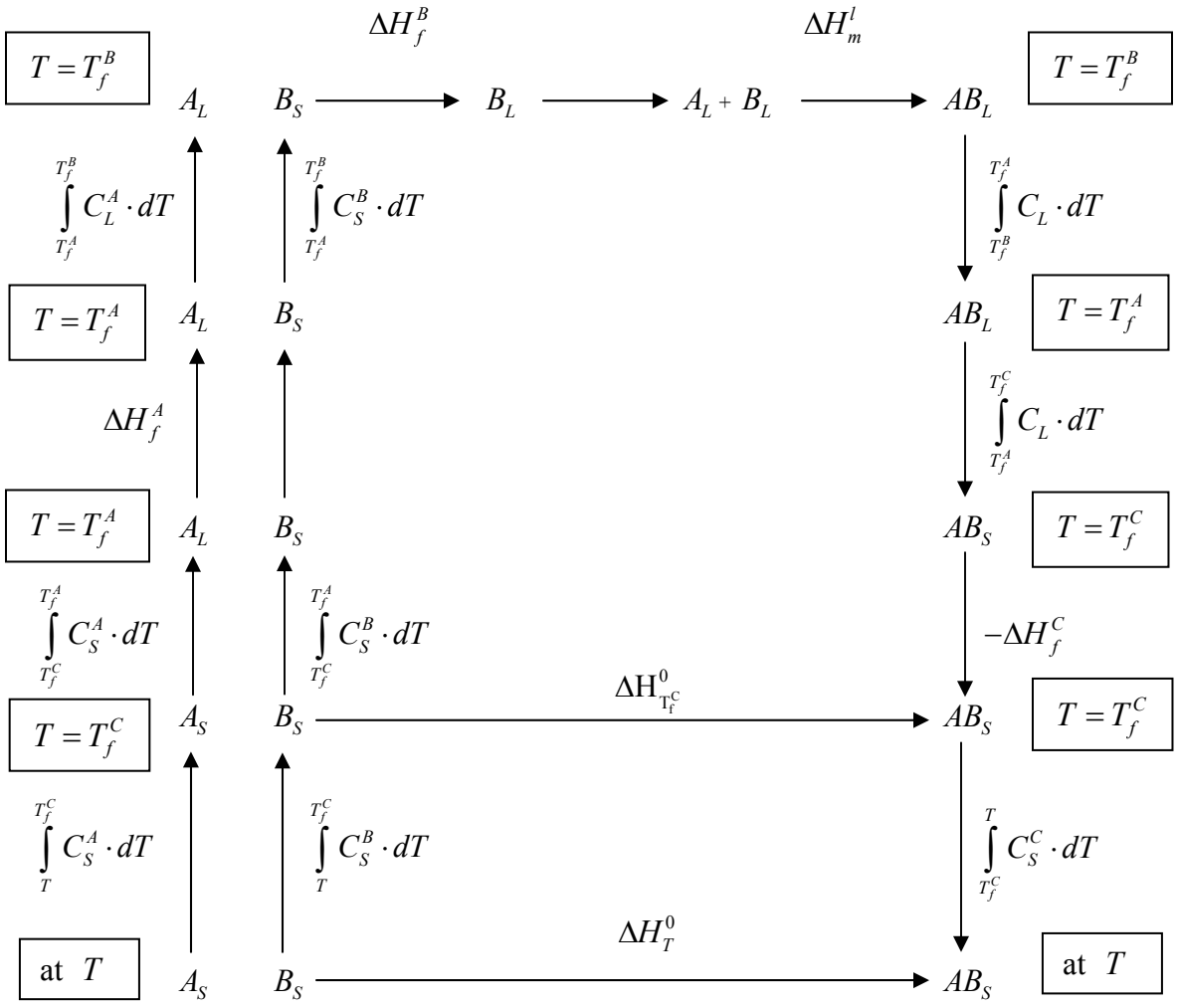

Figure 5.3: The enthalpy changes during various steps of a TDC involving the cocrystal reactants A and B and cocrystal C, when cocrystal melting point is lower then that of its components. ΔH_f, C_s, C_L and T_f represent the enthalpy of fusion, heat capacity of the solid and liquid and fusion temperature respectively. Subscripts l and s denote the liquid and solid phases. ΔH^m and ΔH^o denote the enthalpy of mixing and the enthalpy of formation respectively.

From the TDC shown in Figure 5.3, enthalpy of formation at fusion temperature of component C ($\Delta H^0_{T_f^C}$) and the entropy of formation ($\Delta S^0_{T_f^A}$) can be derived. Assuming that the contribution of heat capacity is negligible, the expression to calculate the free energy of formation ($\Delta G^0_{T_f^C}$) at T_f^C is given by,

$$\Delta G^0_{T_f^C} = \Delta S_f^A (T_f^A - T_f^C) + \Delta S_f^B (T_f^B - T_f^C) - T_f^C R \ln 2 + \Delta H_m^l \qquad (5.8)$$

By applying Walden's rule equation (5.8) can be further simplified to,

$$\Delta G^0_{T_f^C} = \Delta S_f (T_f^A + T_f^B - 2T_f^C) - T_f^C R \ln 2 + \Delta H_m^l \qquad (5.9)$$

According to the Walden's rule, for non-spherical rigid molecules the ratio of heat of fusion to the fusion temperature is roughly constant at around 50-60 JK^{-1} mol^{-1}, more specifically a value of 56.5 JK^{-1} mol^{-1} is assigned. However, spherical or close to spherical molecules are not bound by this rule because they often yield anomalously low values of ΔS_f. Neither are flexible molecules, with elements of structure that can assume different conformations in the liquid state. For example, in a set of 739 compounds studied by Gilbert, two subsets were generated, one with 358 rigid compounds and the other with 381 flexible compounds[21]. It was found that there was a strong correlation between ΔS_f and ΔH_f with flexible molecules tending to yield higher values of ΔS_f for a given ΔH_f. Thus Walden's constant although a good first approximation to estimate the entropy of fusion must be carefully inspected on a case by case basis.

Equation (5.9) indicates that if the enthalpy of mixing is zero, then if T_f^C is greater than the sum of T_f^A and T_f^B by a factor of 2.2 than $\Delta G^0_{T_f^C}$ will be negative. Thus the melting point of cocrystal relative to its components is a good indicator of solid to solid transformation of reactants to cocrystal. For practical applications, value of ΔG_f^o at room

temperature would be of great interest. Expressions for ΔG_f^o at a temperature T are derived from the TDCs shown in Figure 5.2 and Figure 5.3 and are given by,

$$\Delta G_T^0 = \Delta S_f^A (T_f^A - T) + \Delta S_f^B (T_f^B - T) - \Delta S_f^C (T_f^C - T) - TR \ln 2 + \Delta H_m^l \quad (5.10)$$

By taking average entropies, equation (5.10) can be expressed in terms of $\Delta G_{T_f^A}^0$ and $\Delta G_{T_f^C}^0$ as,

$$\Delta G_T^0 = \Delta G_{T_f^A}^A + (T_f^A - T)(\Delta S_f + R \ln 2) + \Delta H_m^l \quad (5.11)$$

$$\Delta G_T^0 = \Delta G_{T_f^C}^0 + T_f^C \Delta S_f + (T_f^C - T)(R \ln 2) + \Delta H_m^l \quad (5.12)$$

According to equations (5.11) ΔG_T^0 is likely to remain negative over a wider temperature range below the cocrystal melting temperature i.e., for the case when $T_f^A < T_f^C < T_f^B$. When ΔG_T^0 has a small negative in equation (5.11), then the sign of ΔG_T^0 may become positive depending on the sign and magnitude of heat capacity and entropy terms. This is because of the larger negative value of $\Delta G_{T_f^A}^0$ relative to $\Delta G_{T_f^C}^0$ in equation (5.12) as well as due to the positive contribution of $T_f^C \Delta S_f$ to $\Delta G_{T_f^C}^0$ in equation (5.12)

Materials and Methods

Materials

GBPL (97+% purity) was purchased from Waterstone-Technology, LLC. Carmel IN. All other chemicals were purchased from Sigma-Aldrich and were of 99+ % purity and were used as received. Materials were characterized by X-Ray powder diffraction (XRPD) and DSC prior to use. All the new forms were synthesized according to reaction crystallization method (RCM).[13]

Cocrystal Synthesis

The cocrystals were synthesized according to the reaction crystallization method previously described by where cocrystals were precipitated from near saturated aqueous solutions of the higher solubility component.[14] The slurry was left to stir for 12-24 hours followed by filtration of the crystallized solid using a vacuum filtration assembly. The filtered material was air dried and the solid phase confirmation and purity analyses were carried out by PXRD, DSC and HPLC.

X-ray Powder Diffraction (XRPD)

XRPD was used to identify solid phases after to determine cocrystal formation. XRPD patterns of solid phases were recorded with a Rigaku MiniFlex X-ray diffractometer (Danvers, MA) using Cu Kα radiation (λ = 1.5418 Å), a tube voltage of 30 kV, and a tube current of 15 mA. The intensities were measured at 2θ values from 2° to 30° with a continuous scan rate of 2.5°/min.

Thermal Analysis

Crystalline samples of 2-4 mg were analyzed by differential scanning calorimetry (DSC) using a TA instrument (Newark, DE) 2910 MDSC system equipped with a refrigerated cooling unit. DSC experiments were performed by heating the samples at a rate of 10 K/min under a dry nitrogen atmosphere. Temperature and enthalpy calibration of the instruments was achieved using a high purity indium standard. Standard aluminum sample pans were used for all measurements. All samples were measured in triplicates with standard deviation less than 5%. Cocrystal samples for DSC analysis comprised several large crystals grown by slow partial evaporation of solutions containing the

reactants. These crystals were isolated from solution, washed, and characterized by X-Ray diffraction before DSC analysis. Heat capacities were measured by modulated differential scanning calorimetry (MDSC).

Results and discussion

Thermal data of several cocrystals that have melting point in between the melting point of its components is listed in Table 5.1. The table shows the free energy of cocrystal formation at the temperature of melting of the highest melting components as well as at 25ºC. It is apparent that the values of free energy of formation are more negative at the melting temperature of the highest melting component for all cocrystals. However at room temperature some cocrystals have larger value of free energy of formation while others have negative value. This difference is due to the contribution of the enthalpy of mixing in the liquid state, while we assumed that this mixing enthalpy is negligible when the reactants are in the solid form.

Table 5.1: For the case $T_f^A < T_f^C < T_f^B$ table presents cocrystal and component melting points, fusion enthalpies, free energies at fusion temperature of lower melting component and temperature T and the difference in the fusion temperature of higher melting component and cocrystal melting point.

Cocrystal	CC MP (K)	Drug MP (K)	Coformer MP (K)	CC ΔH_f (KJ/mol)	Drug ΔH_f (KJ/mol)	Coformer ΔH_f (KJ/mol)	$\Delta G^0_{T_f^A}$ (KJ/mol)	ΔG^0_T (T=25°C) (KJ/mol)	$T_f^B - T_f^C$	ΔH_l^m (KJ/mol)
CBZ-SUCC	461.9	465.1	460.0	28.3	24.2	32.9	-2.6	-0.40	3.2	-0.25
CBZ-SLC	433.0	465.1	432.0	26.1	24.2	24.6	-0.7	-0.23	32.1	-1.3
CBZ-GA	398.9	465.1	370.7	23.7	24.2	26.7	1.35	1.80	66.2	-1.75*
CBZ-NCT	433.8	465.1	403.5	27.2	24.2	26.6	-0.8	-0.45	31.3	-1.6
GBPL-SUCC	368.7	365.0	460.0	13.4	19.0	32.9	2.8	4.96	89.3	-12.6
GBPL-4ABA	393.4	365.0	459.2	16.6	19.0	18.4	0.9	1.92	65.6	-2.1
GBPL-GA	398.9	365.0	481.0	23.7	19.0	26.7	1.95*	7.89	82.1	0.85*
THP-NCT	448	548.2	403.5	14.6	29.1	26.6	3.9	2.49	100.2	-12.0

**The magnitude and sign on ΔH_l^{mix} would depend on the entropy of fusion value of GA. Walden's constant of 56.5 $Jmol^{-1}K^{-1}$ and a melting temperature of 200C were used to calculate the ΔH_{fus}. The value of ΔH_l^{mix} would depend on error associated with the value of fusion temperature as well as the Walden's constant. A 10% higer value of Walden's constant would change the value of ΔH_l^{mix} of GBPL-GA cocrystal from 0.85 to -0.5 $kJmol^{-1}$. Thus a positive value of $\Delta G^0_{T_f^A}$ for GBPL-GA cocrystal could be due to the generalized value used for the entropy of fusion to calculate the enthalpy of fusion of GA.*

Table 5.1 shows the free energy of formation as a function of temperature difference between cocrystal components. However the analysis shown in figure assumes that the enthalpy of mixing in the liquid state is negligible or that the mixing is ideal. As discussed previously this assumption does not apply to cocrystals since the components are chemically different, however the figure implies that in the absence of heat of mixing the dependence of free energy on the temperature difference of cocrystal components would be linear. These results are similar to the findings for about 25 racemic species studied by Li et al[22] which assumes ideal enthalpy of mixing for racemic species.

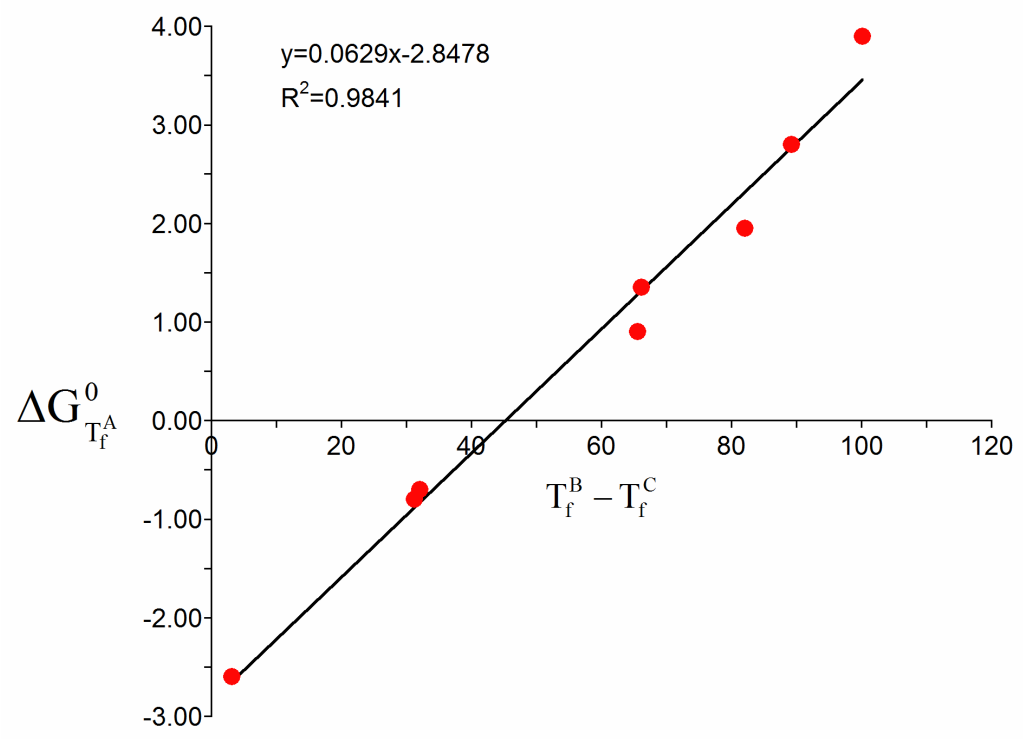

Figure 5.4: Free energy values of cocrystals against the difference between the fusion temperature of higher melting component and cocrystal for the case when the cocrystal melting point is between the melting point of its components ($T_f^A < T_f^C < T_f^B$).

Table 5.2 summarizes the thermal behavior of cocrystals and its components for the case where cocrystal melting point is below that of its components ($T_f^C < T_f^A < T_f^B$). Equation (5.9) is used to calculate the free energy of cocrystal formation for this case. It is observed that when ΔH_l^m is calculated and used in equation (5.9) then the free energy of formation of all cocrystals belonging to this category is negative. However, if we assume that ΔH_l^m is negligible then the value of free energy for all cocrystals is positive. These results are similar to the previous investigation using racemic species[22]. This implies that these cocrystals can form from the melt or the solutions phase, however their spontaneous crystallization from the reactant in the solid state is not thermodynamically favorable. It is evident from equation (5.9) that for ΔG_T^0 to be negative the fusion

temperature of the cocrystal must be 2.1 times the sum of the fusion temperatures of its components. When ΔG_T^0 is close to zero, the driving force for spontaneous cocrystal formation would be small and the kinetic factors such as temperature, disorder in material and moisture can have large dominance on the rate of formation. Equations (5.7) and (5.9) are used to study the dependence of difference of fusion temperature on ΔG_T^0 as shown in Figures 5.4 and 5.5. The entropy of mixing term is always negative and will contribute towards cocrystal formation suggesting that the entropy of mixing of the melt contributes towards the driving force for cocrystal formation.

Table 5.2: For the case $T_f^C < T_f^A < T_f^B$ table presents cocrystal and component melting points, fusion enthalpies, free energies at fusion temperature of lower melting component and temperature T and the difference in the fusion temperature of higher melting component and cocrystal melting point.

Cocrystal	CC MP (K)	Drug MP (K)	Coformer MP (K)	CC ΔH_f (KJ/mol)	Drug ΔH_f (KJ/mol)	Coformer ΔH_f (KJ/mol)	$\Delta G^0_{T_f^C}$ (KJ/mol)	ΔG^0_T (T=25°C) (KJ/mol)	$T_f^A + T_f^B - 2T_f^C$	ΔH_l^m (KJ/mol)
CBZ-4HBA	446.7	465.1	492.3	25.1	24.2	30.4	1.0	22.7	64.0	-2.2
CBZ-SAC	450.9	465.1	502.3	25.3	24.2	29.2	1.1	24.7	65.6	-1.4
CBZ-4ABA	422.5	465.1	461.9	18.8	24.2	18.4	2.2	21.8	82.0	-2.5
CBZ-BA	385.5	465.1	395.8	17.0	24.2	18.6	2.9	16.3	89.9	-4.4
GBPL-BA	356.9	365	395.8	15.5	19.0	18.6	0.6	14.5	47.0	-3.3

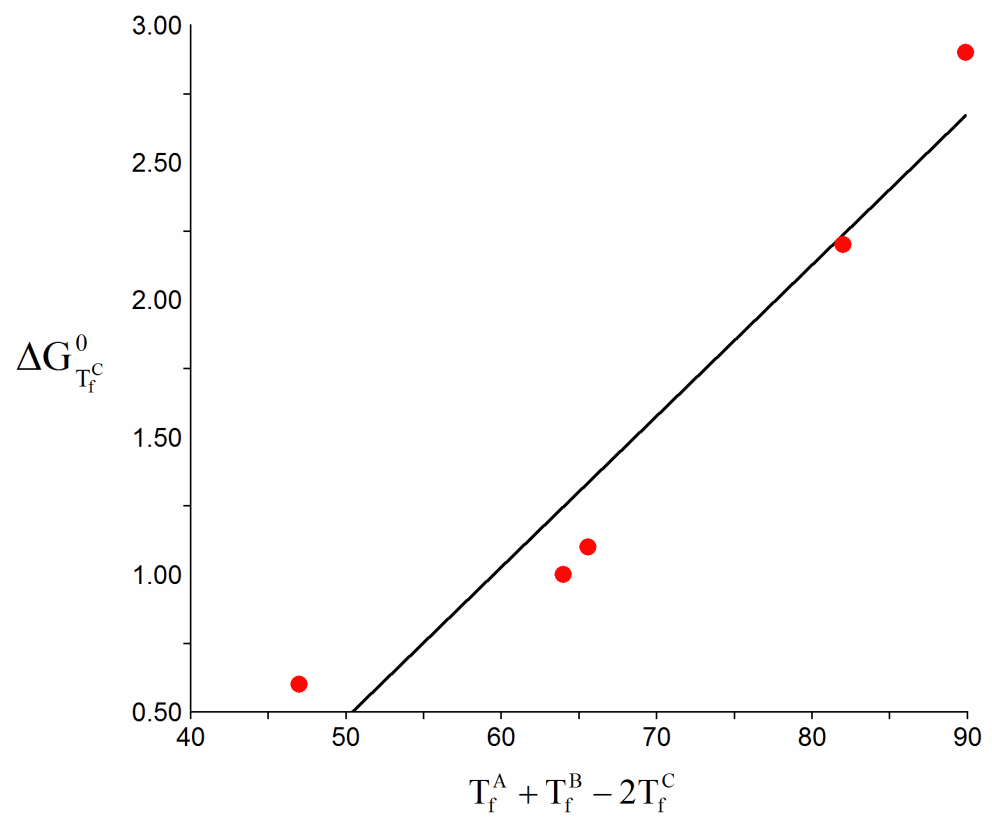

Figure 5.5: Free energy values of cocrystals listed in Table 5.2 against the difference between the sum of fusion temperatures of cocrystal components and twice the fusion temperature of cocrystal for the case when the cocrystal melting point is lower than the melting point of its components ($T_f^C < T_f^A < T_f^B$).

Investigation of all cocrystals listed in this chapter for spontaneous crystallization from its reactants is beyond the scope of this work. This type of theoretical formalism to calculate the free energy of cocrystal formation is developed for the first time to the best of our knowledge. Further work will be needed to experimentally test the models with several systems, investigate possible exceptions and develop theoretical refinement. However, we investigated the thermal behavior of CBZ-NCT cocrystal in detail which is described in the following sections. This investigation provides detailed insights to several stages through which the reaction proceeds when exposed to temperatures up to

the melting temperature of the highest melting component. The solid-liquid phase equilibrium data for the CBZ/NCT system is shown in Figure 5.6 in the form of temperature-composition phase diagram. The plot shows the formation of a 1:1 CBZ-NCT cocrystal with congruent melting point (represented by B) and the two eutectic melting points, E_1 and E_2. The eutectic compositions as well as the experimental and calculated eutectic temperatures are reported in Table 5.3. Figure 5.6 indicates that the melting point of CBZ decreases with the addition of NCT until it reaches a minimum value at E_1, which is the eutectic between CBZ and the cocrystal. On further addition of NCT, the melting point rises slightly to a maximum value at B. At the point B, the components of the solid and liquid phases are identical. This maximum temperature is the congruent melting temperature of the CBZ-NCT cocrystal. Beyond the congruent melting point, a further increase in the NCT composition causes a decrease in the melting point of the physical mixture approaching a second minimum temperature E_2, which is the eutectic between NCT and cocrystal. The lowering of CBZ and NCT melting points shown in the binary melting phase diagram in Figure 5.6 is generated by plotting the melting temperature of pure components (CBZ and NCT) recorded by DSC as a function of composition of the mixture. The experimental points were compared with the theoretical liquidus curves calculated with the simplified equation of Schröder-Van Laar (5.13).

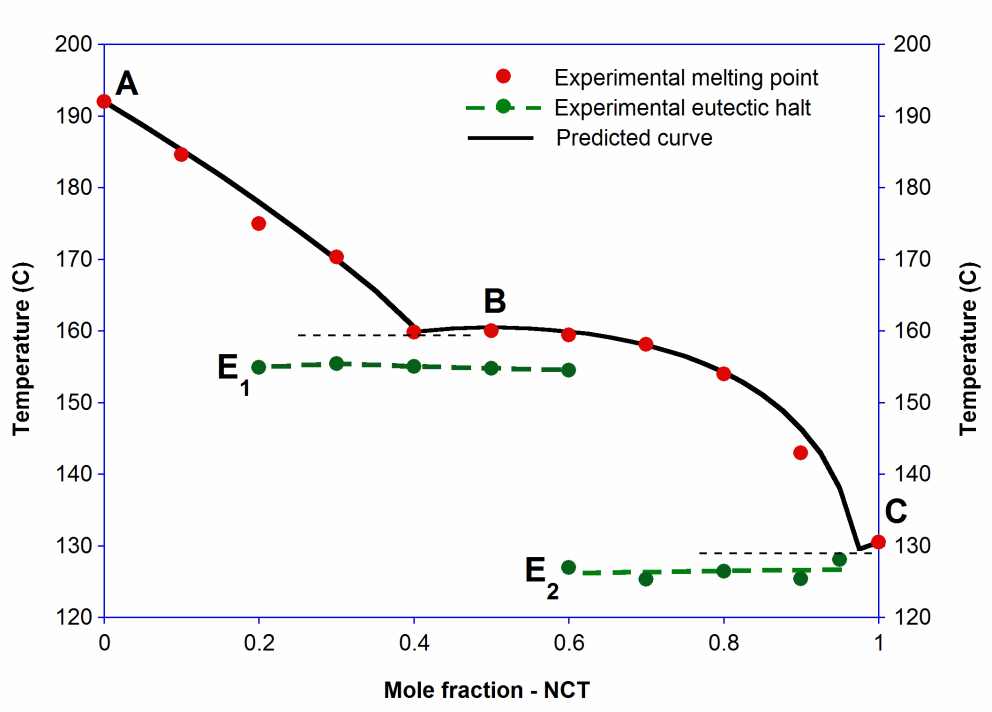

Figure 5.6: Phase diagram showing the thermal behavior of CBZ/NCT binary mixture. A, B and C are the melting points of CBZ, NCT and CBZ-NCT cocrystal respectively, the theoretical thermodynamic eutectic temperature is represents by (-----), E_1 and E_2 are the observed eutectic temperatures between CBZ and cocrystal and between NCT and cocrystal respectively. (●) represents the experimental melting points and (—) is the predicted melting curve generated by model equations (5.13) and (5.14).

$$\ln \chi_A = \frac{\Delta H^A_{fus}}{R}\left(\frac{1}{T^A_{fus}} - \frac{1}{T_{fus}}\right) \qquad (5.13)$$

Where, χ_A is the mole fraction of the component A in the mixture melting at temperature T_{fus}. ΔH^A_{fus} and T^A_{fus} are the enthalpy and the temperature of fusion (in Kelvin) of the pure constituents respectively and R is the gas constant (8.314 $JK^{-1}mol^{-1}$).[20] The part of the phase diagram where the solid phase consists of the cocrystal is a function of the temperature of fusion of the mixture and its composition. The temperature of fusion

of the mixture can be calculated for a mixture of known composition using the Prigogine-Defay model given by,

$$\ln 4\chi(1-\chi) = \frac{2\Delta H_{fus}^{cc}}{R}\left(\frac{1}{T_{fus}^{cc}} - \frac{1}{T_{fus}}\right) \qquad (5.14)$$

Where, χ is the mole fraction of one of the components in the mixture whose melting point is T_{fus} and T_{fus}^{cc} and ΔH_{fus}^{cc} are the melting point and heat of fusion of the pure cocrystal respectively.

Table 5.3: CBZ/NCT binary mixture eutectic data showing the eutectic compositions, experimental and calculated eutectic temperatures.

Composition	Mole fraction (χ_{CBZ})	Temperature (C) (Experimental)	Temperature (C) (Calculated)
Eutectic 1	0.6	125	129.1
Eutectic 2	0.03	155	159.8

From the data in Table 5.3 and Figure 5.6, it is evident that the Schröder-Van Laar and Prigogine-Defay equations over predict the eutectic temperatures. For the eutectic points, E_1 and E_2 the calculated temperatures are 4.1 and 4.8°C above the experimental temperatures respectively. These temperature differences are presumably due to some degree of non ideality in the molten state of mixtures. A mixture is considered to behave ideally in the liquid state if the enthalpy of mixing (ΔH_{mix}) were equal to zero. The enthalpy of mixing is calculated using the following equation,[26]

$$\Delta H_{mix} = \Delta H_{fus}^{exp} - \chi_1 \Delta H_{fus}^{1} + \chi_2 \Delta H_{fus}^{2} \qquad (5.15)$$

where, χ and ΔH_{fus} are the mole fraction and enthalpy of fusion of the components 1 and 2.

From the values of the enthalpies of fusion of cocrystal and cocrystal constituents, various thermodynamic parameters can be estimated to understand the crystallization behavior from the melt, specifically the eutectics and the interaction between the components forming the cocrystal can be calculated. If a eutectic is a simple mechanical mixture of two components involving no enthalpy of mixing or any type of association in the melt, then the enthalpy of eutectic melt is given by,

$$\Delta H_{fus}^{eu} = \chi_1 \Delta H_{fus}^{1} + \chi_2 \Delta H_{fus}^{2} \qquad (5.16)$$

where, χ and ΔH_{fus} are the mole fraction and enthalpy of fusion of components 1 and 2.[26] A mixture is considered to behave ideally in the liquid state if the enthalpy of mixing (ΔH_{mix}) is equal to zero. However, mixtures in the liquid state may not behave ideally. This is due to the fact that the energy of intermolecular homomeric interactions in the liquid or solution state is different from the energy of corresponding heteromeric interactions. Depending on whether heteromeric interactions are stronger or weaker than the homomeric interactions there would be either evolution or absorption of heat involved resulting in either an exotherm or an endotherm.[20] The experimental and calculated eutectic temperatures are shown in Table 5.3. The deviation in the experimental and calculated temperature values of the two eutectics as well as the negative enthalpies of mixing is due to the heteromeric interaction between CBZ and NCT, most likely due to the hydrogen bond formation in the molten state. The formation of intermolecular hydrogen bonds causes the liberation of heat resulting in lower experimental values of enthalpy of fusion relative to the calculated values. The cocrystal formed between the two components follows the reaction scheme given below.

$$A_{melt} + B_{melt} \rightarrow AB_{melt} \rightarrow AB_{solid}$$

This simple reaction scheme can be easily delineated from the DSC thermograms shown.

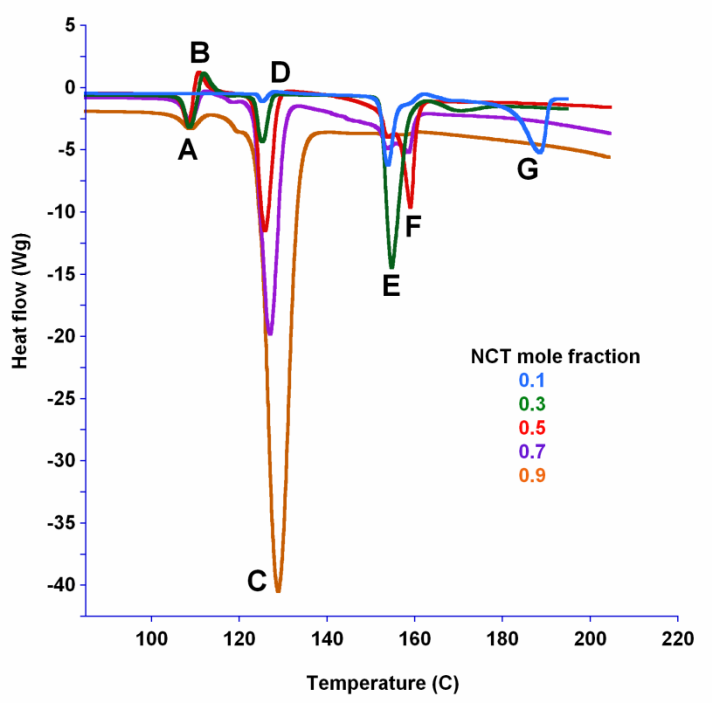

Figure 5.7: DSC thermogram representing the thermal events of CBZ/NCT mixtures with increasing mole fraction of NCT in the mixtures. Thermal event A is the eutectic endotherm between the CBZ and NCT (~108°C), B is crystallization of CBZ-NCT, C is eutectic between the cocrystal and NCT (~127°C) and D is the exotherm due to continued cocrystal formation, E is the eutectic between cocrystal and CBZ (~155°C), F is melting of the cocrystal (~160°C) and G is melting of CBZ.

Thermal event A is the first eutectic event which is between the cocrystal components, CBZ and NCT in the physical mixture. Event B pertaining to the cocrystallization from the eutectic melt was confirmed by halting the DSC immediately after this crystallization exotherm B was completed (at 120°C) and analyzed by PXRD (Figure 5.8). CBZ-NCT cocrystal can be identified by PXRD, while the un-reacted components are still present in the mixture leading to the thermal events observed in Figure 5.7. These thermal events were confirmed by performing DSC experiments with mixtures of pure cocrystal and NCT as well as pure cocrystal and CBZ as shown in Figure 5.9 and Figure 5.10.

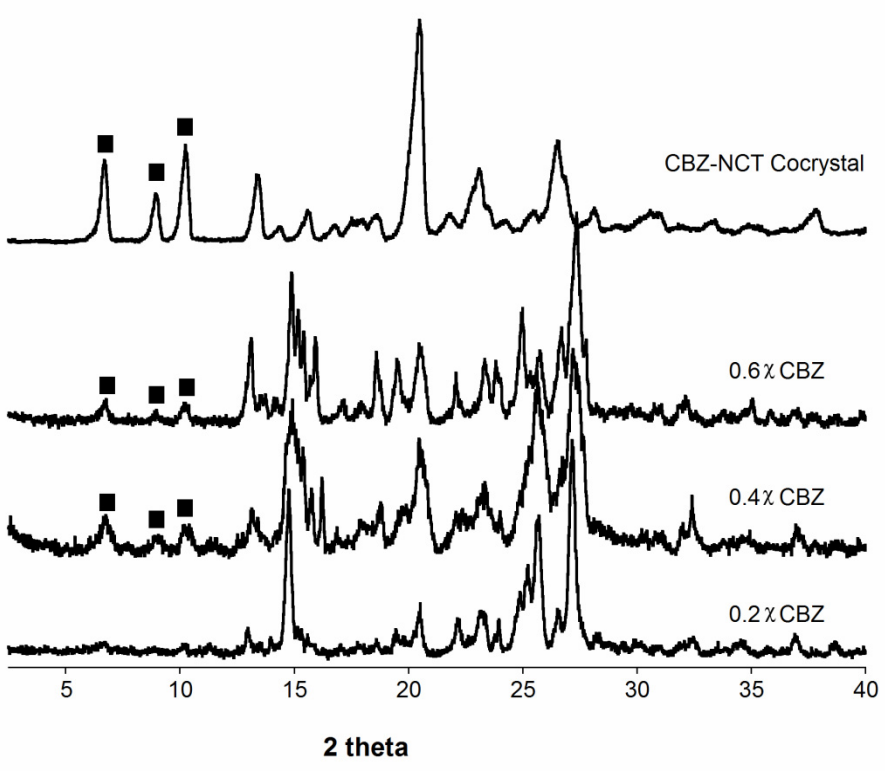

Figure 5.8: PXRD showing the formation of CBZ-NCT cocrystal upon completion of the thermal event B (and before event C) in Figure 5.7.

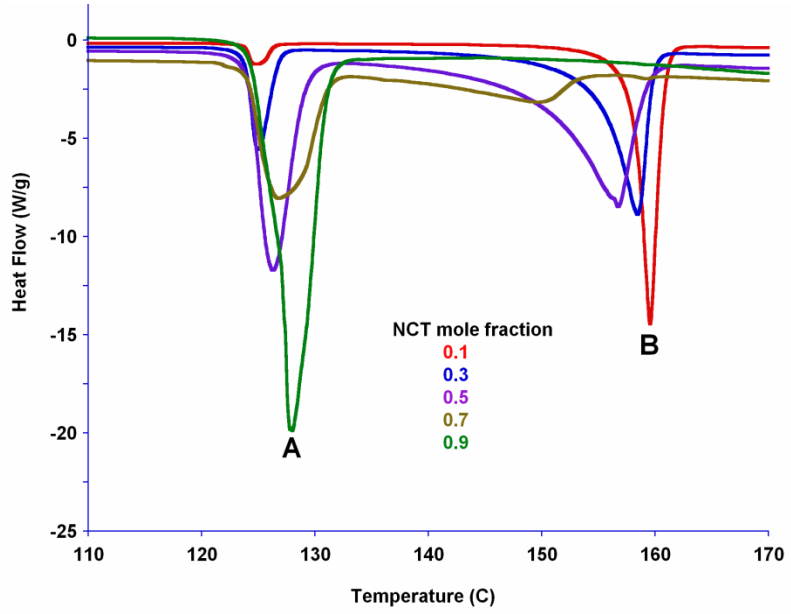

Figure 5.9: DSC thermograms of CBZ-NCT cocrystal and NCT mixtures. Thermal events A and B are the eutectic between NCT and the cocrystal and melting of the cocrystal respectively.

Figure 5.9 indicates that the eutectic between NCT and cocrystal is between 0.9 and 1.0 mole fraction of NCT in the mixture as predicted by equations (5.13) and (5.14). Cocrystal melting is shown by the thermal event B, which approaches the melting endotherm of the pure cocrystal with increasing mole fraction of the cocrystal.

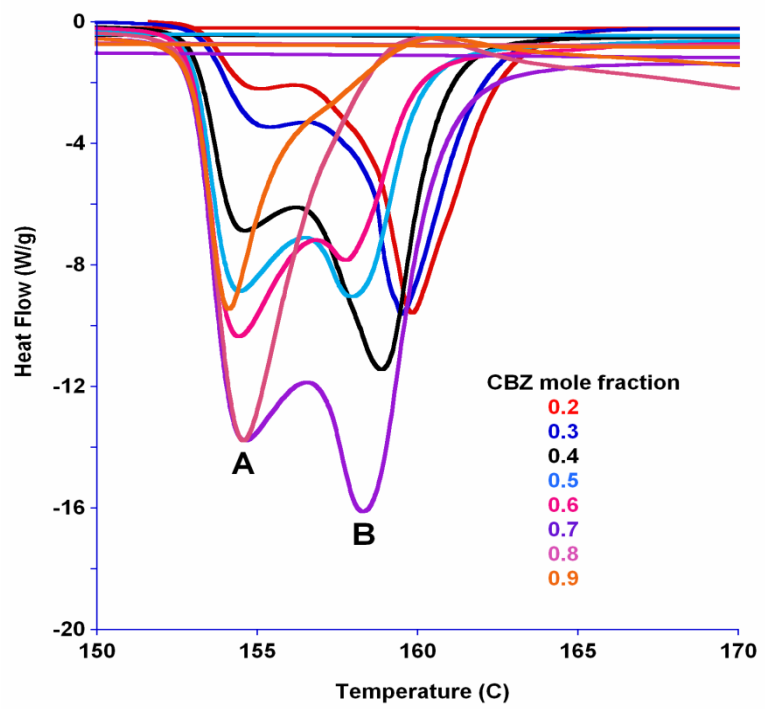

Figure 5.10: DSC thermograms of CBZ-NCT cocrystal and CBZ mixtures. Thermal even A is the eutectic between CBZ and CBZ-NCT cocrystal and B represents cocrystal melting.

Figure 5.10 shows the DSC thermograms of mixtures of CBZ and cocrystal. A eutectic halt can be observed at about 155ºC. The endotherm associated with the melt of the cocrystal shifts to that of the pure cocrystal melting endotherm with higher proportion of cocrystal in the mixtures.

Hot stage microscopy (HSM)

HSM was performed to confirm the results seen by the DSC. Figure 5.11 shows the hot stage polarized light microscopic images of the CBZ/NCT mixture.

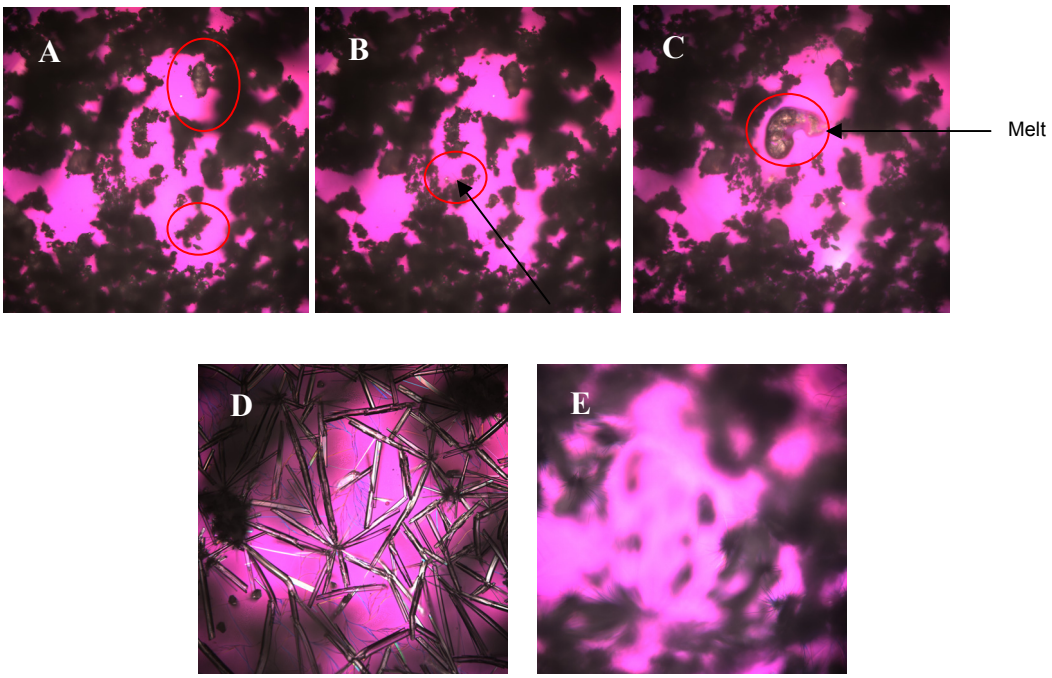

Figure 5.11: HSM showing the thermal events of CBZ/NCT mixture upon constant rate heating. A: small melting at 108°C due to the eutectic event A as seen in the DSC; B: New crystals growing due to event B shown in the DSC; C: Melting at 127°C due to the event C observed by the DSC; D: Crystallization of cocrystal continues at 135°C after the melting of NCT; and E: Melting of cocrystal at 158°C.

These thermal events confirm the thermal events observed in the DSC thermograms of CBZ/NCT mixtures in Figure 5.7. Although a binary phase diagram is useful in the assessment of stability of cocrystals, however from the cocrystal and component fusion temperatures and enthalpies spontaneous cocrystal formation cannot be predicted, and the models presented here are useful to calculate the driving force for cocrystal formation. Similar analysis has been shown for racemic compounds, where the free energy of formation of a racemic compound is proportional to the difference in the fusion

temperature between the racemic compound and its enantiomers.[21] However, in some cases both racemic compounds as well as racemic conglomerates have been observed despite large differences in the melting point.

Cocrystal Stoichiometry

The DSC thermograms were used to analyze the cocrystal stoichiometry. This was done by measuring the experimental heats of crystallization (ΔH_{cryst}) for the crystallization event represented by **B** in Figure 5.7.

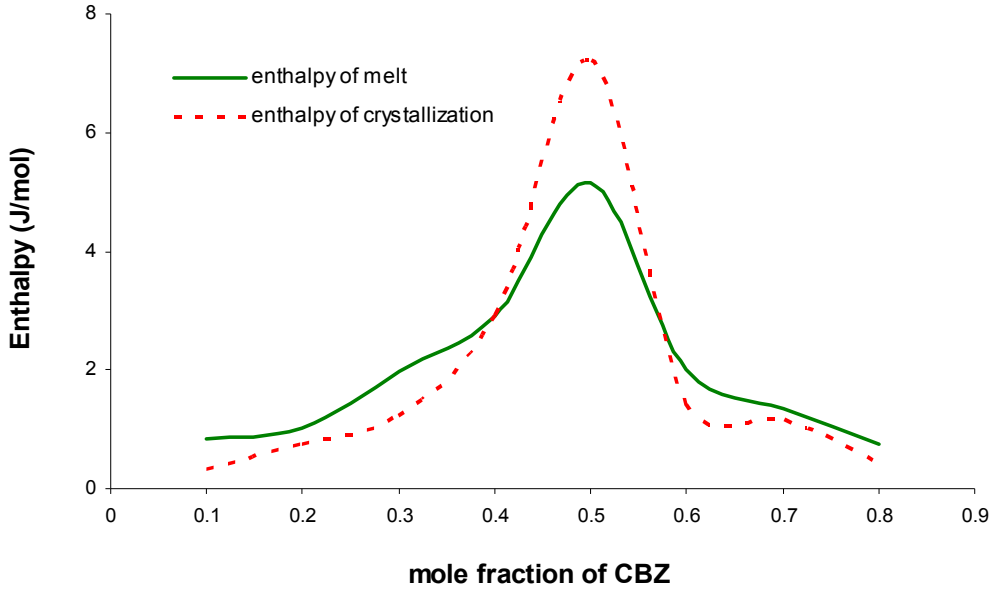

Figure 5.12: Enthaply of crystallization and melting of cocrystal at various concentrations of CBZ in the mixtures.

Figure 5.12 shows the data for ΔH_{cryst} of cocrystal formation and enthalpy of fusion of cocrystal at various mole fractions of CBZ in the mixture. Interestingly the greatest value of enthalpy of crystallization and fusion is observed at CBZ mole fraction of 0.5 suggesting that the 1:1 stoichiometry is thermodynamically preferred. This is because at

the mole fraction composition equivalent to cocrystal stoichiometry, both cocrystal components are available to their maximum concentration for reaction with the other component. As the concentration of any one component falls, less cocrystal formation takes place as reflected in Figure 5.12. Thus a careful analysis of the DSC thermograms might be useful in determining the cocrystal stoichiometry. The difference in the values of crystallization and fusion enthalpies of the mixture could be due to the embedded crystallization event occurring concurrently with melting resulting in an overall reduced observed heat of crystallization. Rodríguez-Hornedo and Suryanaranayan have shown that cocrystals can be screened by thermal methods such as DSC[27]. It is reported that a cocrystal can be anticipated if a eutectic melt is seen followed by the melting point of the cocrystal. However a more careful analysis of the DSC thermograms is needed. We address the examination of complex DSC thermograms using our studies with CBZ/NCT mixtures. Careful attention to the thermograms revealed 1st eutectic event occurs at 108°C immediately followed by cocrystallization at 111°C. While the eutectic melt could still be observed for any binary mixture, it is not necessary that it would result in formation of a cocrystal or an addition compound. We observe this behavior with CBZ/Citric acid mixture where there was no crystallization exotherm following the eutectic melt of the two components. These thermal events should indeed be confirmed with additional testing using other complimentary methods such as variable temperature XRD and HSM.

Conclusion

Experimentally accessible thermodynamic parameters can be utilized in determining the spontaneous cocrystal formation in the solid state. In the case when the free energy of formation largely depends on the difference of the fusion temperature between the higher melting component and the cocrystal. The data set analyzed suggests that for ΔG_f^o to be negative, i.e., for spontaneous cocrystal formation to occur, the difference in the temperature between the higher melting component and the cocrystal must be approximately 45°C or less. In the case when the free energy would be negative if the sum of the fusion temperature of cocrystal components is less than 2.1 times the cocrystal melting temperature. The ideal entropy of mixing contributes toward the cocrystal formation. At any temperature T, below the MP of the lowest melting component, the cocrystal formation would be more favorable with the rise in temperature, as the contribution from the ideal entropy of mixing towards free energy of formation would be more negative.

APPENDIX 3

Derivation of equations that describe the free energy of formation at the melting temperature of the lowest melting component. These equations pertain to the case when cocrystal melting point is between the melting point of its components ($T_f^A < T_f^C < T_f^B$). From the thermodynamic cycles developed in the chapter the following equation can be written as,

Heat of formation at T_f^A *:*

$$\Delta H^0_{T_f^A} = \int_{T_f^A}^{T_f^C} C_S^B \cdot dT + \int_{T_f^C}^{T_f^B} C_S^B \cdot dT + \int_{T_f^B}^{T_f^C} C_L \cdot dT + \int_{T_f^C}^{T_f^A} C_S^C \cdot dT + \int_{T_f^C}^{T_f^B} C_S^C \cdot dT + \Delta H_f^A + \Delta H_f^B - \Delta H_f^C + \Delta H_m^I$$

Solving the above integral gives

$$\Delta H^0_{T_f^A} = C_S^B (T_f^A - T_f^B) + C_L (T_f^C - T_f^B) + C_S^C (T_f^A - T_f^C) + \Delta H_f^A + \Delta H_f^B - \Delta H_f^C + \Delta H_m^I$$

Entropy of formation at T_f^A *:*

$$\Delta S^0_{T_f^A} = \int_{T_f^A}^{T_f^C} C_S^B \cdot \frac{dT}{T} + \int_{T_f^C}^{T_f^B} C_S^B \cdot \frac{dT}{T} + \int_{T_f^B}^{T_f^C} C_L \cdot \frac{dT}{T} + \int_{T_f^C}^{T_f^A} C_S^C \cdot \frac{dT}{T} + \Delta S_f^A + \Delta S_f^B - \Delta S_f^C + R \ln 2$$

Solving the above integral gives

$$\Delta S^0_{T_f^A} = (C_S^B - C_S^C)(\ln \frac{T_f^C}{T_f^A}) + (C_L - C_S^B)(\ln \frac{T_f^C}{T_f^B}) + \Delta S_f^A + \Delta S_f^B - \Delta S_f^C + R \ln 2$$

Solving for the enthalpy and entropy of fusion terms yields,

$$\Delta H_f^A + \Delta H_f^B - \Delta H_f^C - T_f^A(\Delta S_f^A + \Delta S_f^B - \Delta S_f^C + R\ln 2)$$

Substituting the $\Delta H^0_{T_f^A}$ *and* $\Delta S^0_{T_f^A}$ *in* $\Delta G = \Delta H - T\Delta S$ gives**,**

$$\Delta G^0_{T_f^A} = C_S^B(T_f^A - T_f^B) + C_L(T_f^C - T_f^B) + C_S^C(T_f^A - T_f^C) - (C_S^B - C_S^C)(T_f^A \ln\frac{T_f^C}{T_f^A}) - (C_L - C_S^B)(T_f^A \ln\frac{T_f^C}{T_f^B})$$
$$+\Delta S_f^B(T_f^B - T_f^A) - \Delta S_f^C(T_f^C - T_f^A) - T_f^A R\ln 2 + \Delta H_l^m$$

The heat capacity of solids is ignored as well as $C_L(T_f^C - T_f^B)$ due to no phase change and therefore insignificant contribution from heat capacity and simplifying the above equation gives,

$$\Delta G^0_{T_f^A} = \Delta S_f^B(T_f^B - T_f^A) - \Delta S_f^C(T_f^C - T_f^A) - T_f^A R\ln 2 + \Delta H_l^m$$

The above equation can be further simplified by applying Walden's rule and taking average entropies of fusion of component A and cocrystal,

$$\Delta G^0_{T_f^A} = \Delta S(T_f^B - T_f^C) - T_f^A R\ln 2 + \Delta H_l^m$$

Derivation of equations that describe the free energy of formation at a temperature T. These equations pertain to the case when cocrystal melting point is between the melting point of its components ($T_f^A < T_f^C < T_f^B$). From the thermodynamic cycles developed in the chapter the following equation can be written as,

Heat of formation at T:

$$\Delta H_T^0 = \int_T^{T_f^A} C_S^A \cdot dT + \int_{T_f^A}^{T_f^C} C_L^A \cdot dT + \int_{T_f^C}^{T_f^B} C_L^A \cdot dT + \int_T^{T_f^A} C_S^B \cdot dT + \int_{T_f^A}^{T_f^C} C_S^B \cdot dT + \int_{T_f^C}^{T_f^B} C_S^B \cdot dT + \int_{T_f^B}^{T_f^C} C_L \cdot dT + \int_{T_f^C}^{T_f^A} C_S^C \cdot dT + \int_{T_f^A}^{T} C_S^C \cdot dT + \Delta H_f^A + \Delta H_f^B - \Delta H_f^C$$

$$\Delta H_T^0 = C_S^A (T_f^A - T) + C_L^A (T_f^B - T_f^A) + C_S^B (T_f^B - T) + C_L (T_f^C - T_f^B) + C_S^C (T - T_f^C) + \Delta H_f^A + \Delta H_f^B - \Delta H_f^C$$

Entropy of formation at T:

$$\Delta S_T^0 = \int_T^{T_f^A} C_S^A \cdot \frac{dT}{T} + \int_{T_f^A}^{T_f^C} C_L^A \cdot \frac{dT}{T} + \int_{T_f^C}^{T_f^B} C_L^A \cdot \frac{dT}{T} + \int_T^{T_f^A} C_S^B \cdot \frac{dT}{T} + \int_{T_f^A}^{T_f^C} C_S^B \cdot \frac{dT}{T} + \int_{T_f^C}^{T_f^B} C_S^B \cdot \frac{dT}{T} + \int_{T_f^B}^{T_f^C} C_L \cdot \frac{dT}{T} + \int_{T_f^C}^{T_f^A} C_S^C \cdot \frac{dT}{T} + \int_{T_f^A}^{T} C_S^C \cdot \frac{dT}{T} + \Delta S_f^A + \Delta S_f^B - \Delta S_f^C + R \ln 2$$

$$= C_S^A \cdot \ln \frac{T_f^A}{T} + C_L^A \cdot \ln \frac{T_f^C}{T_f^A} + C_L^A \cdot \ln \frac{T_f^B}{T_f^C} + C_S^B \cdot \ln \frac{T_f^C}{T_f^A} + C_L \cdot \ln \frac{T_f^C}{T_f^B} + C_S^C \cdot \ln \frac{T_f^A}{T_f^C} + C_S^C \cdot \ln \frac{T}{T_f^A} + \Delta S_f^A + \Delta S_f^B - \Delta S_f^C + R \ln 2$$

$$= (C_S^A + C_S^B - C_S^C)(\ln \frac{T_f^A}{T}) + (C_L^A + C_S^B - C_S^C)(\ln \frac{T_f^C}{T_f^A}) + (C_L^A + C_S^B - C_L)(\ln \frac{T_f^B}{T_f^C}) + \Delta S_f^A + \Delta S_f^B - \Delta S_f^C + R \ln 2$$

Simplifying the enthalpy and entropy terms we get,

$$\Delta S_f^A (T_f^A - T) + \Delta S_f^B (T_f^B - T) - \Delta S_f^C (T_f^C - T) - R \ln 2$$

Free energy of formation at T: Substituting the ΔH_T^0 *and* ΔS_T^0 *in* $\Delta G = \Delta H - T\Delta S$

$$\Delta G_T^0 = C_S^A(T_f^A - T) + C_L^A(T_f^B - T_f^A) + C_S^B(T_f^B - T) + C_L(T_f^C - T_f^B) + C_S^C(T - T_f^C) - T[(C_S^A + C_S^B - C_S^C)(\ln\frac{T_f^A}{T}) +$$

$$(C_L^A + C_S^B - C_S^C)(\ln\frac{T_f^C}{T_f^A}) + (C_L^A + C_S^B - C_L)(\ln\frac{T_f^B}{T_f^C}) + \Delta S_f^A(T_f^A - T) + \Delta S_f^B(T_f^B - T) - \Delta S_f^C(T_f^C - T) - TR\ln 2$$

The above equation can be simplified by eliminating the heat capacity terms involving the solids,

$$\Delta G_T^0 = C_L^A(T_f^B - T_f^A) + C_L(T_f^C - T_f^B) - (C_L^A + C_S^B - C_S^C)(T\ln\frac{T_f^C}{T_f^A}) - (C_L^A + C_S^B - C_L)(T\ln\frac{T_f^B}{T_f^C}) + \Delta S_f^A(T_f^A - T) + \Delta S_f^B(T_f^B - T) - \Delta S_f^C(T_f^C - T) - TR\ln 2$$

The above equation can be further simplified to,

$$\Delta G_T^0 = \Delta S_f^A(T_f^A - T) + \Delta S_f^B(T_f^B - T) - \Delta S_f^C(T_f^C - T) - TR\ln 2$$

By taking average entropies, the above equation can be expressed in terms of $\Delta G^0_{T_f^A}$

$$\Delta G_T^0 = \Delta G^0_{T_f^A} + (T_f^A - T)(\Delta S_f + R\ln 2) + \Delta H_l^m$$

Derivation of equations that describe the free energy of formation when cocrystal melting point is below that of its components ($T_f^C < T_f^A < T_f^B$). From the thermodynamic cycles developed in the chapter the following equation can be written as,

Heat of formation at T_f^C *:*

$$\Delta H^0_{T_f^C} = \int_{T_f^C}^{T_f^A} C_S^A \cdot dT + \int_{T_f^A}^{T_f^B} C_L^A \cdot dT + \int_{T_f^C}^{T_f^B} C_S^B \cdot dT + \int_{T_f^B}^{T_f^A} C_L \cdot dT + \int_{T_f^C}^{T_f^A} C_S^C \cdot dT + \Delta H_f^A + \Delta H_f^B - \Delta H_f^C + \Delta H_m^l$$

$$\Delta H^0_{T_f^C} = C_S^A (T_f^A - T_f^C) + C_L^A (T_f^B - T_f^A) + C_S^B (T_f^B - T_f^C) + C_L (T_f^A - T_f^B) + C_S^C (T_f^A - T_f^C) + \Delta H_f^A + \Delta H_f^B - \Delta H_f^C$$

Entropy of formation at T_f^C *:*

$$\Delta S^0_{T_f^C} = \int_{T_f^C}^{T_f^A} C_S^A \cdot \frac{dT}{T} + \int_{T_f^A}^{T_f^B} C_L^A \cdot \frac{dT}{T} + \int_{T_f^C}^{T_f^B} C_S^B \cdot \frac{dT}{T} + \int_{T_f^B}^{T_f^A} C_L \cdot \frac{dT}{T} + \int_{T_f^C}^{T_f^A} C_S^C \cdot \frac{dT}{T} + \Delta S_f^A + \Delta S_f^B - \Delta S_f^C + R \ln 2$$

$$\Delta S^0_{T_f^C} = (C_S^A - C_S^C)(\ln \frac{T_f^A}{T_f^C}) + (C_L^A + C_S^B)(\ln \frac{T_f^B}{T_f^A}) + (C_S^B + C_L)(\ln \frac{T_f^A}{T_f^C}) + \Delta S_f^A + \Delta S_f^B - \Delta S_f^C + R \ln 2$$

Substituting the $\Delta H^0_{T_f^C}$ *and* $\Delta S^0_{T_f^C}$ *in* $\Delta G = \Delta H - T\Delta S$ gives,

$$\Delta G^0_{T_f^C} = C_S^A (T_f^A - T_f^C) + C_L^A (T_f^B - T_f^A) + C_S^B (T_f^B - T_f^C) + C_L (T_f^A - T_f^B) + C_S^C (T_f^A - T_f^C) - T_f^C [(C_S^A - C_S^C)(\ln \frac{T_f^A}{T_f^C}) + (C_L^A - C_S^B)(\ln \frac{T_f^B}{T_f^A}) +$$

$$(C_S^B + C_L)(\ln \frac{T_f^A}{T_f^C}) + \Delta S_f^A (T_f^A - T_f^C) + \Delta S_f^B (T_f^B - T_f^C) - T_f^C R \ln 2 + \Delta H_m^l$$

The heat capacity of solids is ignored as well as $C_L(T_f^B - T_f^C)$ and $C_L(T_f^A - T_f^B)$ due to no phase change and therefore insignificant contribution from heat capacity and simplifying the above equation gives,

$$\Delta G^0_{T_f^C} = \Delta S_f^A (T_f^A - T_f^C) + \Delta S_f^B (T_f^B - T_f^C) - T_f^C R \ln 2 + \Delta H_m^l$$

By applying Walden's rule the above equation can be further simplified to,

$$\Delta G^0_{T_f^C} = \Delta S_f (T_f^A + T_f^B - 2T_f^C) - T_f^C R \ln 2 + \Delta H_m^l$$

Derivation of equations that describe the free energy of formation at a temperature T. These equations pertain to the case when cocrystal melting point is between the melting point of its components ($T_f^C < T_f^A < T_f^B$). From the thermodynamic cycles developed in the chapter the following equation can be written as,

Heat of formation at T:

$$\Delta H_T^0 = \int_T^{T_f^C} C_S^A \cdot dT + \int_{T_f^C}^{T_f^A} C_S^A \cdot dT + \int_{T_f^A}^{T_f^B} C_L^A \cdot dT + \int_T^{T_f^C} C_S^B \cdot dT + \int_{T_f^C}^{T_f^A} C_S^B \cdot dT + \int_{T_f^A}^{T_f^B} C_S^B \cdot dT + \int_{T_f^B}^{T_f^A} C_L \cdot dT + \int_{T_f^A}^{T_f^C} C_S^C \cdot dT + \int_{T_f^C}^{T} C_S^C \cdot dT + \Delta H_f^A + \Delta H_f^B - \Delta H_f^C$$

$$\Delta H_T^0 = C_S^A (T_f^A - T) + C_L^A (T_f^B - T_f^A) + C_S^B (T_f^B - T) + C_L (T_f^A - T_f^B) + C_S^C (T - T_f^A) + \Delta H_f^A + \Delta H_f^B - \Delta H_f^C$$

Entropy of formation at T:

$$\Delta S_T^0 = \int_T^{T_f^C} C_S^A \cdot \frac{dT}{T} + \int_{T_f^C}^{T_f^A} C_S^A \cdot \frac{dT}{T} + \int_{T_f^A}^{T_f^B} C_L^A \cdot \frac{dT}{T} + \int_T^{T_f^C} C_S^B \cdot \frac{dT}{T} + \int_{T_f^C}^{T_f^A} C_S^B \cdot \frac{dT}{T} + \int_{T_f^A}^{T_f^B} C_S^B \cdot \frac{dT}{T} + \int_{T_f^B}^{T_f^A} C_L \cdot \frac{dT}{T} + \int_{T_f^A}^{T_f^C} C_S^C \cdot \frac{dT}{T} + \int_{T_f^C}^{T} C_S^C \cdot \frac{dT}{T} + \Delta H_f^A + \Delta H_f^B - \Delta H_f^C$$

$$= C_S^A \cdot \ln\frac{T_f^C}{T} + C_S^A \cdot \ln\frac{T_f^A}{T_f^C} + C_L^A \cdot \ln\frac{T_f^B}{T_f^A} + C_S^B \cdot \ln\frac{T_f^C}{T} + C_L \cdot \ln\frac{T_f^B}{T_f^A} + C_S^C \cdot \ln\frac{T_f^C}{T_f^A} + C_S^C \cdot \ln\frac{T_f^C}{T} + \Delta S_f^A + \Delta S_f^B - \Delta S_f^C + R \ln 2$$

$$= (C_S^A + C_S^B - C_S^C)(\ln\frac{T_f^C}{T}) + (C_S^A + C_S^B - C_L)(\ln\frac{T_f^A}{T_f^C}) + (C_S^B + C_L^A - C_L)(\ln\frac{T_f^B}{T_f^A}) + \Delta S_f^A + \Delta S_f^B - \Delta S_f^C + R \ln 2$$

Simplifying the enthalpy and entropy terms we get,

$$\Delta S_f^A (T_f^A - T) + \Delta S_f^B (T_f^B - T) - \Delta S_f^C (T_f^C - T) - R \ln 2$$

Free energy of formation at T: Substituting the ΔH_T^0 *and* ΔS_T^0 *in* $\Delta G = \Delta H - T\Delta S$

$$\Delta G_T^0 = C_S^A (T_f^A - T) + C_L^A (T_f^B - T_f^A) + C_S^B (T_f^B - T) + C_L (T_f^C - T_f^B) + C_S^C (T - T_f^C) - T[(C_S^A + C_S^B - C_S^C)(\ln \frac{T_f^C}{T}) + (C_L - C_S^A - C_S^B)(\ln \frac{T_f^C}{T_f^A}) +$$

$$(C_L^A + C_S^B - C_L)(\ln \frac{T_f^B}{T_f^A}) + \Delta S_f^A (T_f^A - T) + \Delta S_f^B (T_f^B - T) - \Delta S_f^C (T_f^C - T) - TR \ln 2$$

The heat capacity of solids is ignored as well as $C_L (T_f^B - T_f^A)$ and $C_L (T_f^C - T_f^B)$ due to no phase change and therefore insignificant contribution from heat capacity and simplifying the above equation gives,

$$\Delta G_T^0 = \Delta S_f^A (T_f^A - T) + \Delta S_f^B (T_f^B - T) - \Delta S_f^C (T_f^C - T) - TR \ln 2$$

By taking average entropies, the above equation can be expressed in terms of $\Delta G_{T_f^C}^0$

$$\Delta G_T^0 = \Delta G_{T_f^C}^0 + T_f^C \Delta S_f + (T_f^C - T)(R \ln 2) + \Delta H_m^1$$

References

(1) Bak, A.; Gore, A.; Yanez, E.; Stanton, M.; Tufekcic, S.; Syed, R.; Akrami, A.; Rose, M.; Surapaneni, S.; Bostick, T.; King, A.; Neervannan, S.; Ostovic, D.; Koparkar, A., The co-crystal approach to improve the exposure of a water-insoluble compound: AMG 517 sorbic acid co-crystal characterization and pharmacokinetics. *Journal of Pharmaceutical Sciences* **2008,** 97, (9), 3942-3956.

(2) McNamara, D. P.; Childs, S. L.; Giordano, J.; Iarriccio, A.; Cassidy, J.; Shet, M. S.; Mannion, R.; O'Donnell, E.; Park, A., Use of a glutaric acid cocrystal to improve oral bioavailability of a low solubility API. *Pharmaceutical Research* **2006,** 23, (8), 1888-1897.

(3) Stanton, M. K.; Bak, A., Physicochemical properties of pharmaceutical co-crystals: A case study of ten AMG 517 co-crystals. *Crystal Growth & Design* **2008,** 8, (10), 3856-3862.

(4) Bethune, S. J.; Huang, N.; Jayasankar, A.; Rodríguez-Hornedo, N., Understanding and Predicting the Effect of Cocrystal Components and pH on Cocrystal Solubility. *Crystal Growth & Design* **2009,** 9, (9), 3976-3988.

(5) Jayasankar, A.; Good, D. J.; Rodriguez-Hornedo, N., Mechanisms by which moisture generates cocrystals. *Molecular Pharmaceutics* **2007,** 4, (3), 360-372.

(6) Huang, N.; Rodriguez-Hornedo, N., Effect of Micelliar Solubilization on Cocrystal Solubility and Stability. *Crystal Growth & Design* **2010,** 10, (5), 2050-2053.

(7) Chency, M. L.; Shan, N.; Healey, E. R.; Hanna, M.; Wojtas, L.; Zaworotko, M. J.; Sava, V.; Song, S. J.; Sanchez-Ramos, J. R., Effects of Crystal Form on Solubility and Pharmacokinetics: A Crystal Engineering Case Study of Lamotrigine. *Crystal Growth & Design* **2010,** 10, (1), 394-405.

(8) Remenar, J. F.; Peterson, M. L.; Stephens, P. W.; Zhang, Z.; Zimenkov, Y.; Hickey, M. B., Celecoxib : Nicotinamide dissociation: Using excipients to capture the cocrystal's potential. *Molecular Pharmaceutics* **2007,** 4, (3), 386-400.

(9) Guzman, H. R.; Tawa, M.; Zhang, Z.; Ratanabanangkoon, P.; Shaw, P.; Gardner, C. R.; Chen, H.; Moreau, J. P.; Almarsson, O.; Remenar, J. F., Combined use of crystalline salt forms and precipitation inhibitors to improve oral absorption of celecoxib from solid oral formulations. *Journal of Pharmaceutical Sciences* **2007,** 96, (10), 2686-2702.

(10) Jayasankar, A.; Reddy, L. S.; Bethune, S. J.; Rodriguez-Hornedo, N., Role of Cocrystal and Solution Chemistry on the Formation and Stability of Cocrystals with Different Stoichiometry. *Crystal Growth & Design* **2009,** 9, (2), 889-897.

(11) Nehm, S. J.; Rodriguez-Spong, B.; Rodriguez-Hornedo, N., Phase solubility diagrams of cocrystals are explained by solubility product and solution complexation. *Crystal Growth & Design* **2006,** 6, (2), 592-600.

(12) Friscic, T.; Childs, S. L.; Rizvi, S. A. A.; Jones, W., The role of solvent in mechanochemical and sonochemical cocrystal formation: a solubility-based approach for predicting cocrystallisation outcome. *Crystengcomm* **2009,** 11, (3), 418-426.

(13) Childs, S. L.; Rodriguez-Hornedo, N.; Reddy, L. S.; Jayasankar, A.; Maheshwari, C.; McCausland, L.; Shipplett, R.; Stahly, B. C., Screening strategies based on solubility and solution composition generate pharmaceutically acceptable cocrystals of carbamazepine. *Crystengcomm* **2008,** 10, (7), 856-864.

(14) Rodriguez-Hornedo, N.; Nehm, S. J.; Seefeldt, K. F.; Pagan-Torres, Y.; Falkiewicz, C. J., Reaction crystallization of pharmaceutical molecular complexes. *Molecular Pharmaceutics* **2006,** 3, (3), 362-367.

(15) Trask, A. V.; Motherwell, W. D. S.; Jones, W., Solvent-drop grinding: green polymorph control of cocrystallisation. *Chemical Communications* **2004**, (7), 890-891.

(16) Chadwick, K.; Davey, R.; Cross, W., How does grinding produce co-crystals? Insights from the case of benzophenone and diphenylamine. *CrystEngComm* **2007,** 9, 732-734.

(17) Maheshwari, C.; Jaysankar, A.; Khan, N. A.; Amidon, G. E.; Rodriguez-Hornedo, N., Factors that influence the spontaneous formation of pharmaceutical cocrystals by simply mixing solid reactants. . *CrystEngComm* **2009,** 11, 493-500.

(18) Neau, S. H.; Shinwari, M. K.; Hellmuth, E. W., Melting point phase diagrams of free base and hydrochloride salts of bevantolol, pindolol and propanolol. *International Journal of Pharmaceutics* **1993,** 99, 303-310.

(19) Prankard, R. J.; Elsabee, M., Thermal Analysis of Chiral Drug Mixtures: The DSC behavior of mixtures of ephedrine·HCl. *Thermochimica Acta* **1995,** 248, 147-160.

(20) Jacques, J.; Collet, A.; Wilen, S. H., *Enantiomers, Racemates and Resolutions*. ed.; John Wiley & Sons, Inc.: New York, 1981.

(21) Glbert, A.S.; Entropy-enthalpy compensation in the fusion of organic molecules: implications for Walden's rule and molecular freedom in the liquid state. *Thermochimica Acta* 1999, 339, 131-142.

(22) Li, Z. J.; Zell, M. T.; Munson, E. J.; Grant, D. J. W., Characterization of racemic species of chiral drugs using thermal analysis, thermodynamic calculation, and structural studies. *Journal of Pharmaceutical Sciences* **1999,** 88, (3), 337-346.

(23) Schartman, R. R., On the thermodynamics of cocrystal formation. *International Journal of Pharmaceutics* **2009,** 365, (1-2), 77-80.

(24) Ainouz, A.; Authelin, J. R.; Billot, P.; Lieberman, H., Modeling and prediction of cocrystal phase diagrams. *International Journal of Pharmaceutics* **2009,** 374, (1-2), 82-89.

(25) Rodriguez-Hornedo, N.; Nehru, S. J.; Seefeldt, K. F.; Pagan-Torres, Y.; Falkiewicz, C. J., Reaction crystallization of pharmaceutical molecular complexes. *Molecular Pharmaceutics* **2006,** 3, (3), 362-367.

(26) Rai, U. S.; George, S., Thermochemical studies on the eutectics and addition compounds in the binary systems of benzidine with p-nitrophenol, m-aminophenol and resorcinol. *Thermochimica Acta* **1994,** 243, 17-25.

(27) Lu, E., Rodriguez-Hornedo, N., Suryanarayanan, R., A rapid thermal method for cocrystal screening, *CrystEngComm* **2008**, 10, 665-668.

CHAPTER 6

CONCLUSION AND FUTURE WORK

This dissertation has focused on the thermodynamic solubility and stability of pharmaceutical cocrystals. The specific goals of this dissertation were to (i) Investigate the role of coformer solubility influencing the cocrystal solubility and developing new cocrystals of lower solubility relative to the reference compound, (ii) Provide understanding on the role of lattice properties and solute-solvent interactions as parameters that govern the observed equilibrium solubility, (iii) Describe the pH_{max} for cocrystals and how this critical phenomenon can regulate the cocrystal solution stability. Lay out generalized guidelines that describe the parameters that affect the value of pH_{max} for cocrystals, (iv) Compare the solubility of cocrystals and salts and how cocrystals can offer solubility advantage over salts, (v) Importance of thermodynamic solubility measurements to access the true solubility of metastable cocrystals, by showing how kinetic solubility measurements of highly soluble solid forms could lead to misinterpretation of solubility due to phase transformation as well as the effect of common ions on such phase transitions, (vi) The role of surfactants is examined in the synthesis of cocrystals and how micellar concentration affects the solubility of a cocrystal of weakly basic drug and a non-ionic coformer, (vii) Thermal behavior of cocrystal components was studied by means of calorimetry and mechanism of cocrystal formation

from the melt is presented. Assuming ideality of a binary mixture, a phase diagram can be generated from a few experiments, yielding valuable information about the eutectics. (vii) Spontaneous cocrystal formation in solid mixtures was investigated and thermodynamic cycles were developed to estimate free energy of cocrystal formation from its reactants. Several mathematical models were developed and presented in the research chapters for a robust understanding of cocrystal solid and solution phase chemistry and stability.

The quest is not always about improving the solubility of a poorly soluble compound, but attaining the right solubility, which might involve lowering the solubility of a highly soluble compound due to its toxicity and for drug delivery. Cocrystals allow us to tailor the drug solubility and dissolution kinetics and thereby facilitate the development of solid forms with customizable drug absorption and bioavailability profiles. While a direct solubility measurement of thermodynamically stable cocrystals of gabapentin-lactam was possible as described in chapter 2, for high solubility cocrystal of lamotrigine, direct solubility measurement was not possible. This is due to supersaturation and subsequent phase transformations to less soluble forms. However, pH is an important factor in altering the thermodynamic solubility, such that beyond a critical pH value known as pH_{max} the thermodynamic stability of forms reverses and high solubility forms can be made stable. This is investigated and presented in detail for both, (i) the relatively low solubility cocrystals of gabapentin-lactam, and (ii) for high solubility cocrystal of lamotrigine with nicotinamide as coformer. pH_{max} is a eutectic point where in the three-component system (components A, B and solution) at constant temperature and pressure, two solid phases (A and B) are in equilibrium with solution

(Gibbs phase rule). One of the solid phases is the cocrystal while the other could be a cocrystal component or its solvate, different stoichiometry cocrystal, cocrystal solvate. Thus a eutectic point allows the measurement of the thermodynamic solubility of the cocrystal and to estimate the maximum stoichiometric solubility. Analogous to salts, cocrystal are shown to exhibit pH_{max} and generalized models are derived to show the affect of K_{sp}, component solubility and ionization properties (pK_a) on the value of pH_{max}. The advantage of these methods is that they are accessible and correspond to a thermodynamic equilibrium that is a reference point for describing solution phase behavior. For a cocrystal of a non ionic compound with an acidic coformer, higher the value of drug solubility and coformer pKa, higher is the pH_{max}, while the cocrystal solubility (K_{sp}) is inversely proportional to the value of pH_{max}. The contributions of fusion enthalpy and melting temperatures of several gabapentin-lactam cocrystals were compared to the experimentally measured solubility. These correlations showed considerable deviations in the observed aqueous cocrystal solubility values from the ideal solubility behavior based on the contributions of crystal lattice alone. For this small series of gabapentin-lactam cocrystals with weakly acidic coformers the key learning are (i) solvent-solute interactions quantified by activity coefficient, in water, were dominant relative to the ideal solubility estimated from fusion of the crystal lattice, (ii) solubilities increased exponentially when pH > pKa, while cocrystals with amphoteric coformer had U-shaped solubility-pH profile in accordance with coformer's two pK_a values, (iii) mathematical models provide a rational basis for selecting coformers to customize cocrystal solubility-pH behavior, (iv) solution pH can promote (or avoid) cocrystal formation. Thus understanding both the solid phase and solution chemistry of cocrystals

is important toward expanding cocrystal-solubility relationships. Future considerations of cocrystal solubility should seek to combine the observed solubility trends with the crystal lattice energy. All gabapentin-lactam cocrystals studied in this dissertation have solubilities lower than both cocrystal components, this is a subject of further research where studying the crystal lattice properties would shed information as why the solubility is lower than both components. Many cocrystals studied in the past have shown solubility values which is between that of its components. Understanding these behaviors would enhance the rational selection of coformers as well as prediction of solubility behavior.

In the case of lamotrigine-nicotinamide hydrate cocrystal discussed in chapter 3, the solubility of cocrystal is found to be 30 fold higher than that of lamotrigine hydrate. The estimation of this higher thermodynamic solubility relative to lamotrigine hydrate was possible by measuring the eutectic concentration of cocrystal components. Thermodynamic solubility of two cocrystals and two salts were compared with the reported solubility values determined by kinetic methods. There is a large discrepancy in the reported solubility values which were determined by kinetic methods compared to the values obtained from the equilibrium methods presented in this thesis. This is due to the solution phase mediated transformation of high solubility solid forms to more stable forms. All solid forms studied transform to the lamotrigine hydrochloride salt since this salt has the lowest solubility and is the most stable form. Cocrystal and salt solubility-pH dependencies revealed that experiments were in excellent agreement with those predicted by the solubility equations. The key leanings are, (i) By using the solid solution phase equilibria and solubility models, such solution phase behavior can be predicted and a

rationale experimental design to assess true solubility can be utilized, (ii) RCM was successfully used to synthesize lamotrigine-nicotinamide hydrate cocrystal. Various methods presented in the literature were tried but did not result in a cocrystalline solid phase. RCM with 2% SLS with NCT concentration above its eutectic concentration successfully generated pure cocrystalline phase, (iii) Critical stabilization concentration (CSC) was investigated in the presence of 2% SLS. Although no CSC exists between lamotrigine-nicotinamide hydrate and lamotrigine hydrate, there is an approximately 8 fold higher lamotrigine concentrations in 2% SLS solution. This increase in the reactant concentration likely provides a conducive environment for cocrystal formation. Future work should investigate the critical SLS concentration that is needed for cocrystallization as well as the mechanism by which SLS (micelles) aid in cocrystal formation. This will expand the understanding of cocrystal formation *via* micellar solubilization and relate it to molecular structure and solubility differences of cocrystal components.

Spontaneous cocrystal formation in reactant mixtures was investigated and presented in chapter 4 of this dissertation, where physical mixtures of cocrystal reactants were prepared. We hypothesized that if cocrystal formation is thermodynamically favored then cocrystal should form in simple physical mixtures without milling the reactants together. Carbamazepine-nicotinamide and carbamazepine-saccharin cocrystals were tested and the factors that influence the kinetics were investigated. Temperature, relative humidity as well as milling of individual reactants influence the cocrystallization rates. Cocrystallization rates were higher when physical mixtures were stored at higher temperature, higher relative humidity and when prepared from individually milled reactants. Results indicate that defects caused by milling of the reactants may have a role

in enhancing the kinetics of cocrystal formation. When reactants were annealed after milling and prior to mixing, the rates of cocrystal formation were slower compared to milled and un-annealed reactants. Other mechanism such as eutectic melt, deliquescence or vapor phase mediated cocrystal formation were not observed indicating that this was a solid to solid conversion of reactants to cocrystals. Future work should investigate the role of reactant properties and mechanisms such as self catalysis, and progression of defects in the formation of cocrystals from solid reactants.

The driving force for cocrystal formation from solid reactants was modeled by developing thermodynamic cycles presented in chapter 5. The thermodynamic cycles were used to derive the free energy expressions and estimating the sign and magnitude of free energy of formation of cocrystals. From simple thermal parameters such as enthalpy of fusion (ΔH_f), temperature of fusion (T_f), entropy of fusion (ΔS_f) and mixing (ΔS_m), heats of mixing (ΔH_m) and heat capacities differences ΔC_p, mathematical expressions for free energy of formation are derived. Cocrystals were classified into two categories, one where the cocrystal melting point is between that of its components, and second where the cocrystal melting point is below that of its components. Generalized equations were derived for both the classes of cocrystals and it was found that cocrystal melting point relative to that of its components is a key parameter that governs the sign and magnitude of molar free energy of formation (ΔG_f^o). Unlike racemic compounds, cocrystal components are chemically different with different fusion temperatures and enthalpies. As a consequence the assumption applicable to racemates, that heat of mixing will be negligible would not hold for cocrystals and there can be significant contribution from mixing to the overall free energy of formation. From the mathematical models developed,

free energies of formation of several cocrystals were calculated and it was found that higher the cocrystal melting point relative to its components more likely the value of ΔG_f^o to be negative. Future work should investigate a much larger sample of cocrystals and also include the contributions from heat capacity measurements, especially when the free energy of formation is close to zero. A comparison of calculated and experimental evaluation of the enthalpy of mixing of cocrystal components would provide insights to the propensity of interaction between the components, which will enhance the accuracy of the models.